

Soils and Rocks

An International Journal of Geotechnical
and Geoenvironmental Engineering



Volume 40, N. 1
January-April 2017

**Soils and Rocks is an International Journal of Geotechnical and
Geoenvironmental Engineering published by**

**ABMS - Brazilian Association for Soil Mechanics and Geotechnical Engineering
Av. Queiroz Filho, 1700 - Torre A Sky, Sala 106 - Vila Hamburguesa
05319-000, São Paulo, SP
Brazil**

**SPG - Portuguese Geotechnical Society
LNEC, Avenida do Brasil, 101
1700-066 Lisboa
Portugal**



Issue Date: April 2017

Issue: 400 copies and 800 online-distributed copies

Manuscript Submission: For review criteria and manuscript submission information, see Instructions for Authors at the end.

Disclaimer: The opinions and statements published in this journal are solely the author's and not necessarily reflect the views or opinions of the publishers (ABMS and SPG). The publishers do not accept any liability arising in any way from the opinions, statements and use of the information presented.

Copyright: Authors and ABMS-Brazilian Society for Soil Mechanics and Geotechnical Engineering

SOILS and ROCKS

An International Journal of Geotechnical and Geoenvironmental Engineering

Editor Paulo Scarano Hemsí - Aeronautics Institute of Technology, Brazil

Co-editor José Couto Marques - University of Porto, Portugal

Executive Board

Waldemar Coelho Hachich
University of São Paulo, Brazil
António Topa Gomes
University of Porto, Portugal

Gustavo Ferreira Simões
Federal University of Minas Gerais, Brazil
Rafaela Cardoso
University of Lisbon, Portugal

Associate Editors

H. Einstein
MIT, USA
John A. Hudson
Imperial College, UK
Kenji Ishihara
University of Tokyo, Japan
Michele Jamiolkowski
Studio Geotecnico Italiano, Italy
Willy A. Lacerda
COPPE/UFRJ, Brazil

E. Maranha das Neves
Lisbon Technical University, Portugal
Nielen van der Merve
University of Pretoria, South Africa
Paul Marinos
NTUA, Greece
James K. Mitchell
Virginia Tech., USA
Lars Persson
SGU, Sweden

Harry G. Poulos
University of Sidney, Australia
Niek Rengers
ITC, The Netherlands
Fumio Tatsuoka
Tokyo University of Science, Japan
Luiz González de Vallejo
UCM, Spain
Roger Frank
ENPC-Cermes, France

Editorial Board Members

Roberto F. Azevedo
Federal University of Viçosa, Brazil
Milton Kanji
University of São Paulo, Brazil
Kátia Vanessa Bicalho
Federal University of Espírito Santo, Brazil
Omar Y. Bitar
IPT, Brazil
Lázaro V. Zuquette
University of São Paulo at São Carlos, Brazil
Fabio Taioli
University of São Paulo, Brazil
Tarcisio Celestino
University of São Paulo at São Carlos, Brazil
Edmundo Rogério Esquível
University of São Paulo at São Carlos, Brazil
Nilo C. Consoli
Federal Univ. Rio Grande do Sul, Brazil
Sandro S. Sandroni
Consultant, Brazil
Sérgio A.B. Fontoura
Pontifical Catholic University, Brazil
Ennio M. Palmeira
University of Brasília, Brazil
Luciano Décourt
Consultant, Brazil
Façal Massad
University of São Paulo, Brazil
Marcus Pacheco
University of the State of Rio de Janeiro, Brazil
Paulo Maia
University of Northern Rio de Janeiro, Brazil
Renato Cunha
University of Brasília, Brazil

Orencio Monje Vilar
University of São Paulo at São Carlos, Brazil
Maria Eugenia Boscov
University of São Paulo, Brazil
Eda Freitas de Quadros
BGTECH, Brazil
Tácio de Campos
Pontifical Catholic University of Rio de Janeiro, Brazil
Richard J. Bathurst
Royal Military College of Canada
Robert Mair
University of Cambridge, UK
Serge Leroueil
University of Laval, Canada
Mario Manassero
Politécnico di Torino, Italy
Luis Valenzuela
Consultant, Chile
Jorge G. Zornberg
University of Texas/Austin, USA
Andrew Whittle
MIT, USA
Pierre Bérest
LCPC, France
Peter Kaiser
Laurentian University, Canada
He Manchao
CUMT, China
Teruo Nakai
Nagoya Inst. Technology, Japan
Claudio Olalla
CEDEX, Spain
Frederick Baynes
Baynes Geologic Ltd., Australia

R. Kerry Rowe
Queen's University, Canada
R. Jonathan Fannin
University of British Columbia, Canada
Laura Caldeira
LNEC, Portugal
António S. Cardoso
University of Porto, Portugal
José D. Rodrigues
Consultant, Portugal
António G. Coelho
Consultant, Portugal
Luís R. Sousa
University of Porto, Portugal
Rui M. Correia
LNEC, Portugal
João Marcelino
LNEC, Portugal
António C. Mineiro
University of Lisbon, Portugal
António P. Cunha
LNEC, Portugal New
António G. Correia
University of Minho, Portugal
Carlos D. Gama
Lisbon Technical University, Portugal
José V. Lemos
LNEC, Portugal
Nuno Grossmann
LNEC, Portugal
Luís L. Lemos
University of Coimbra, Portugal
Ricardo Oliveira
COBA, Portugal

“Ad hoc” Reviewers (2015-2017)

Adilson do Lago Leite
UFOP, Brazil

Alexandre Duarte Gusmão
UPE, Brazil

Ana Cristina Seira
UERJ, Brazil

André Luis Brasil Cavalcante
UnB, Brazil

Antônio Roque
LNEC, Portugal

Antonio Thomé
UPF, Brazil

Antônio Topa Gomes
FEUP, Portugal

Armando Manuel Nunes Antão
Univ. Nova de Lisboa, Portugal

Arsenio Negro Jr.
Bureau, Brazil

Bengt Fellenius
Consultant, Canada

Bernadete Ragoni Danziger
UERJ, Brazil

Braja Das
California State Univ., USA

Carlos Medeiros Silva
Embre, Brazil

Celso Romanel
PUC-RJ, Brazil

Charles Shackelford
Colorado State Univ., USA

Claudio Fernando Mahler
UFRJ, Brazil

Claudio Michael Wolle
USP-Poli, Brazil

David Martins Geraldo Taborda
Imperial College, UK

Denise Gerscovich
UERJ, Brazil

Eda Quadros
BGTECH, Brazil

Edgar Odebrecht
Geoforma, Brazil

Edgard Poiate
Petrobrás, Brazil

Elizabeth Ritter
UERJ, Brazil

Ennio Marques Palmeira
UnB, Brazil

Euripedes Vargas
PUC-RJ, Brazil

Faiçal Massad
USP-Poli, Brazil

Fernando Antonio Medeiros Marinho
USP-Poli, Brazil

Fernando Olavo Franciss
Progeo, Brazil

Fernando Saboya
UENF, Brazil

Fidelis Suorineni
UNSW, Australia

Francisco Chagas da Silva Filho
UFC, Brazil

Francisco de Rezende Lopes
UFRJ, Brazil

Frederico Falconi
ZF, Brazil

Gisleine Coelho de Campos
IPT, Brazil

Giulliana Mondelli
UFABC, Brazil

Heraldo Luiz Giacheti
USP-S.Carlos, Brazil

Hossein Soltani-Jigheh
Azarbaijan Shahid Madani Univ., Iran

Isabel Lopes
IST, Portugal

João Manuel Marcelino Mateus da Silva
LNEC, Portugal

Jorge Augusto Pereira Ceratti
UFRGS, Brazil

José Camapum de Carvalho
UnB, Brazil

José Jorge Nader
USP-Poli, Brazil

José Renato Baptista de Lima
USP-Poli, Brazil

José Tadeu Balbo
USP-Poli, Brazil

Kátia Vanessa Bicalho
UFES, Brazil

Leonardo Becker
UFRJ, Brazil

Luís de Almeida Prado Bacellar
UFOP, Brazil

Luís Lemos
Univ. Coimbra, Portugal

Luís Ribeiro e Souza
FEUP, Portugal

Marc Vinches
Ecole des Mines d'Alès, France

Marcia Maria dos Anjos Mascarenhas
UFG, Brazil

Maria Cláudia Barbosa
UFRJ, Brazil

Maria de Lurdes Lopes
FEUP, Portugal

Maria Eugénia G. Boscov
USP-Poli, Brazil

Maurício Ehrlich
UFRJ, Brazil

Nelson Aoki
USP-S.Carlos, Brazil

Newton Moreira de Souza
UnB, Brazil

Nilo Cesar Consoli
UFRGS, Brazil

Nuno M. da Costa Guerra
Univ. Nova de Lisboa, Portugal

Paulo José Rocha Albuquerque
Unicamp, Brazil

Pedro Guedes de Melo
Consulgeo, Portugal

Pedro Sêco Pinto
Consultant, Portugal

Pérsio Leister de Almeida Barros
Unicamp, Brazil

Pierre Berest
Ecole Polytechnique, France

Renato Pinto da Cunha
UnB, Brazil

Sérgio A. Barreto da Fontoura
PUC-RJ, Brazil

Sussumu Niyama
Tecnum, Brazil

Tácio Mauro Pereira de Campos
PUC-RJ, Brazil

Terezinha Espósito
UFMG, Brazil

Thiago Luiz Coelho Morandini
CEFET-MG, Brazil

Tiago Miranda
Univ. do Minho, Portugal

Waldyr Lopes de Oliveira Filho
UFOP, Brazil

Werner Billfinger
Vector, Brazil

Soils and Rocks publishes papers in English in the broad fields of Geotechnical Engineering, Engineering Geology and Geoenvironmental Engineering. The Journal is published in April, August and December. Subscription price is US\$ 90.00 per year. The journal, with the name “Solos e Rochas”, was first published in 1978 by the Graduate School of Engineering, Federal University of Rio de Janeiro (COPPE-UFRJ). In 1980 it became the official magazine of the Brazilian Association for Soil Mechanics and Geotechnical Engineering (ABMS), acquiring the national character that had been the intention of its founders. In 1986 it also became the official Journal of the Brazilian Association for Engineering Geology and the Environment (ABGE) and in 1999 became the Latin American Geotechnical Journal, following the support of Latin-American representatives gathered for the Pan-American Conference of Guadalajara (1996). In 2007 the journal acquired the status of an international journal under the name of *Soils and Rocks*, published by the Brazilian Association for Soil Mechanics and Geotechnical Engineering (ABMS), Brazilian Association for Engineering Geology and the Environment (ABGE) and Portuguese Geotechnical Society (SPG). In 2010, ABGE decided to publish its own journal and left the partnership.

Soils and Rocks

1978,	1 (1, 2)
1979,	1 (3), 2 (1,2)
1980-1983,	3-6 (1, 2, 3)
1984,	7 (single number)
1985-1987,	8-10 (1, 2, 3)
1988-1990,	11-13 (single number)
1991-1992,	14-15 (1, 2)
1993,	16 (1, 2, 3, 4)
1994-2010,	17-33 (1, 2, 3)
2011,	34 (1, 2, 3, 4)
2012-2016,	35-39 (1, 2, 3)
2017,	40 (1,

ISSN 1980-9743

CDU 624.131.1

SOILS and ROCKS

An International Journal of Geotechnical and Geoenvironmental Engineering

Publication of**ABMS - Brazilian Association for Soil Mechanics and Geotechnical Engineering****SPG - Portuguese Geotechnical Society****Volume 40, N. 1, January-April 2017****Table of Contents**

ARTICLES

<i>A Microstructural Cam Clay Model for Hydro-Mechanical Behavior of Unsaturated Soils</i> M.P. Cordão Neto, B.C.F.L. Lopes, M.M.A. Mascarenha, E. Romero	3
<i>Pile Setup over a Period of Seven Years Based on Dynamic Load Tests in Overconsolidated Clay</i> L.B. Passini, L.B. Benetti, A.C.M. Kormann	17
<i>Study of the Shear Strength of a Tropical Soil with Grass Roots</i> M.I. Miranda Neto, C.F. Mahler	31
<i>Cavity Expansion Analysis to Predict Side Shear Set-Up in Clayey Soils</i> P.C.R. Silva, F. Massad	39
<i>Statistical Modeling of Municipal Solid Waste Settlement from a Lysimeter</i> C.L. Araújo Neto, B.M.A. Nóbrega, R.B.A. Sousa, M.C. Melo, W. Paiva, V.E.D. Monteiro	51
<i>An Evaluation of the Shaft Resistance of Piles Embedded in Gneissic Rock</i> E.L. Juvencio, F.R. Lopes, A.L.L.S. Nunes	61

Articles

Soils and Rocks
v. 40, n. 1

A Microstructural Cam Clay Model for Hydro-Mechanical Behavior of Unsaturated Soils

M.P. Cordão Neto, B.C.F.L. Lopes, M.M.A. Mascarenha, E. Romero

Abstract. In this paper, two new state variables are included in a conventional elastoplastic model, Modified Cam-clay, to incorporate the influence of pore size distribution changes in the mechanical behavior of unsaturated soils. The first state variable allows capturing the influence of large pore changes in the mechanical behavior, and is controlled by an evolution law that incorporates plastic volumetric strain. The second state variable is added to reproduce suction effects and the evolution of this variable is also controlled by plastic volumetric strain. The new approach is validated against a variety of experimental data of high porosity soils.

Keywords: high porosity soils, mechanical behavior, unsaturated soils, new state variables.

1. Introduction

Over the past decades, several constitutive models have been developed to reproduce the hydro-mechanical behavior of unsaturated soils. Alonso *et al.* (2010) state that nowadays, the development of constitutive models for unsaturated soils is tightly linked to the concept of effective stress. Indeed, the apparent success of this concept is also substantially connected to the fact that this effective stress takes into account the influence of the degree of saturation (Wheeler *et al.*, 2003) or effective degree of saturation (Alonso *et al.*, 2010).

On the other hand, some research trends aim at investigating the influence of the microstructure in the behavior of the soil; for instance: Prapaharan *et al.* (1985), Griffiths & Joshi (1989), Delage *et al.* (1996), Qi *et al.* (1996), Penumadu & Dean (2000), Simms & Yanful (2005), Cuisinier & Laloui (2004), Kong *et al.* (2005), Li & Zhang (2009), Tarantino & de Col (2008), Delage (2010), Romero *et al.* (2011), Munoz-Castelblanco *et al.* (2012) among others. This paper aims to advance this discussion.

Figure 1 presents the results of a collapsible and porous soil of Brasília, DF, Brazil (Silva, 2009). The figure illustrates some evidences of how loading and wetting can change the pore size density function (PSD). The PSD relates the log differential intrusion curve - obtained by mercury intrusion porosimetry- vs. entrance pore size D , which aids in the visual detection of the dominant pore modes. Results of three soil samples are presented: one as compacted on the dry side ($e = 1.16$), a second sample loaded at constant water content up to 800 kPa of vertical stress ($e = 0.98$), and the last one loaded at constant water content

up to 800 kPa followed by collapse induced by saturation ($e = 0.77$). It can be observed from Fig. 1 that both loading and collapse have an effect mostly in the largest pore sizes, which agrees with findings from Delage & Lefebvre (1984) and Griffiths & Joshi (1989). These authors reported that irreversible strains were caused by changes in the volume of the largest pores.

Based on the previous discussions, it can be concluded that any new constitutive model should take into account how the change in the fabric is affecting the mechanical response of the soil in terms of deformability and strength. This can be reached by introducing a new state variable associated with the soil fabric and the influence of large pore changes.

Probably, the best way to obtain this variable is by observing the evolutions of the PSD when it is subjected to different stress paths, *i.e.*, it is necessary to define a model that allows evaluating the changes that occur in the PSDs along different stress paths (Romero *et al.*, 2011). Figure 2 shows the evolution of the PSD when the soil is loaded and dried. It is clear that the PSD is differently affected by loading and suction changes. Moreover, the PSD of different soils is expected to have different responses.

Thus, this paper attempts to link the macroscopic behavior of the soil with its fabric by the introduction of two new state variables into a constitutive model. One of those variables is linked to the pore size distribution and the second one takes into account how the plastic volumetric strain affects the suction effect in the mechanical behavior. Those variables are used to adapt the Modified Cam-clay model to reproduce the behavior of unsaturated soils that present

Manoel Porfírio Cordão Neto, D.Sc., Professor Adjunto, Departamento de Engenharia Civil e Ambiental, Universidade de Brasília, 70910-900 Brasília, DF, Brasil. e-mail: mporfirio76@gmail.com.

Bruna de Carvalho Faria Lima Lopes, D.Sc., Research Associate, Department of Civil and Environmental Engineering, University of Strathclyde, Glasgow, United Kingdom. e-mail: bruna.lopes@strath.ac.uk.

Márcia Maria dos Anjos Mascarenha, D.Sc., Professora Adjunta, Escola de Engenharia Civil e Ambiental, Universidade Federal de Goiás, 74605-220 Goiânia, GO, Brazil. e-mail: marciamascarenha@gmail.com.

Enrique Romero, D.Sc., Director of Research, Departamento de Ingeniería del Terreno, Cartográfica e Geosférica, Universitat Politècnica de Catalunya, Campus Diagonal Nord, 08034 Barcelona, Spain. e-mail: enrique.romero-morales@upc.edu.

Submitted on January 7, 2016; Final Acceptance on February 10, 2017; Discussion open until August 31, 2017.

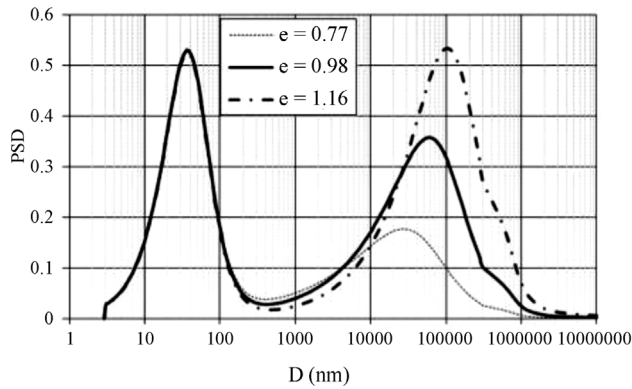


Figure 1 - Changes in pore size density functions of a collapsible soil (Silva, 2009).

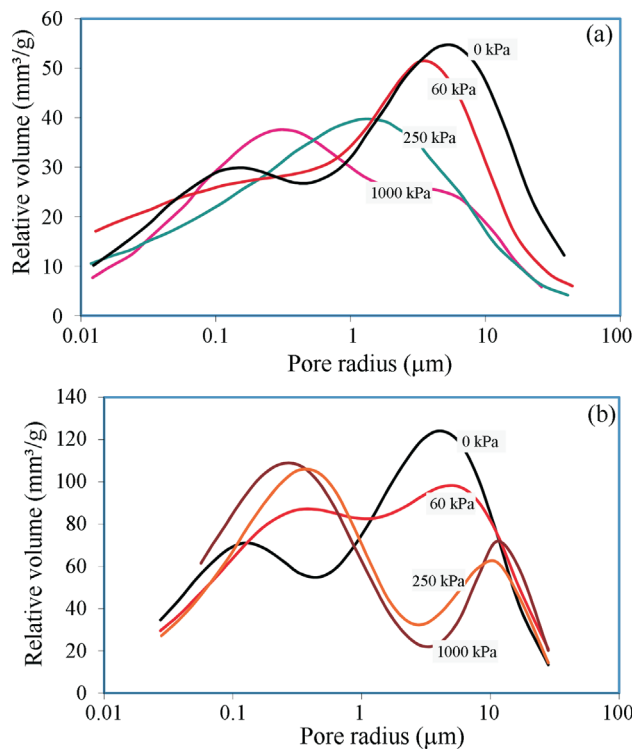


Figure 2 - Evolution of the PSDs as a result of (a) loading and (b) suction changes (after Cuisinier & Laloui, 2004).

strong changes in their fabric, for instance, natural and compacted soils that display two distinct levels of dominant pores (large and small pores).

2. New Model Concepts

2.1. Analyses of the mechanical behavior of soils using PSD

As mentioned previously, PSD analyses may be used in the modelling process to help understand the hydro-mechanical behavior of soils and also assist in defining new

state variables that provide a relationship between the macroscopic behavior and the microscopic response of the soil.

Figure 1 illustrates the case of a collapsible and highly porous soil, in which soil bonding effects are negligible. Thus, when analysing this graph it is possible to conclude that the region of the largest pores (macrofabric level) is easily destroyed when the soil is loaded and the smallest voids remain unchanged. A way to reproduce this hypothesis is to admit a superposition of effects between large pores and small pores, meaning:

$$d\varepsilon = d\varepsilon^L + d\varepsilon^S \quad (1)$$

where $d\varepsilon$ is the total strain or the strain measured in the laboratory, $d\varepsilon^L$ is the strain that occurs due to changes of the large pore volume (macrofabric level) and $d\varepsilon^S$ is the strain due to changes of the small pore volume (microfabric level). Considering that initially $d\varepsilon^L$ is much greater than $d\varepsilon^S$, the total strain may then be associated only with $d\varepsilon^L$. However, as the macrofabric level is reduced, strain in the microfabric level will start to gain significance and for larger loading levels it will be predominant. Hence, it is possible to associate the mechanical response of the soil with the pore size distribution. In the following sections, the concepts necessary to complete the definition of the new model introduced in this paper are presented.

2.2. Classical admissible state region

In order to understand the new concepts presented in this paper it is necessary to introduce the idea of admissible states. Figure 3 shows two classical examples: the Mohr-Coulomb envelope (on the left) and the surface of elastoplastic constitutive models (on the right). In the latter, the surface delimits both the elastic region and the admissible states of the soil, as once the stress path reaches the surface it has to keep on it, given that beyond the surface is the region of impossible states. In this plot, e is the void ratio and p' the mean effective stress.

In Fig. 3(b) a stress path can be seen where AB is elastic. If the condition of stress applied on the soil is such that it ends up in C' (an impossible state) the soil will be forced to rearrange its fabric leading it to C on the Normal Consolidated Line (NCL), which is the limit of admissible state in this space. This is a result of the inability of the soil fabric to sustain this stress state. Thereby, a rearrangement of the fabric occurs bringing the soil to a new state able to sustain the stress. This change is irreversible and it generates elastoplastic strains.

2.3. Intrinsic state

Some features of the soil such as anisotropy, suction, bonding and structural metastability modify the limit of admissible states of the soil, defined in the previous section. Although soils in their natural condition present some of those effects, it is possible to idealise a material with no alteration at all. This ideal state of the soil resembles the soil

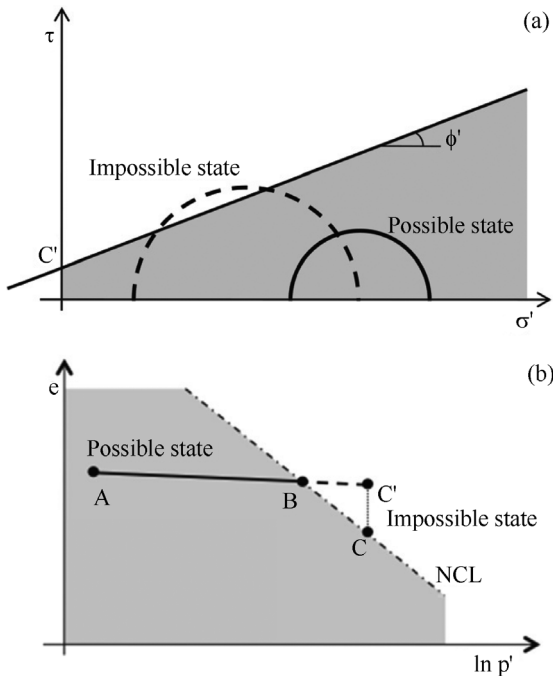


Figure 3 - Admissible state concept. (a) Mohr Coulomb envelope and (b) Void ratio (e): $\ln p'$ relationship - Elastoplastic models.

paste used to determine the liquid limit and is defined in this paper as the Intrinsic State. In this state the soil has the greatest possible void ratio, but it is still solid and without any additional effect.

If from that idealized state a loading path is drawn in the p' - e space, then the Normal Consolidated Line (NCL) will be renamed as the Intrinsic Consolidated Line (ICL) (Fig. 4). This line (ICL) is a function of compositional factors such as: type and shape of minerals, particles size distribution, mineral fractions, type of absorbed cations, pore water composition, and type and amount of other constituents such as organic matter, silica, alumina and iron oxides (Mitchell & Soga, 2005).

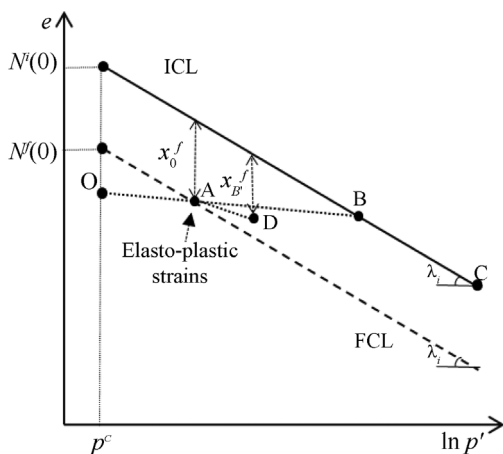


Figure 4 - Intrinsic and Fabric (non-intrinsic) consolidation lines.

The ICL can be determined by two terms. The first one is the void ratio of the sample as if it were in the paste condition used to determine its liquid limit, *i.e.*, $w(\%) = w^L$. This void ratio can be given by:

$$e^{w^L} = G_s w^L \quad (2)$$

where G_s is the specific gravity of the soil grains and w^L is the liquid limit. Besides the void ratio, the other term required is its slope. In this paper it is assumed to be given by λ^i . In section 3.1 a way to determine its value is presented.

2.4. Fabric effect

All features mentioned in the previous section change the domain of admissible states. As a result, the limit line for another condition incorporating one or more features does not correspond to the ICL. For all new features incorporated into the intrinsic state there will be a corresponding new limit line, which could reduce or increase the region of admissible states.

Figure 5 can help understand how the existing different pore levels could affect the soil behavior and the change in the admissible states. In the graph of Fig. 5, two samples of soils with an identical void ratio are shown, however with different pore size distributions. It is reasonable to as-

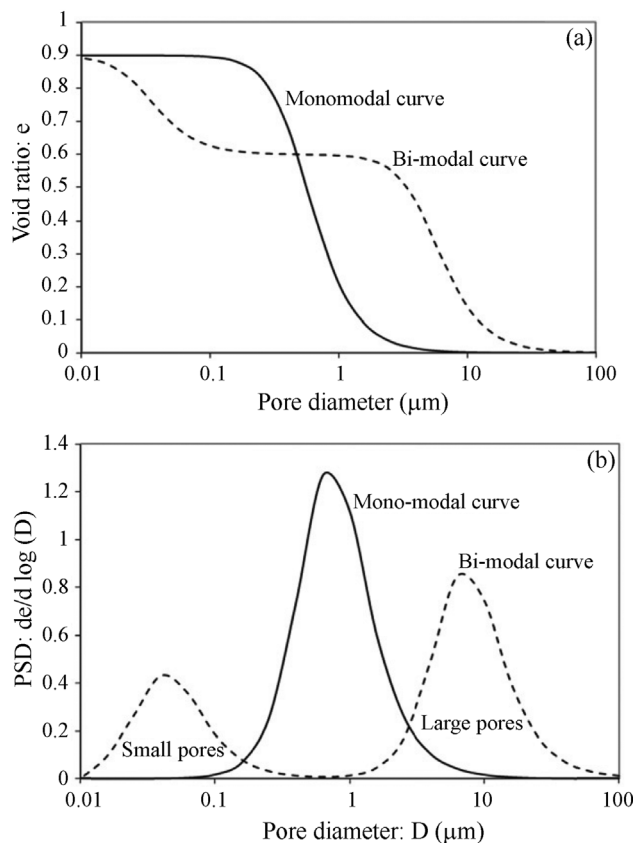


Figure 5 - Soils with an identical void ratio and different structures: (a) Cumulative pore size distribution curve; (b) pore size density function.

sume that the largest pores are more easily affected by a loading path than the smallest pores. Nevertheless, as the largest pores are being destroyed, both soils will tend to present similar behavior, as their pore size distribution curves will tend to be similar. This hypothesis was shown by Otálvaro (2013), Borges (2014) and Otálvaro *et al.* (2016).

Thus, the simplest fact that large pores exist reduces the area of admissible states, as shown in Fig. 4, which originates the new admissible line as a consequence of the fabric influence (FCL- Fabric Consolidated Line). The distance between the ICL and the FCL is defined as the state variable x^f .

This new variable is used to measure the influence of the macrofabric (largest pores) level in the mechanical response of the soil and as soon as plastic strains start to develop, x^f will gradually begin to degrade. Therefore, the mechanical response approaches the behavior of the soil in the intrinsic state. State variable, x^f , can be defined as:

$$x^f = e^{wL} - e^0 \quad (3)$$

where e^0 is the initial void ratio of the sample in the natural condition and e^{wL} is the void ratio of the sample in the intrinsic state, defined by Eq. 2.

Figure 4 shows the path OABC that represents a loading in a soil sample in the intrinsic state, where only elastic strains occur in OAB, and elastoplastic strains occur in BC. For double structure soils the elastic region will be reduced, and elastoplastic strains will start occurring at A. At this point, large porosity effect is maximum and associated with x_0^f . As shown in Fig. 4, when plastic strain occurs (path AD), x^f will gradually degrade according to its evolution law, given by:

$$x^f = x_0^f e^{(-a^f \varepsilon_v^p)} \quad (4)$$

where x^f is the new state variable associated with macrofabric level strain; x_0^f is the initial value of x^f ; a^f controls the absolute rate of degradation; and ε_v^p is the plastic volumetric strain. The effect of parameter a^f can be seen in Fig. 6. High values of a^f increase the degradation effect of the macrofabric level in the mechanic response of the soil while $a^f = 0$ brings the model to the conventional Modified Cam-Clay Model.

The plastic volumetric strains take place based on the ICL. Thus, it is necessary to project the current stress state point on the ICL and then plastic volumetric strain rates are given by:

$$d\varepsilon_v^p = \frac{\lambda^i - \kappa}{1 + e} \frac{dp_0^i}{p_0^i} \quad (5)$$

where $d\varepsilon_v^p$ is the plastic volumetric strain rate; λ^i is the slope of the ICL; κ is the slope of the elastic path; e is the void ratio; dp_0^i is the pre-consolidation stress rate in the ICL; and p_0^i is the projection of the pre-consolidation stress

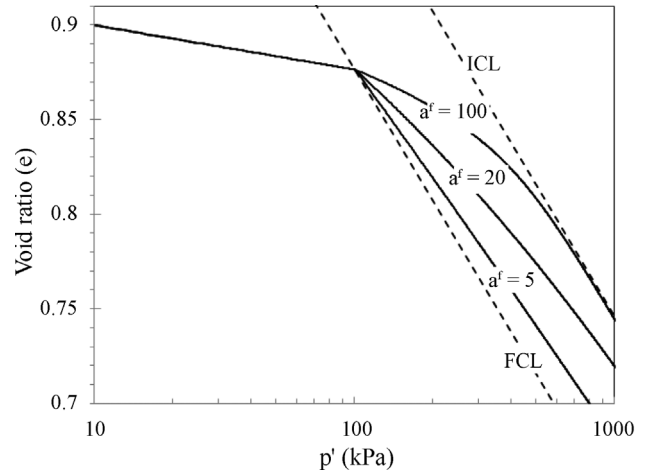


Figure 6 - Void ratio (e): $\ln p'$ relationship. Influence of parameter a^f on loading paths.

on the ICL. Finally, pre-consolidation stresses are calculated by:

$$p_0^s = p_0^i e^{\left(\frac{-x^f}{\lambda^i - \kappa}\right)} \quad (6)$$

where p_0^s is the pre-consolidation stress on the FCL, and x^f measures the influence of the double structure on soil behavior. In Fig. 4, p_0^s and p_0^i are the stress on the points A and B, respectively.

2.5. Suction effect

Suction effect shifts the limit of admissible states of the soil, amplifying its domain. This is due to the fact that suction effect increases soil capacity to sustain stresses without inducing plastic straining. As a result, the limit line for unsaturated soils (UCL) is shifted by x^s above the ICL which is a limit for fully saturated soils.

Figure 7 explains suction effect in the $p''-e$ space, where p'' represents the mean net stress. An unsaturated soil is loaded following elastic path DE, where point E is on the UCL. At this stage, x^s is the maximum and the region below UCL is elastic while above this line is a region of impossible states. From point E, elastoplastic strains start to occur on loading. Thus the UCL shifts towards the ICL and x^s will then be reduced originating path EF'. Therefore, the distance between UCL and ICL is reduced and consequently if a wetting path is applied to the soil, the resulting collapse will also be reduced. The pre-consolidated stress for both conditions, saturated and unsaturated, is defined by p_0^* and p_0 , and these variables are used to define ICL and UCL.

State variable x^s will gradually degrade as plastic strains occur, in the same way as it occurs for x^f , and following an equivalent evolution law given by:

$$x^s = x_0^s e^{(-a^s \varepsilon_v^p)} \quad (7)$$

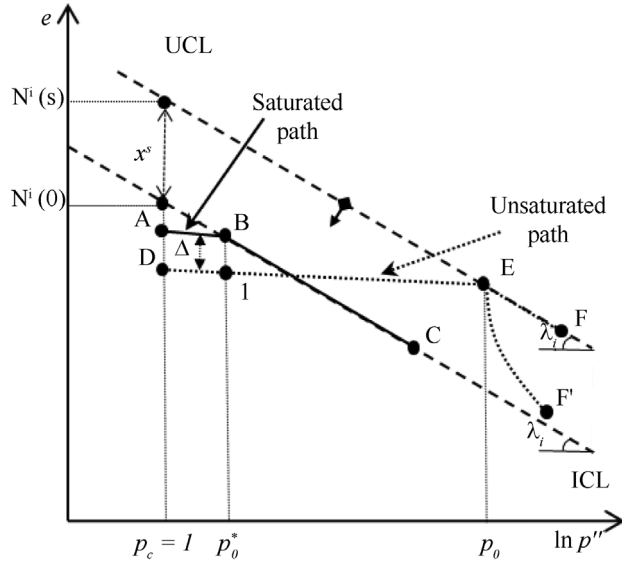


Figure 7 - Void ratio (e) : $\ln p''$ curve - unsaturated and saturated limits.

where x^s is the suction effect on the soil; x_0^s is its initial value; a^s controls the absolute rate of suction degradation; and $\varepsilon_v^p x$ is the plastic volumetric strain. The effect of parameter a^s can be seen in Fig. 8.

Figure 7 shows two different stress paths followed by the same soil under saturated and unsaturated conditions. It can be observed that due to the expansion of the soil the initial void ratio of the saturated soil is greater than in the case of the unsaturated soil (the difference being equal to Δ). Although both elastic stress paths have the same slope (κ), unsaturated soil starts yielding at a greater stress value, point E, compared to the stress value for the soil in the saturated condition, point B.

The physical meaning of suction effect degradation can be understood as a reduction of suction influence on

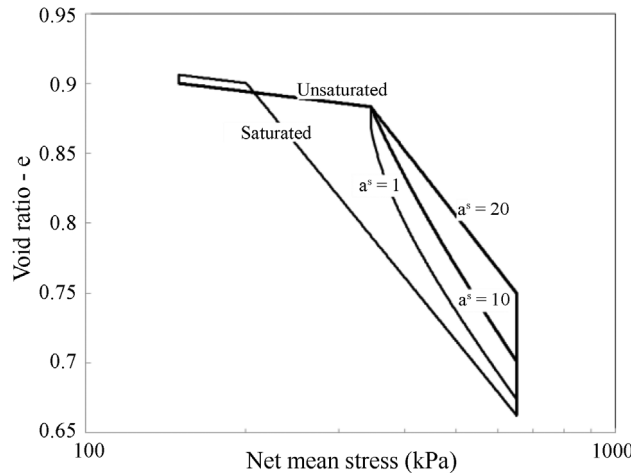


Figure 8 - Influence of a^s parameter along unsaturated loading paths.

compression in the global stiffness of the soil (on loading at constant suction, the degree of saturation increases and affects soil compressibility). This effect is in agreement with models that use Bishop's stress as a state variable, such as Wheeler *et al.* (2003), Sheng *et al.* (2004), Alonso *et al.* (2010) and Della Vecchia *et al.* (2013).

From Fig. 7, it is also possible to obtain the relationship between saturated and unsaturated pre-consolidation stresses, *i.e.*, the Loading Collapse curve (LC), as follows. The void ratio when mean net stress is p_c on the ICL is given by:

$$N^i(0) = e_1 + \Delta + \lambda^i \ln \left(\frac{p_0^s(0)}{p^c} \right) \quad (8)$$

where $N^i(0)$ is the void ratio when the mean net stress is p_c on the ICL; e_1 is the void ratio at point 1; Δ is the difference between the saturated and unsaturated initial void ratios for a suction unloading (wetting) in the elastic domain; p_0^s is the pre-consolidation stress for the saturated path; and p^c is a reference mean net stress, in this case 1 kPa. Similarly, the value of void ratio when the mean net stress is p^c on the UCL is given by:

$$N^i(s) = e_1 - \kappa \ln \left(\frac{p_0^i(s)}{p_0^i(0)} \right) + \lambda^i \ln \left(\frac{p_0^i(s)}{p^c} \right) \quad (9)$$

where $N^i(s)$ is the void ratio when the mean stress is p_c on the UCL; κ is the slope of the elastic path; and $p_0^i(s)$ is the pre-consolidation stress for the unsaturated path. Suction effect (x^s) is given by:

$$x^s = N^i(s) - N^i(0) \quad (10)$$

Thus, x^s can be rewritten as:

$$x^s = -\Delta + (\lambda^i - \kappa) \ln \left(\frac{p_0^i(s)}{p_0^i(0)} \right) \quad (11)$$

and the Loading Collapse (LC) equation can be given by:

$$p_0^i(s) = p_0^i(0) e^{\left(\frac{\Delta + x^s}{\lambda^i - \kappa} \right)} \quad (12)$$

where $p_0^i(s)$ is the mean net stress on the UCL, and $p_0^i(0)$ is the mean net stress on the ICL. Similarly to what has been indicated for the state variable, x^f , the authors consider that x^s could also be described through analysis of the PSD curve. However, in the absence of more experimental data, x^s is described as follows:

$$x^s = 1 - \left[(1-r)e^{-\beta s} + r \right] \quad (13)$$

where x^s is the suction effect degradation; s is suction; β and r are parameters similar to BBM parameters (Alonso *et al.*, 1990).

For moderately expansive soils, Δ can be calculated according to Alonso *et al.* (1990), as follows:

$$\Delta = \kappa_s \ln \left(\frac{s + p_{atm}}{p_{atm}} \right) \quad (14)$$

where p_{atm} is the atmospheric pressure, s is suction, κ_s is the slope on the wetting path in the elastic region. The relationship presented in Eq. 14 is valid on the elastic region for wetting and drying paths only.

The analysis of Eq. 14 allows a better interpretation of Δ and x^s parameters, which control the mechanical response of the model under unsaturated conditions. While x^s is affected by plastic volumetric strains (Eq. 7) and suction variations (Eq. 13), parameter Δ is affected solely by suction variations (Eq. 14).

It is important to point out that Δ can be described by any law that allows reproducing the volume changes that occur due to wetting and drying stress paths for expansive soils. In case these variations result in plastic strains, they will be taken into account through updates of x^s and x^f state variables.

2.6. Fabric and suction coupling effects

In general, both effects mentioned previously appear combined in natural and compacted soils. As a result, limit states that were described separately above are now combined: the fabric (large and small pores) and suction effects. In Fig. 9 UFCL is a limit line that combines suction effect (x^s), responsible for the elastic domain expansion, and the fabric effect (x^f) that reduces it. It is also important to highlight that both effects are degraded through plastic straining, which means that as plastic volumetric strains develop, x^s and x^f will be gradually destroyed.

Hypothetical stress paths have been drawn in Fig. 9 to explain the behavior of a soil that presents both high porosity and suction effects. Path OA is elastic and A is the yield-

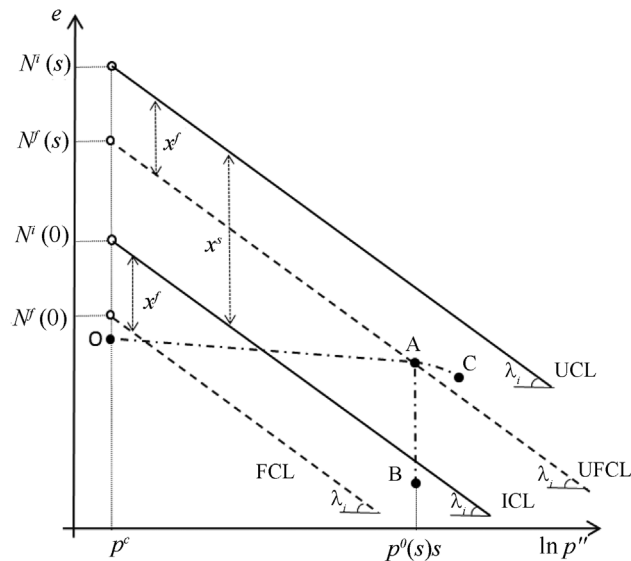


Figure 9 - Void ratio (e) : $\ln p'''$ relationship - limits (fabric and suction effects).

ing point. If the soil sample is wetted, it follows path AB, indicating volumetric collapse. In this case, not only a reduction of suction effect is expected, but also destruction of the initial fabric of the soil. This results in the displacement of FCL towards the ICL. The new position of FCL can be calculated through the evaluation of plastic volumetric strains according to Eq. 4.

On the other hand, if the soil was loaded at constant suction from point A, the stress path would follow path AC, tending towards the UCL. This happens because the distance between UFCL and UCL reduces as plastic strains occur and x^f degrades. However, besides degradation of the fabric effect, the suction effect is also degraded. Therefore, it could be observed that the path followed will depend on the values of d^f and a^s , which control the velocity of degradation effects of the fabric and suction, respectively.

2.7. Model formulation

The yield surface proposed for the new model is similar to the one presented by Alonso *et al.* (1990) to define the Barcelona Basic Model. It is described by the following equations:

$$f^1(p, q, s, \varepsilon^p) = q^2 - M^2(p_0^s(s) - p)(p + p^s) = 0 \quad (15)$$

$$f^2(p, q, s, \varepsilon^p) = (s^i - s) = 0 \quad (16)$$

$$p_0^s(s) = p_0^s(0) e^{\left(\frac{\Delta + x^s}{\lambda^i - \kappa} \right)} \quad (17)$$

$$p^s = \kappa^c s \quad (18)$$

$$x^s = 1 - \left[(1-r)e^{-\beta s} + r \right] \quad (19)$$

where p , q and s are the stress state variables; ε^p is the vector of plastic strain; s^i is the suction increase yield locus; $p_0^i(0)$ is the pre-consolidation stress for saturated condition soil; λ^i and κ are the slopes of the Intrinsic Consolidation Line and Unloading Line; κ^c is the rate of cohesion increase with suction; and finally β and r are parameters related to suction effects on the LC yield locus (Eq. 17, which is equivalent to Eq. 12). In this work, the formulation presented will not take into account suction paths that go beyond s^i (Eq. 16).

Figure 10 presents a 3D view of the yield surface under saturated conditions in the $p''-q-e$ space, in which it is possible to observe the effects induced by state variable x^f . In this figure, the Intrinsic Critical State Line (ICSL) and the Fabric Critical State Line (FCSL) are presented. Both lines tend to converge as x^f is degraded, in the same way as it happens with ICL and FCL.

Hardening laws are defined relating plastic volumetric strain to the size of the yield surface. They can be expressed as follows:

$$\frac{dp_0^i}{d\varepsilon_v^p} = \frac{1+e}{\lambda^i - \kappa} p_0^i \quad (20)$$

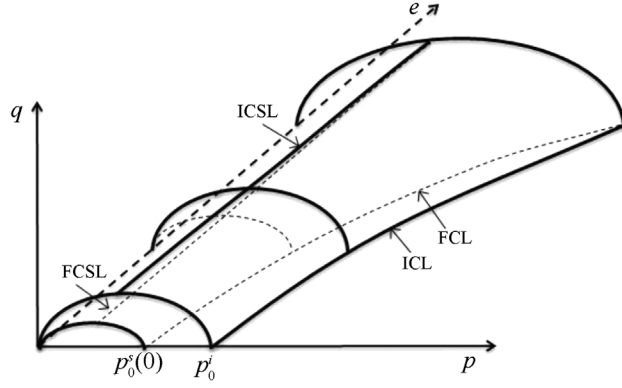


Figure 10 - Yield surface for saturated conditions.

$$p_0^i = p_0^s(0) e^{\left(\frac{x^f}{\lambda^i - \kappa}\right)} \quad (21)$$

$$\frac{dx^f}{d\varepsilon_v^p} = -a^f x^f \quad (22)$$

$$\frac{ds^f}{d\varepsilon_v^p} = -a^s x^s \quad (23)$$

All variables and parameters presented in Eq. 21 to 23 have been defined previously, except for p_0^i which is the projection of the pre-consolidation stress $p_0^s(0)$ on the ICL at constant void ratio (refer also to Eq. 6). This allows isolating plastic strain effects that occur at the microfabric level ($\frac{dp_0^i}{d\varepsilon_v^p}$), at the macrofabric level ($\frac{dx^f}{d\varepsilon_v^p}$) and the strains associated with suction variations ($\frac{ds^f}{d\varepsilon_v^p}$). This translates the natural coupling between these three effects and can be materialised in the following expression:

$$d\varepsilon_v^p = \frac{\lambda^i - \kappa}{1 + e} \frac{dp_0^i}{p_0^i} - \left(\frac{1}{a^f x^f} dx^f + \frac{1}{a^s x^s} ds^s \right) \quad (24)$$

The new model considers associated flow rule, and then plastic strain can be determined by:

$$d\varepsilon_v^p = \Lambda \frac{\partial f^1}{\partial \sigma_i} \quad (25)$$

where Λ is the plastic multiplier which is calculated as:

$$\Lambda = \frac{-a_i d\sigma_i}{Y} + \frac{-cds}{Y} \quad (26)$$

or

$$\Lambda = \frac{a_i D_{kl} d\varepsilon_k}{a_m D_{nm} b_n - Y} + \frac{(c - a_i D_{kl} H_k) ds}{a_m D_{nm} b_n - Y} \quad (27)$$

where $a_i = \frac{\partial f^1}{\partial \sigma_i}$, $b_i = \frac{\partial g^1}{\partial \sigma_i}$ and $c = \frac{\partial f^1}{\partial s}$.

Terms a_i and b_i are easily determined, since they are similar to those terms of other constitutive models, such as BBM (Alonso *et al.*, 1990), but here the associated flow, *i.e.*, the $f^1 \equiv g^1$ is assumed. On the other hand, $c = \frac{\partial f^1}{\partial s}$ requires more attention, since its derivative depends on other terms:

$$c = \frac{\partial f^1}{\partial s} = \frac{\partial f^1}{\partial p_0^s(s)} \frac{\partial p_0^s(s)}{\partial x^s} \frac{\partial x^s}{\partial s} + \frac{\partial f^1}{\partial p_0^s(s)} \frac{\partial p_0^s(s)}{\partial \Delta} \frac{\partial \Delta}{\partial s} + \frac{\partial f^1}{\partial p^s} \frac{\partial p^s}{\partial s} \quad (28)$$

The term Y that appears in Eqs. 26 and 27, represents hardening and can be expressed as follows:

$$Y = \left(\frac{\partial g^1}{\partial \sigma_x} + \frac{\partial g^1}{\partial \sigma_y} + \frac{\partial g^1}{\partial \sigma_z} \right) \left(\frac{\partial f^1}{\partial p_0^s(s)} \frac{\partial p_0^s(s)}{\partial p_0^s(0)} \frac{\partial p_0^s(0)}{\partial p_0^i} \frac{\partial p_0^i}{\partial \varepsilon_v^p} \right) + \left(\frac{\partial f^1}{\partial p_0^s(s)} \frac{\partial p_0^s(s)}{\partial x^s} \frac{\partial x^s}{\partial \varepsilon_v^p} + \frac{\partial f^1}{\partial p_0^s(s)} \frac{\partial p_0^s(s)}{\partial p_0^s(0)} \frac{\partial p_0^s(0)}{\partial x^f} \frac{\partial x^f}{\partial \varepsilon_v^p} \right) \quad (29)$$

where all terms can be determined through Eqs. 6 and 13 to 23.

In the next section the model validation will be presented, which was accomplished through simulations of isotropic and oedometer stress paths. The model results were then compared to experimental test results.

3. Model Validation

To demonstrate the model capability, simulations results from different soils, where two of them were sampled at natural conditions, will be presented in the paper. In an initial stage, simulation results will be dealing with saturated soils. Then, unsaturated soil features will be addressed.

3.1. Saturated soil modelling

Table 1 presents different soils and their main properties are indicated, as well as the parameters used for the saturated modelling. Some details on the choice of parameters is presented in the following.

The first variable to be discussed is the pre-consolidation stress. When analysing this variable, it should be remarked that most of the values presented in Table 1 are somewhat lower than the values used in the original studies (see references in the table). It is worth mentioning that in this paper, pre-consolidation stress is defined as the stress from which the soil no longer has linear-logarithm behavior with κ slope, which differs from other criteria, as presented by Cui & Delage (1996), where pre-consolidation stress values are defined from the intersection of the extension lines with κ and λ slopes.

Parameter κ is defined in the same way as most constitutive models, where it represents the elastic slope determined as:

Table 1 - Parameters for saturated soils.

Soil	x^f	a^f	λ	κ	$p_{(0)}$ (kPa)	w^l (%)	PI (%)	G_s
Cataluña Silty Clay ⁽¹⁾	0.10	15	0.115	0.006	50	22	7	2.70
Pereira Barreto Clayey Sand ⁽²⁾	0.46	15	0.200	0.008	20	22	< 10	2.69
Brasilia Clay ⁽³⁾	0.40	10	0.250	0.003	30	26	10	2.74
Residual silty sand derived from gneiss ⁽⁴⁾	0.06	15	0.112	0.006	40	31	12	2.64

⁽¹⁾Mascarenha (2008), ⁽²⁾Rodrigues (2007), ⁽³⁾Silva (2009), ⁽⁴⁾Pereira (1996).

$$\kappa = \frac{e_i - e_0}{\ln \frac{\sigma_0}{\sigma_i}} \quad (30)$$

where σ_i and σ_0 vertical net stresses and e_i and e_0 void ratios are defined in the elastic line under oedometer conditions. Parameter λ^i is defined as the slope of the elastoplastic (intrinsic) line, given by the following expression:

$$\lambda^i = e_i - e_0 \ln \frac{\sigma_0}{\sigma_i} \quad (31)$$

where σ_i and σ_0 vertical net stresses and e_i and e_0 void ratios are defined in the region where all the high porosity effect has been already destroyed, *i.e.* $x^f = 0$, which differentiates the new model from others. However, none of the test results used in this paper were defined to reach such a condition, therefore there is no clear evidence that the final portion of loading stage is in this condition. Figure 11(a) present λ^i values used in the simulations (λ (model) in the figure) and the values obtained from the portion where it is believed x^f is close to 0, which corresponds to the highest vertical stresses of the tests (λ (data) in the figure). In general, values used in the simulations are larger than experimentally determined values.

Variable x^f can be obtained from Eq. 3. Due to the high variability of liquid limit values (w^l) it is necessary to slightly adjust the values obtained from Eq. 3. Figure 11 (b) shows good agreement between values estimated from Eq. 3 (x^f (data) in the figure) and values used in the simulations to obtain best fit (x^f (model) in the figure).

On the other hand, parameter a^f controls the rate at which the high porosity effect is destroyed due to plastic volumetric straining. Eq. 4 is used to obtain a^f , where at least two points of x^f are required. The initial value of x^f is known. Besides this, it is also possible to estimate its final value that corresponds to the difference between the void ratio of the sample and the void ratio on the ICL at high vertical net stresses. Plastic strains are also known, since an unloading path is usually carried out. Even using test data that were not specifically performed for the proposed model calibration, it was possible to obtain a good agreement as presented in Fig. 12. In this figure, the FCL and ICL lines of each soil considered are also plotted. The results presented in this work are a clearly better fit that the

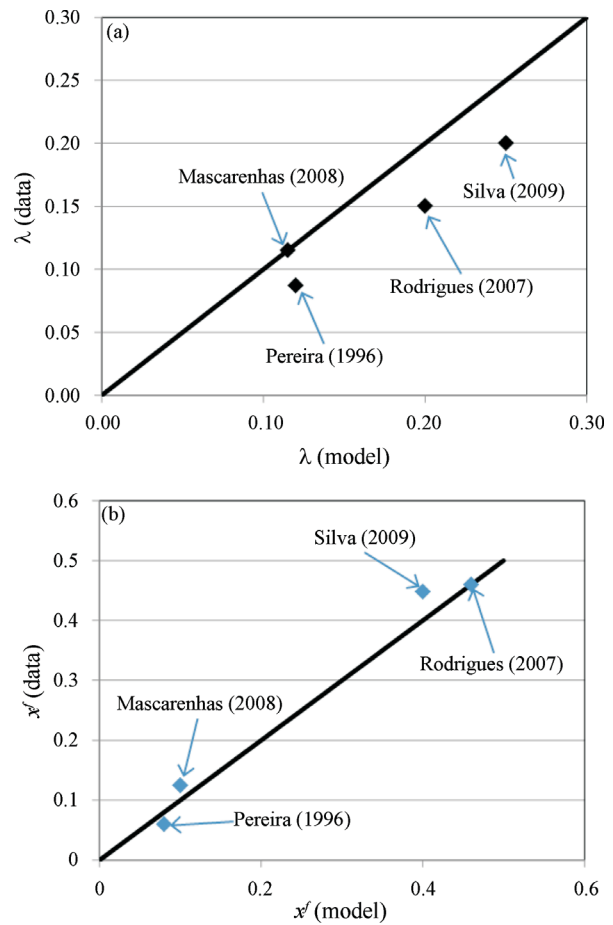


Figure 11 - λ^i and x^f calculated from experimental data and values used in the simulations.

ones presented by Pereira (1996), Mascarenha (2008) and Silva (2009), the original sources of data, where Nonlinear Elastic models (Pereira, 1996) and Modify Cam-clay models (Mascarenha, 2008 and Silva, 2009) were used.

In the case of the Brasilia Clay (Fig. 12(d)), it is possible to note that x^f is nearly zero, which corresponds to a total destruction of the largest pores, as indicated in Fig. 1.

3.2. Unsaturated soil modelling

3.2.1. Theoretical case

Although the hypotheses used in the new model are different from the ones used in BBM (Alonso *et al.*, 1990),

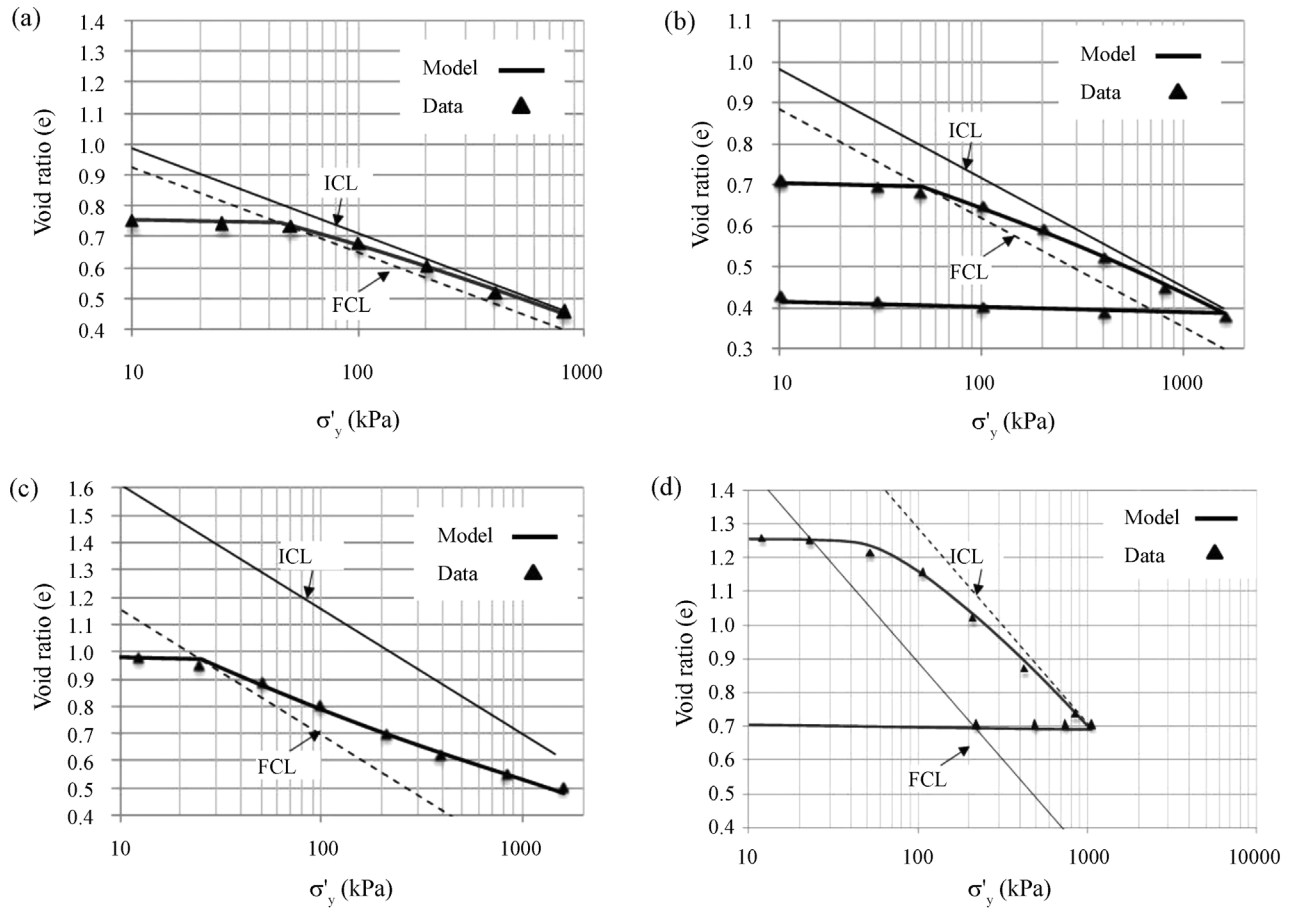


Figure 12 - Simulation results of saturated oedometer paths. (a) Residual silty sand derived from gneiss - Pereira (1996); (b) Cataluña Silty Clay - Mascarenha (2008); (c) Residual silty sand derived from gneiss - Rodrigues (2007); and (d) Brasília Clay - Silva (2009).

the new model is able to reproduce, with some agreement, the results foreseen by BBM. Therefore, the first results presented in this section will be a comparison between the behavior foreseen by the new model and BBM.

Parameters used in BBM simulations are the same presented in Alonso *et al.* (1990) and they are summarised in Table 2 along with the parameters used in the new model. Parameters λ^i and κ are assumed to display the same values as the ones proposed by Alonso *et al.* (1990). This means that λ^i can be considered the slope of ICL, since BBM is an extension of Modified Cam Clay. Variables ($p_0^s(0)$ and x_0^f) and a^f parameter were determined to obtain best fit results along a saturated path.

Parameters r and β were obtained so that a best fit between LC curves of the new model and BBM were reached. Figure 13 shows a comparison between both LC curves. It is also possible to observe the high porosity effect in the curve, which corresponds to a drastic reduction of the pre-consolidation stress in the low suction range. In this case, it was compensated for by an increase of parameters β and r with respect to BBM values indicated in Table 2.

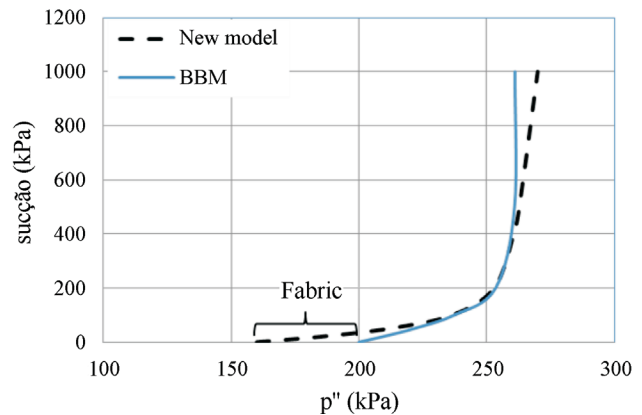


Figure 13 - LC curves of BBM and New Model.

In Fig. 14 comparative results are presented for both saturated and unsaturated conditions, where the unsaturated paths considered were associated with an isotropic loading at constant suction $s = 200$ kPa, followed by saturation inducing volumetric collapse. The saturated path considered is a loading path starting from the same initial void ratio.

Table 2 - Parameters used in the new model.

	λ^i	κ	$p_0^s(0)$ kPa	p^c (kPa)	r	β (MPa)	x_0^f	a^f	a^s	κ^s
BBM	0.2	0.02	200	100	0.75	12.5	-	-	-	0.008
New model	0.2	0.02	160	-	0.923	20	0.04	50	1.5 (10)*	0.008

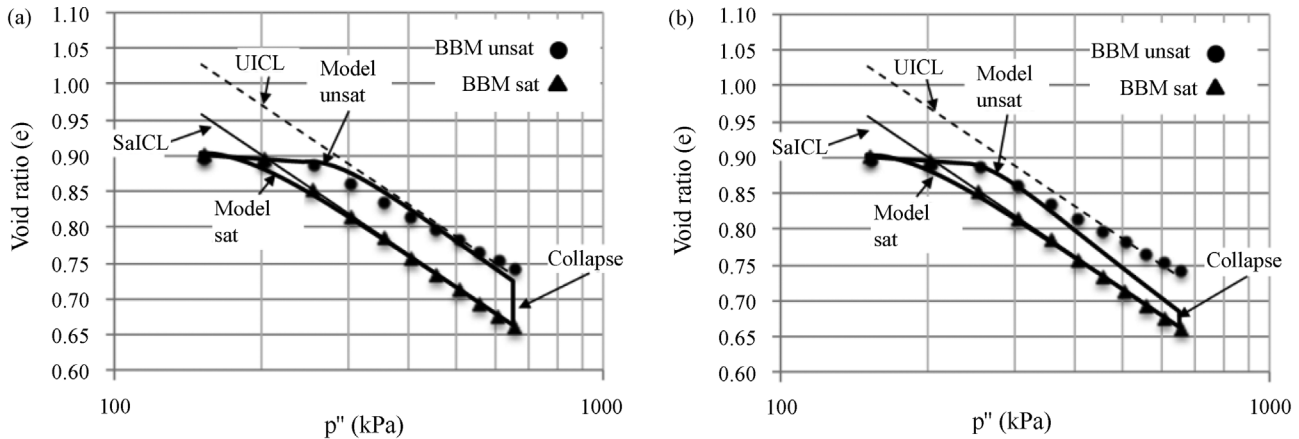


Figure 14 - Comparison between results of the new model and BBM: (a) Low velocity of suction degradation ($a^s = 1.5$). (b) High velocity of suction degradation ($a^s = 10$).

It is important to remark some aspects reproduced by the new model. First, the smooth transition that is observed between the elastic and intrinsic segments, which occurs during the degradation of the high porosity effect. A second point to be highlighted is the degradation of the suction effect (associated with the increase in degree of saturation as a consequence of loading at constant suction). This degradation results in a progressive approach between the saturated and unsaturated curves as plastic straining is induced. The velocity associated with this process is controlled by parameter a^s that also affects the collapsible response. This may be visualized through comparisons between Fig. 14(a) and (b), in which low suction degradation effects on compressibility ($a^s = 1.5$) are compared to higher degradation effects ($a^s = 10$). Finally, it is possible to observe that even with all other parameters kept constant, collapse value is significantly reduced when comparing both model results. In addition, it allows simulating a maximum collapse at intermediate vertical stresses (Fig. 14(b)).

3.2.2. Loading and wetting stress paths

In this section, loading and wetting results will be presented for compacted (Pereira, 1996) and natural (Mascarenha, 2008) soils. Table 3 presents the calibration of parameters obtained for Pereira (1996) and Mascarenha (2008) tests.

In general, the new model was able to adequately reproduce soil responses for different stress paths. Simulation results of Pereira (1996) data are presented in Fig. 15(a). It shows an oedometer path with application of vertical stress up to 400 kPa, followed by saturation and more application of vertical stress up to 800 kPa. The new model is able to reproduce precisely this path (an oedometer saturated path has already been presented in Fig. 12(a)).

Figure 15(b) presents the results of suction reduction paths under isotropic loading conditions at different mean net stresses. All samples started at the same initial suction ($s = 370$ kPa). The new model was able to satisfactorily reproduce collapse variation associated with different soil

Table 3 - Parameters calibrated for compacted and natural soils.

Soil	λ^i	κ	$p_0^s(0)$ (kPa)	r	β (MPa)	x_0^f	a^f	a^s	κ^s
Cataluña Silty Clay ⁽¹⁾	0.115	0.006	50	0.75	0.13	0.10	15	6	0.008
Residual silty sand derived from gneiss ⁽²⁾	0.12	0.006	40	0.75	8.0	0.06	15	2	0.0

⁽¹⁾Mascarenha (2008), ⁽²⁾Pereira (1996).

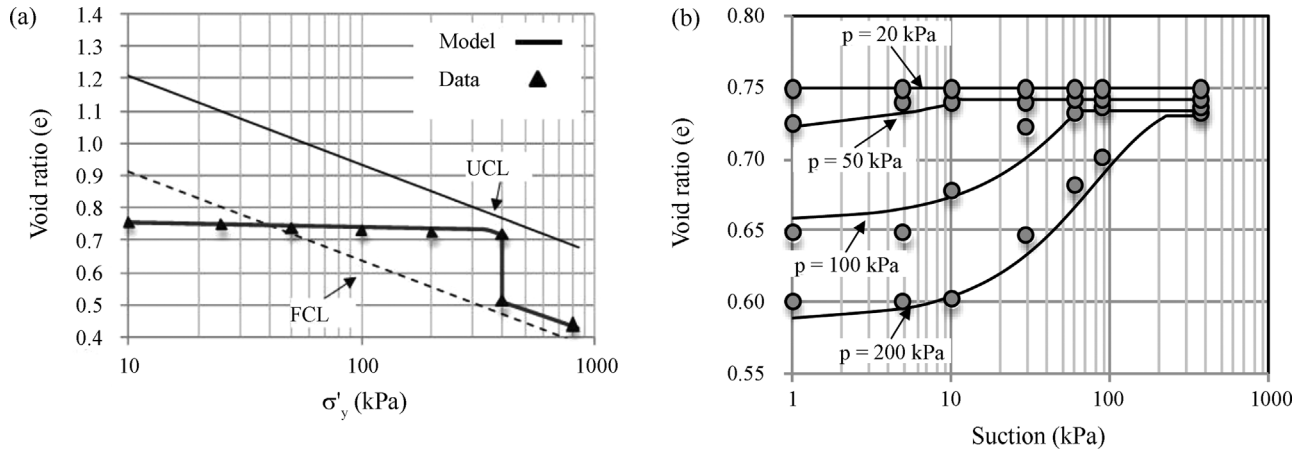


Figure 15 - Pereira test simulations. (a) Loading and wetting paths (b) Wetting paths at different net mean stresses.

stress states (different final suctions at different mean net stresses).

In Fig. 16 it is possible to observe the LC curve for the final condition of the wetting test at constant $p = 200$ kPa. In the same figure, the LC associated with BBM is shown (Farias & Cordão-Neto, 2010). There is a significant difference between both LC curves. This is due to the fact that while for BBM the LC curve depends exclusively on suction, in the new model the LC curve depends on suction and plastic volumetric strains which affect state variables x^i and x^s . If state parameter x^s is strongly affected by plastic strains ($a^s = 10$), then suction, as a consequence, will have less influence on soil behavior.

Two unsaturated stress paths reported by Mascarenha (2008) on a natural high-porosity soil were also used to perform simulations. In both tests, vertical net stress was increased up to 800 kPa (in these paths suction was kept constant, at 50 kPa and 400 kPa, respectively), followed by suction reduction until saturation. From this point on, tests followed the paths indicated in Fig. 17(a) and (b). The new model was able to adequately replicate soil behavior, in-

cluding the volumetric collapse starting from different initial suctions (50 kPa and 400 kPa).

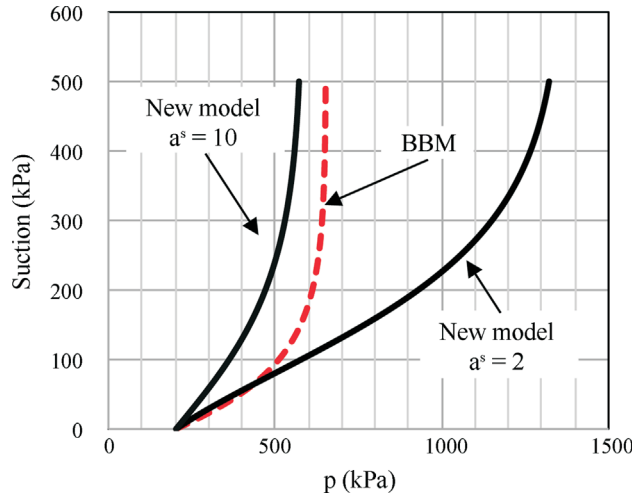


Figure 16 - Wetting test simulation for constant mean net stress $p = 200$ kPa. Comparison between final LC curves, taking into account different a^s values.

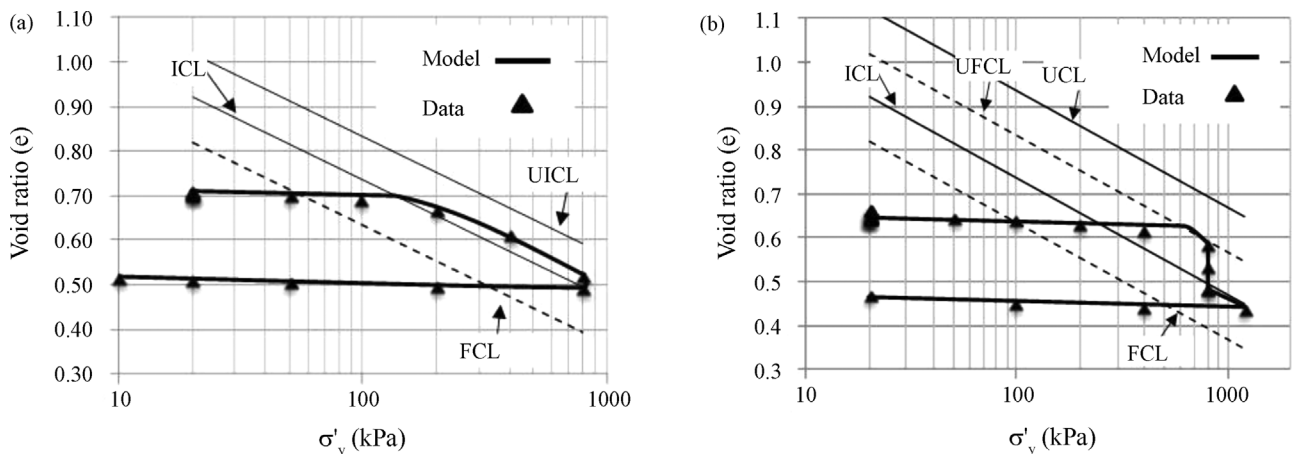


Figure 17 - Mascarenha (2008) test simulations. Reproduction of collapse paths. (a) $s = 50$ kPa; (b) $s = 400$ kPa.

In Fig. 17 it is possible to observe that after saturation the soil is close to the ICL, which means x' is small. Figure 18 displays the evolution of the PSDs of the soil starting from natural conditions ($e = 0.71$) and after being loaded to 800 kPa at constant water content followed by wetting ($e = 0.53$).

As observed, there is a significant change in the pore size distribution, particularly in the region with pore diameters greater than 10,000 nm. Although the resulting PSD is still a bimodal curve, it is possible to observe that the loading tends to convert the bimodal curve into a unimodal one, which is the hypothesis assumed by the model in this paper. Loading and wetting induce an important reduction in the macropore volume, as well as shifting towards smaller values of the dominant macropore size. On the other hand, wetting induces some swelling of micropore volume (a new mode emerges in this micropore volume domain at a dominant pore size around 200 nm).

4. Conclusions

In this paper, a new constitutive model for unsaturated high-porosity soils is proposed, which incorporates two new state variables. These state variables have an important impact on the mechanical response of the soil and are associated with soil fabric (macropore volume that reduces on loading and wetting) and with suction. In order to introduce the model, fundamental aspects of intrinsic and admissible states of soils are first presented, together with pore size distribution changes along loading and wetting (collapse) paths.

The state variables are ruled by plastic volumetric strain. This allows capturing the influence on mechanical behavior of suction effects together with large pore changes (fabric effects) and degree of saturation changes (as a consequence of plastic straining). For example, during loading at constant suction the soil reaches a maximum collapse capability on wetting at an intermediate stress state. This is a consequence of the increase in stress (which increases col-

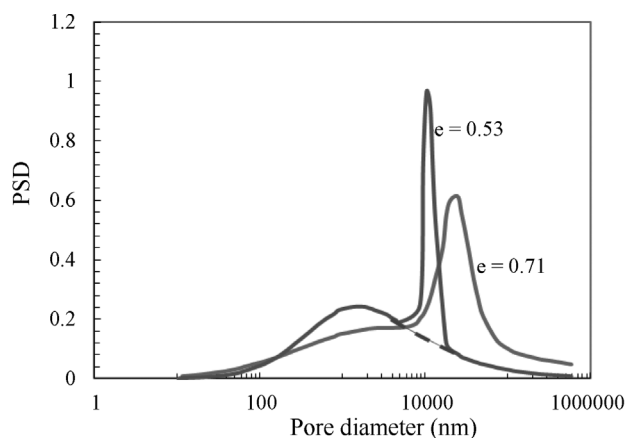


Figure 18 - Evolution of pore size density functions (after Mascarenha, 2008).

lapse), and, on the other hand, to an opposite effect that increases degree of saturation and thus reduces the capability to collapse. Simultaneously tackling these effects (high porosity and suction) together with the evolution of plastic volumetric straining, enables a better reproduction of the behavioral features of high-porosity saturated and unsaturated soils.

The paper presented the model formulation together with the stress-strain relationships. Generally speaking, the model did not lose any of the predecessor's characteristics (such as BBM, Alonso *et al.*, 1990) and new ones were incorporated to enable better capacity to reproduce several aspects of soil behavior. Moreover, additional information associated with high porosity was incorporated in the Cam-clay model and BBM. This new information helps obtain some characteristics that are not captured in conventional models, such as smooth transition between pre- and normally consolidated locus.

As for the next steps, the authors consider that the model could be expanded, with little modifications, to expansive soils, and that state variables related to soil fabric could be directly obtained from the pore size distribution analysis. This way, it is expected that the macroscopic response of the soil could be better described through its microscopic behavior.

Acknowledgments

The authors also acknowledge the support provided by the European Commission by Marie Curie IRSES project GREAT (FP7-PEOPLE-2013-IRSES-612665).

References

- Alonso, E.E.; Gens, A. & Josa, A. (1990). A constitutive model for partially saturated soils. *Géotechnique*, 40(3):405-430.
- Alonso, E.E.; Pereira, J.M.; Vaunat, J. & Olivella, S. (2010). A microstructurally based effective stress for unsaturated soils. *Géotechnique*, 60(12):913-925.
- Borges, C.R. (2014). *Estudo Microestrutural do Comportamento Hidromecânico do Solo de Brasília-DF*. Tese de Doutorado, Universidade de Brasília, Brasília, 112 p.
- Cui, Y.J. & Delage, P. (1996). Yielding and plastic behavior of an unsaturated compacted silt. *Géotechnique*, 46(2):291-311.
- Cuisinier, O. & Laloui, L. (2004). Fabric evolution during hydromechanical loading of a compacted silt. *Int J Numer Anal Meth Geomech*, 28(6):483-499.
- Delage, P. (2010). A microstructure approach to the sensitivity and compressibility of some Eastern Canada sensitive clays. *Géotechnique*, 60(5):353-368.
- Delage, P.; Cui, Y.J. & Howatt, M.D. (1996). Microstructure of a compacted silt. *Can. Geotech. J.*, 33(1):150-158.

- Delage, P. & Lefebvre, G. (1984). Study of the structure of a sensitive Champlain clay and of its evolution during consolidation. *Can. Geotech. J.*, 21:21-35.
- Della Vecchia, G.; Jommi, C. & Romero, E. (2013). A fully coupled elastic-plastic hydromechanical model for compacted soils accounting for clay activity. *Int. J. Numer. Anal. Meth. Geomech.*, 37(5):503-535.
- Farias, M.M. & Cordão Neto, M.P. (2010). Advanced Numerical Simulation of Collapsible Earth Dams. *Canadian Geotechnical Journal*, 47(12):1351-1364.
- Griffiths, F.J. & Joshi, R.C. (1989). Change in pore size distribution due to consolidation of clays. *Géotechnique*, 39(1):159-167.
- Kong, L.W.; Guo, A.G.; Zhao, Y.H. & Liu, Y.Y. (2005). Influence of moisture content on porosity features of red clay. *Proc. International Symposium on Advanced Experimental Unsaturated Soil Mechanics*, Trento, Italy, pp. 419-424.
- Li, X. & Zhang, L.M. (2009). Characterization of dual-structure pore size distribution of soils. *Can. Geotech. J.*, 46(2):129-141.
- Mascarenha, M.M.A. (2008). Influência da Microestrutura no Comportamento Hidro-Mecânico de uma Argila Silteosa Não Saturada Incluindo Pequenas Deformações. Tese de Doutorado, Departamento de Engenharia Civil e Ambiental, Universidade de Brasília, Brasília, 158 p.
- Mitchell, J.K. & Soga, K. (2005). *Fundamentals of Soil Behavior*. 3rd ed. John Wiley & Sons, Hoboken, 577 p.
- Munoz-Castelblanco J.A.; Pereira, J.M.; Delage, P. & Cui, Y.J. (2012). The water retention properties of a natural unsaturated loess from northern France. *Géotechnique*, 62(2):95-106.
- Otálvaro, I.F. (2013). *Comportamento Hidromecânico de um Solo Tropical Compactado*. Tese de Doutorado, Universidade de Brasília, Brasília, Brasil, 122 p.
- Otálvaro, I.F.; Cordão Neto, M.P.; Delage, P. & Caicedo, B. (2016). Relationship between soil structure and water retention properties in a residual compacted soil. *Engineering Geology*, 205:73-80.
- Penumadu, D. & Dean, J. (2000). Compressibility effect in evaluating the pore-size distribution of kaolin clay using mercury intrusion porosimetry. *Can. Geotech. J.*, 37(2):393-405.
- Pereira, J.H.F. (1996). *Numerical Analysis of the Mechanical Behavior of Collapsing Earth Dams During First Reservoir Filling*. PhD Thesis, University of Saskatchewan, Saskatoon, 449 p.
- Prapaharan, S.; Altschaeffl, A.G. & Dempsey, B.J. (1985). Moisture curve of compacted clay: mercury intrusion method. *Journal of Geotechnical Engineering*, 111(9):1139-1143.
- Qi, Y.; Al Mukthar, M.; Alcover, J.F. & Bergaya, F. (1996). Coupling analysis of macroscopic and microscopic behavior in highly consolidated Na-laponite clays. *Appl Clay Sci.*, 11(2):185-197.
- Rodrigues, R.A. (2007). *Modelação das Deformações por Colapso Devidas à Ascensão de Lençol Freático*. Tese de Doutorado, Escola de Engenharia de São Carlos, São Carlos, 262 p.
- Romero, E.; Della Vecchia, G. & Jommi, C. (2011). An insight into the water retention properties of compacted clayey soils. *Géotechnique*, 61(4):313-328.
- Sheng, D.; Sloan, S.W. & Gens, A. (2004). A constitutive model for unsaturated soils: thermomechanical and computational aspects. *Computational Mechanics*, 33(6):453-465.
- Silva, M.T.M.G. (2009). *Metodologia para Determinação de Parâmetros para Solos Não Saturados Utilizando Ensaio com Umidade Conhecida*. Dissertação de Mestrado, Universidade de Brasília, Brasília, 158 p.
- Simms, P.H. & Yanful, E.K. (2005). A pore-network model for hydromechanical coupling in unsaturated compacted clayey soils. *Can. Geotech. J.*, 42(2):499-514.
- Tarantino, A. & De Col, E. (2008). Compaction behavior of clay. *Géotechnique*, 58(3):199-213.
- Wheeler, S.J.; Sharma, R.S. & Buisson, M.S.R. (2003). Coupling of hydraulic hysteresis and stress-strain behavior in unsaturated soils. *Géotechnique*, 53(1):41-54.

List of Symbols

- D : entrance pore size
 d_{it} : elastic constitutive matrix
 dp_0^i : pre-consolidation stress rate in the ICL
 de : total strain or the strain measured in the laboratory
 de^L : strain that occurs due to changes of the large pore volume (macrofabric level)
 de^S : strain due to changes of the small pore volume (microfabric level)
 de_v^p : plastic volumetric strain rate
 e : void ratio
 e^{vol} : void ratio of the sample in the intrinsic state
 e^0 : initial void ratio of the sample in the natural condition
FCL: Fabric Consolidated Line
 f^q : yield surface (p and q axis)
 f^s : yield surface (p and s axis)
 G_s : specific gravity of the soil grains
 h_k : elastic constitutive vector
 g^i : plastic potential function
ICL: Intrinsic Consolidated Line
LC: Loading Collapse curve
M: slope of critical state lines
NCL: Normal Consolidated Line
 $N^r(s)$: void ratio when the mean stress is p_c on the UCL
 $N^r(0)$: void ratio when the mean net stress is p_c on the ICL
 p : net mean stress
 p' : mean effective stress
 p_{atm} : atmospheric pressure
 p^c : reference mean net stress
PI: plasticity index
 p_0^i : projection of the pre-consolidation stress on the ICL

$p_0^i(s)$: mean net stress on the UCL	a^s : parameter that controls the absolute rate of suction degradation
$p_0^i(0)$: mean net stress on the ICL	β : parameter controlling the rate of increase of soil stiffness with suction
p_0^s : pre-consolidation stress on the FCL	Δ : difference between the saturated and unsaturated initial void ratios for a suction unloading (wetting) in the elastic domain
$p_0^s(s)$: pre-consolidation stress for unsaturated condition soil	ε : total strain or the strain measured in the laboratory
$p_0^s(0)$: pre-consolidation stress for saturated condition soil	ε^p : vector of plastic strain
PSD: pore size density function	ε_v^p : plastic volumetric strain
q : deviatoric stress	ϕ : friction angle
r : parameter defining the maximum soil stiffness	κ : slope of the elastic path
s : suction	k^e : rate of shear strength increase with suction
s^i : suction increase yield locus	κ_s : slope on the wetting path in the elastic region
x^f : state variable associated with macrofabric level strain	λ^i : Slope of the ICL
x_0^f : initial value of x^f	σ_i : Net stresses
x^s : suction effect degradation	σ_o : initial net stresses
s_0^f : initial value of x^s	σ'_v : vertical effective stresses
w : water content	
w^l : Liquid limit	
d : parameter that controls the absolute rate of degradation	

Pile Setup over a Period of Seven Years Based on Dynamic Load Tests in Overconsolidated Clay

L.B. Passini, L.B. Benetti, A.C.M. Kormann

Abstract. This paper presents the results of a field investigation into pile setup in overconsolidated clay soil that was conducted during a period of almost seven years, at Guabirota Geological Formation, south of Brazil, where the experimentation site of the Federal University of Paraná is located. One driven precast prestressed concrete pile was subjected to dynamic load tests at four different events: at the end of driving (EOD) and at three re-strikes: after 113.5 h (4.7 days), 288 h (12 days) and 2342 days (6.4 years) of pile installation. Re-strike measurements confirm that pile setup occurred and the shaft resistance component, not the end-bearing, contributes predominantly to the increase in capacity along time.

Keywords: driven piles, dynamic load test, pile setup, overconsolidated clay soil.

1. Introduction

Driven piles are displacement piles where no (or minimal) soil emerges at the surface as a result of their installation (Salgado, 2008). Prestressed concrete piles are displacement piles that offer several benefits compared to other driven pile systems (*e.g.* Gerwick, 1968; Hussein *et al.*, 1993a; Tomlinson, 1994; Fleming *et al.*, 2009). Tensile stresses, which can arise in a pile during driving, can be better resisted due to prestressing forces and the pile is less likely to be damaged during handling. Bending stresses during driving are also less likely to produce cracking than in conventional precast concrete piles.

As is well known in foundation engineering, piles undergo a process of setup after installation (*e.g.* Hussein *et al.*, 1993b; York *et al.*, 1994; Chow *et al.*, 1998; Axelsson, 1998; Axelsson & Westin, 2000; Tan *et al.*, 2004; Fellenius, 2008; Yan & Yuen, 2010; Lee *et al.*, 2010; Steward & Wang, 2011; Lim & Lehane, 2014; Basu *et al.*, 2014; Afshin & Rayhani, 2015), leading to an increase in capacity along time. It is suggested that this happens both because of the dissipation of positive pore pressure excess and of soil aging (particles rearrangement around the pile shaft) along time after installation. Steward & Wang (2011) define aging as the increase of the soil friction angle at a constant effective stress over time, similar to the one of the secondary compression after primary consolidation is finished. However, it is also known that the two phenomena happen almost at the same time.

Increase in pile capacity after initial driving was well observed in clays and sands over decades. This phenomenon is definitely favorable to engineering designs such as in many important practical implications, regarding testing

methods, during the programming of foundation construction and for the reassessment of existing driven pile capacities. Studies related to pile setup have been developed in the field (*e.g.* Fellenius *et al.*, 1989; Axelsson, 1998; Bullock *et al.*, 2005a; Lee *et al.*, 2010; Ng *et al.*, 2013a; Attar & Fakharian, 2013) and in scale models from laboratory tests (*e.g.* Lim & Lehane, 2014; Rimoy *et al.*, 2015; Afshin & Rayhani, 2015). Although literature provides knowledge regarding the subject of the pile setup phenomenon, the complete contributing mechanisms to the setup are not well understood.

Nevertheless, it is known that the setup phenomenon is related to the disturbance caused by pile installations such as buried, monotonically jacked and driven piles, where displacement piles had larger shaft capacity gains along time (*e.g.* Afshin & Rayhani, 2015). In addition, higher stress level (σ'_v - confining vertical effective stress) appears as an important factor in the occurrence of resistance gains along time (*e.g.* Lim & Lehane, 2014). The most part of the engineers do not attempt to assess setup during construction (Bullock, 2008).

The evaluation of pile resistance over time can be achieved by restriking the pile at different times using the tool of dynamic load tests used for foundation control (*e.g.* York *et al.*, 1994; Hussein & Likins, 1995; Axelsson, 1998; Chow *et al.*, 1998; Axelsson & Westin, 2000; Tan *et al.*, 2004; Yan & Yuen, 2010; Lee *et al.*, 2010; Ng *et al.*, 2013a; Attar & Fakharian, 2013; Afshin & Rayhani, 2015). The dynamic load test is a high strain dynamic test used to assess the bearing capacity of a pile (shaft and tip) by applying a dynamic load at its top (a falling mass) while recording acceleration and strain near its head. Additionally, this

Larissa de Brum Passini, PhD., Associate Professor, Construction Engineering Graduate Program, Federal University of Paraná, Curitiba, PR, Brazil. E-mail: larissapassini@hotmail.com (corresponding author)

Laisa Berno Benetti, MSc. Student, Construction Engineering Graduate Program, Federal University of Paraná, Curitiba, PR, Brazil. E-mail: laisabbenetti@hotmail.com
Alessander Christopher Moraes Kormann, PhD., Associate Professor, Construction Engineering Graduate Program, Federal University of Paraná, Curitiba, PR, Brazil. E-mail: alessander@ufpr.br

Submitted on May 2, 2016; Final Acceptance on March 18, 2017; Discussion open until August 31, 2017.

test provides the assessment of time dependent soil strength changes, determining dynamic pile stresses under hammer impacts, pile structural integrity and investigating hammer and driving system performance (Hussein *et al.*, 1993b).

In order to contribute to a better understanding of high strain dynamic testing of driven pile shafts, this paper describes the results of the research about the behaviour of precast prestressed concrete pile regarding the increase of its capacity over time (setup effects), at Guabirota Geological Formation in the State of Paraná, south of Brazil, which is in progress at the experimentation site of the Federal University of Paraná - UFPR.

2. Materials and Methods

2.1. Geotechnical experimental field

The Geotechnical Experimentation Site of the UFPR is located at the Polytechnic Center Campus in Curitiba, Brazil. One of the reasons for choosing this particular site was because its stratigraphy and soil properties have been extensively studied and are very well documented (*e.g.* Salamuni, 1998; Chamecki *et al.*, 1998; Kormann, 1999; Negro *et al.*, 2012). The natural soil belongs to the tertiary Guabirota Geological Formation. Overconsolidated silty clays and clayey silts with high plasticity are soils commonly present in this sedimentary formation. Polished and shiny surfaces are commonly seen in the clayey soil mass. These slickensides follow a pattern of difficult identification. Well defined tectonic structures are also present. Lenses of sands, rich in feldspar, frequently occur inside the clayey mass. Some conglomerate and carbonate deposits may occur at specific sites.

Two Standard Penetration Tests (SPT) and two Cone Penetration Tests (CPTU) were performed in the area very close to this pile location (Kormann, 2002). The clay soil, typical of the Guabirota Geological Formation, is present until approximately 5.0 m of depth in red or variegated shades, which are usually associated with weathering. These layers have a soft to stiff consistency. Below them and until the end of the SPT boring, there are gray clay materials of hard and stiff consistency. Quartz and feldspar grains are disseminated in the silty-clay matrix. The occasional presence of sand is a characteristic of the area of study. Water table is located at about 2.0 m of depth. Between 5.0 and 7.0 m of depth, a tougher layer is evidenced by the cone tip resistance that exceeds 10 MPa. SPT also accuses a greater number of blows in this region. In general, remarkably high pore pressures were generated during cone penetration. Figures 1 and 2 show the geotechnical profiles by SPT and CPTU, respectively.

2.2. Precast prestressed concrete pile

The pile installed and tested is a precast prestressed concrete pile, with a square and solid section of 0.26 x 0.26 m, having no seams. Total pile length is 10 m and

length inside ground is equal to 9 m. The driven system used had a free-fall hammer with a drop height of 0.60 m and weight of 29.4 kN. Figure 3 displays the driven pile record, where the number of blows indicated is the mean for every 0.50 m of pile penetration.

An analysis of Fig. 3 shows that, between 5.0 m and 7.0 m of penetration, the number of blows increased. This behaviour is compatible with the geotechnical investigation data (in particular SPT-7 and CPTU-8), which accused greater resistance in this region.

After penetration reached 6.0 m, the installation of the instrumentation was executed. It consisted of fixing a specific pair of strain transducers and a pair of accelerometers, positioned at 0.60 m from the top of the pile. Sensor pairs were installed diametrically opposite one another, aiming to compensate the bending effect on the pile, which tends to occur when hammer blows are applied. For every blow, sensors data were processed in the field by the Case Method (*e.g.* Goble & Hussein, 1994), providing signals representing the change in intensity force obtained from the measured strain and velocity, integrated from the acceleration data at pile length along time. These signals were monitored and stored using a Pile Driven Analyzer[®] (PDA), a data logger equipped with a memory card. The Case Method is based on simplified pile and soil behaviour assumptions (free end and plastic soil), resulting in a closed form solution related to the impact and its reflection from the tip, by using the wave propagation theory (Paikowski *et al.*, 2004).

During penetration between 6.0 m and 9.0 m, the maximum average axial compression at the instrumentation level (CSX) ranged from 8.0 to 10.0 MPa. Maximum tensile stress below the sensors (TSX) reached 2.6 MPa. These stress levels are acceptable, since the pile structural resistance is greater than that.

2.3. Dynamic load tests

Dynamic load tests were performed at four distinct events. The first immediately after installation, the second after 113.5 h (4.7 days), the third after 228 h (12 days) and the fourth and last one at 2342 days (6.4 years) after installation. The procedure of increasing dropping hammer heights was applied (Aoki, 1989). For the three first tests a hammer with weight of 29.4 kN was used. For the last dynamic test a hammer with weight of 22.6 kN was available. In spite of the fact a distinct hammer was used in the fourth test, the data assessment provided in the following paragraphs will present evidences that full soil resistances were mobilized in all restrikes. In such case, the use of a lighter hammer in the fourth test does not affect the interpretation.

During the first test, the pile received 7 blows, at heights of 0.2, 0.4, 0.6, 0.8, 1.0, 1.2 and 1.4 m. At the second test, the pile received 6 blows, at heights between 0.2 and 1.2 m. In the third test, the pile received 11 blows, at heights between 0.2, 0.4, 0.6, 0.8, 1.0 (twice), 1.2, 1.4, 1.6,

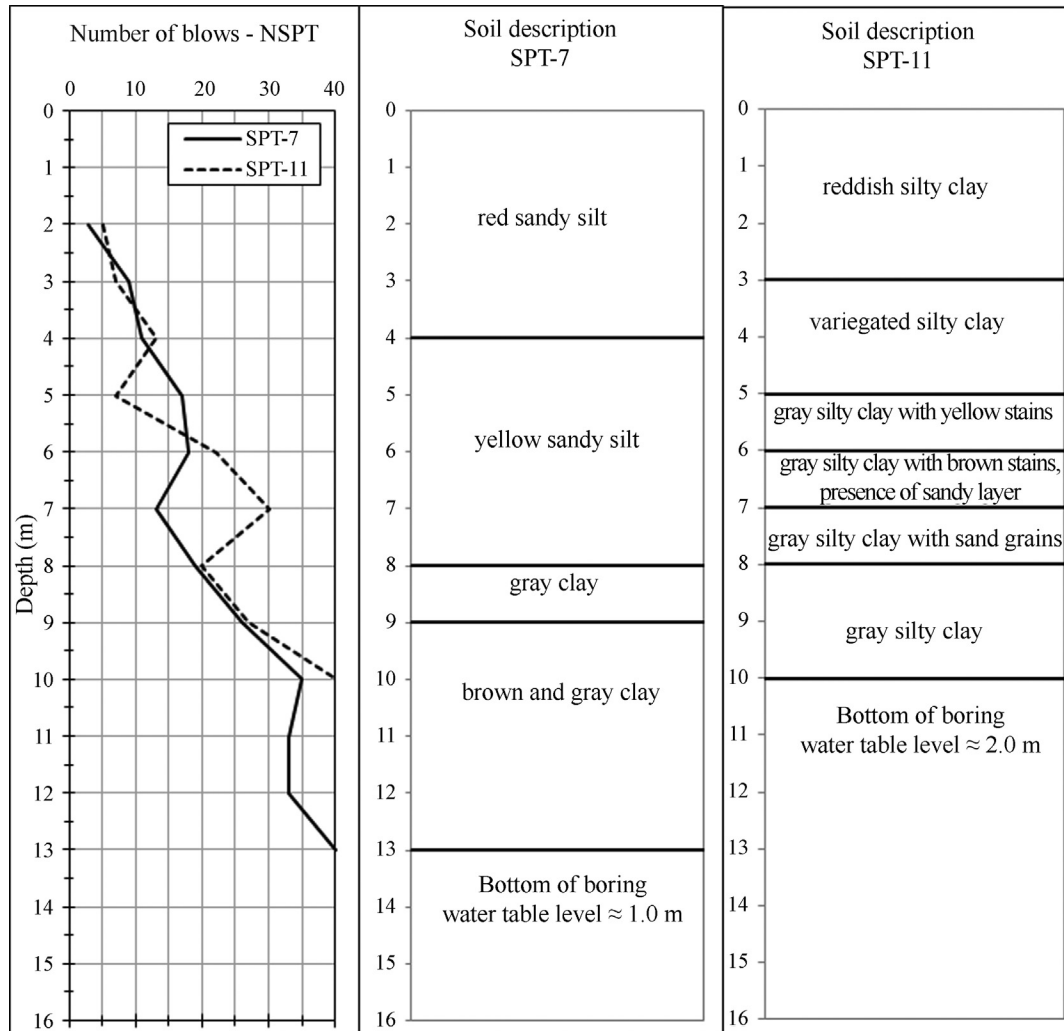


Figure 1 - Geotechnical profiles by SPT.

1.8 and 2.0 m. At the last test, the pile received 5 blows, at heights between 0.2 and 1.0 m.

The set (permanent vertical displacement or penetration of the pile and plastic deformation of the soil) and the rebound (elastic compression of the driving head, pile and soil) resulting from the hammer impact at the pile top were recorded for all blows (as executed during pile installation) and signals from sensors were monitored and stored using the Pile Driven Analyzer® (PDA) for all tests.

Figure 4 illustrates the signals monitored in dynamic load tests. The solid line represents force and the dashed line corresponds to the velocity multiplied by impedance along time. This representative figure refers to the second dynamic load test after 113.5 h (4.7 days) of pile installation (end of driving - EOD), blow number four and drop height equal to 0.80 m.

For all tests, pile length under sensors (L) is equal to 9.40 m and the time required for the wave of the hammer impact to spread until the tip of the pile and return to the top

($2L/c$, where c is the wave travel velocity) is equal to 5.7 ms.

For concrete piles PDI (2003) states that the wave propagation velocity (WS) must be determined for each pile. It can be determined during driving, if wave up indicates some tension reflection (local “valley” in wave up at $2L/c$). With this type of WS determination, the variability in pile properties and the degradation of pile material during repeated hammer blows are considered.

ASTM D4945 (2012) recommends that the wave velocity for concrete piles would preferably be determined from an early impact event if a tensile reflection from the pile toe is clearly identified.

Therefore, for all tests, the wave propagation velocity (WS) equal to 3300 m/s (e.g. Hussein *et al.*, 1993a; Kormann, 2002; Robinson & Iskander, 2008) was measured on the basis of the ascending wave (wave-up), looking to identify tension reflections during the time corresponding to the pile tip response.

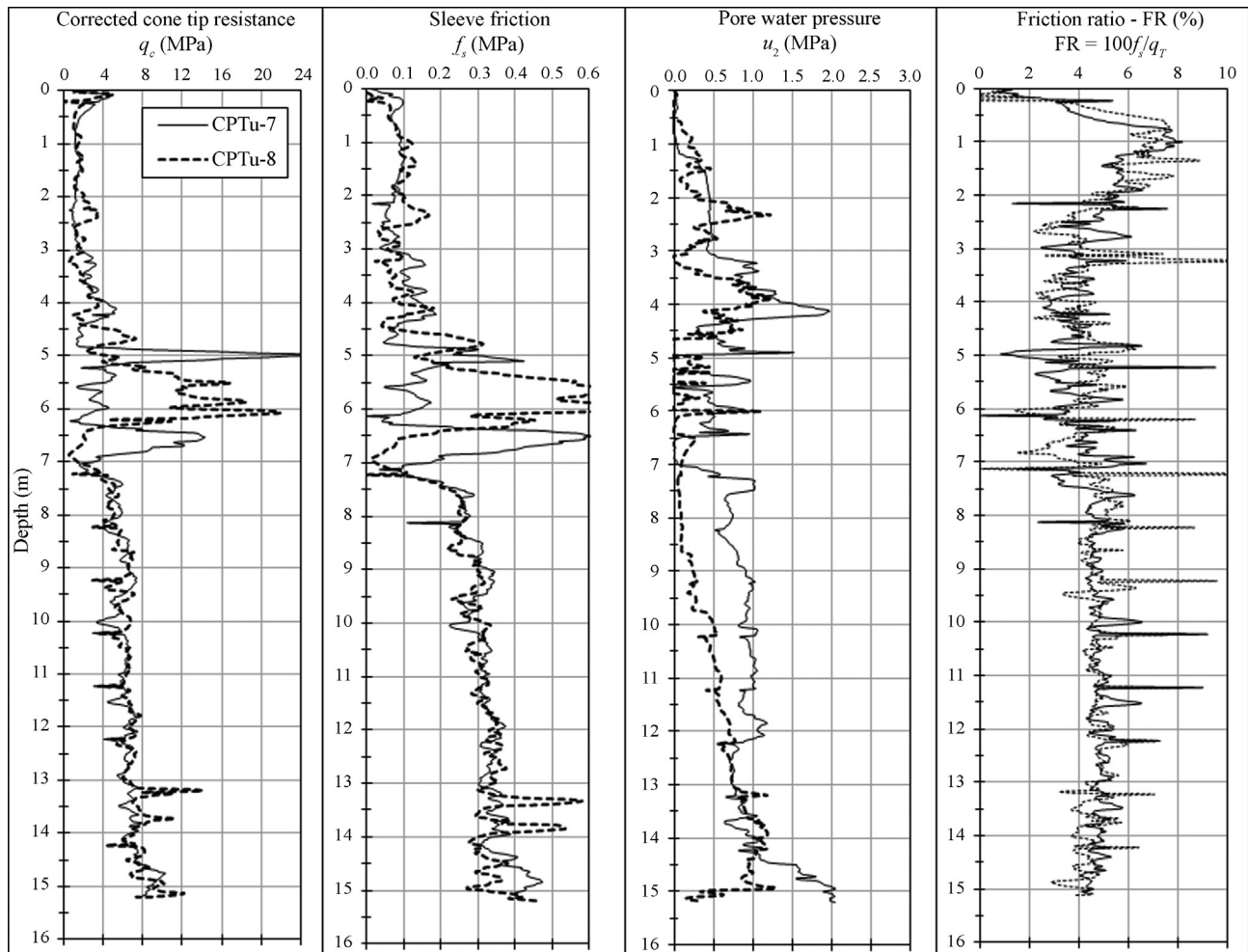


Figure 2 - Geotechnical profiles by CPTU.

Wave propagation velocity is used to calculate the dynamic elastic modulus (EM), which according to the one-dimensional wave propagation theory is given by concrete pile density multiplied by the squared wave propagation velocity ($\rho \times W^2$). Considering concrete pile density as equal to 24.5 kN/m^3 (e.g., Kormann, 2002; PDI, 2003; Robinson & Iskander, 2008; Cintra *et al.*, 2014), the EM obtained was approximately equal to 27 GPa.

During dynamic load tests, compressive and tensile stresses were controlled, in order to prevent damage to the pile. The maximum values for compressive stress (CSX) were obtained at the third test, being equal to 18.5 MPa and for traction stress (TSX) the value was equal to 2.6 MPa, at the fourth test.

The ratio between nominal energy and measured energy, which quantifies efficiency of the hammer, ranged from 11.9% to 35.7%, increasing as the drop height increases. Minimum and maximum values were obtained at the third test.

Table 1 displays the number of blows, drop heights, EMX (measured energy), RMX (total capacity calculated

by Case Method), set and rebound for each dynamic load test.

Figure 5 shows the RMX vs. EMX curve of each test. The shape of the curves indicates that the full capacity of the pile was mobilized since after the RMX value reached a peak there wasn't further growth of the mobilized load capacity as a function of energy increase. From Table 1, it can be seen that after the peak value, the pile starts to penetrate in the soil with high sets and almost constant rebounds, indicating that soil-pile failure was achieved.

The increase of the maximum value of RMX along the tests clearly indicates that the pile load capacity experienced an increase along time.

3. Results and Discussions

3.1. Predicted results

The predicted results of pile load capacity were calculated by selecting some semi empirical methods, routinely applied, which are based on field investigation tests (SPT and CPTU), such as Aoki & Velloso (1975, 1985, 1996), Philipponnat (1979), Bustamante & Gianceselli (1982),

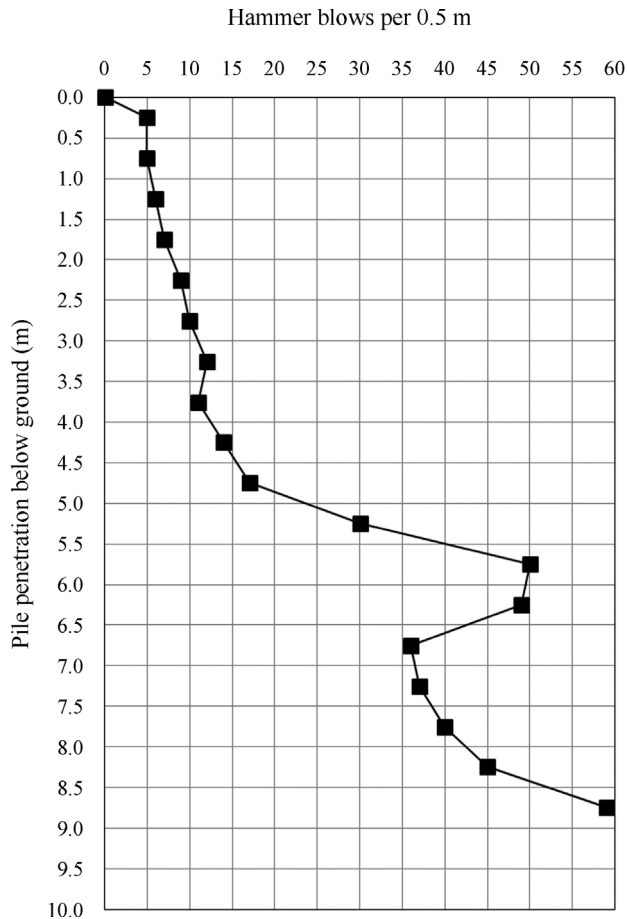


Figure 3 - Driven pile record.

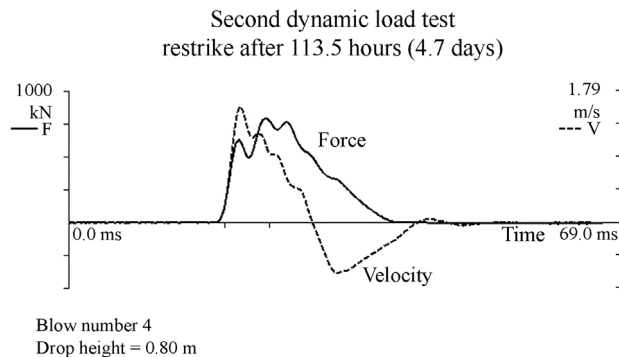


Figure 4 - Example of force and velocity signals multiplied by impedance along time.

Décourt & Quaresma (1978) and Amaral et al. (1999), according to Kormann et al. (2000). The number of blows of SPT was the mean of the two available tests. Tip resistance (q_c) and lateral friction resistance (f_s) of the employed CPTU values came from interpreting the chart in Fig. 2 regarding CPTU-8.

Data in Table 2 show a significant dispersion, suggesting the pile ultimate load capacity ranging between 567 kN and 1033 kN, depending on the semi empirical

method applied. Furthermore, it can be seen that shaft friction contributes most to this wide range. The dispersion can be associated with the empirical factors (related to the soil and pile type, for example) considered in the load capacity predictions, which are influenced by the local geology, regional constructive and field tests practices from the database that was considered in the establishment of the method.

3.2. Measured results

In order to evaluate the mobilized resistance in four dynamic load test events, signals previously selected were submitted to conventional analysis using CAPWAP (CASE Pile Wave Analysis Program). This type of analysis is an iterative process that uses the wave propagation theory involving signals of force or velocity measured in the field as a boundary condition to match a curve modelled by soil parameters like: static resistance and its distribution along the pile shaft and under its tip and dynamic parameters of the pile and of the ground. Additionally, these analyses simulate the top and tip static load-displacement relationships (e.g. Likins et al., 1992; Hussein & Likins, 1995).

The study using the numerical analysis CAPWAP included the four final blows from the first test as well as three, four and two blows from the second, third and fourth tests, respectively. The selected values are justified by the higher total resistance (RMX) mobilized at the field for a specific blow (e.g. Fellenius et al., 1989) obtained by data generated in the Case Method data processor. A reduction in impedance was evidenced by the velocity signal being above the force signal at approximately two and three meters below the pile top, for all tests (Fig. 4). This reduction was modelled with *slacks* and impedance adjustments. Results of the analysis are summarized in Table 3.

The elastic deformation of the soil along the pile shaft (*shaft quake - Qs*) did not show a clear behaviour when comparing all blows and tests (e.g. Alves et al., 2009). However, the elastic deformation of the soil at the pile tip (*toe quake - Qt*) showed a clear increase as the drop height of the hammer was increased. Additionally, it could be observed that *toe quake* values were close to the set values obtained for a specific blow. The high values obtained for the elastic deformation of the soil at the pile tip (*toe quake*) can be associated with the resilient behaviour (e.g. Aoki & Alonso, 1992), as well as with the pile being re-driven into the soil.

Comparing the blows with the same level of measured energy (EMX), it can be seen that the *toe quake* of the re-driven pile tended to be lower than that measured at the end of the first test. For example, the fourth blow of the three initial tests (EMX ranges between 5.80 kNm to 7.50 kNm) and the fifth blow of the last test (EMX equals to 6.67 kNm) present decreasing *toe quake* values, to be specific: 11.16, 5.34, 4.87 and 4.75 mm.

Table 1 - Four dynamic load test records.

Test	Blow	Drop height (cm)	EMX (kNm)	RMX (kN)	Set (mm)	Rebound (mm)
End of driving (EOD)	1	20	0.8	405	1.0	2.0
	2	40	2.4	550	2.0	2.0
	3	60	4.3	570	5.0	3.0
	4	80	7.5	605	11.0	4.0
	5	100	9.4	597	13.0	4.0
	6	120	11.1	618	15.0	4.0
	7	140	13.5	604	20.0	5.0
Restrike after 113.5 h (4.7 days)	1	20	0.9	504	1.0	3.0
	2	40	2.2	732	1.0	4.0
	3	60	3.4	778	2.0	4.0
	4	80	6.0	796	5.0	5.0
	5	100	8.4	799	8.0	5.0
	6	120	11.3	794	12.0	4.0
Restrike after 288 h (12 days)	1	20	0.7	469	1.0	3.0
	2	40	1.9	709	1.0	4.0
	3	60	2.9	791	1.0	5.0
	4	80	5.8	826	4.0	5.0
	5	100	8.5	838	8.0	4.0
	6	100	8.4	836	10.0	-
	7	120	10.7	848	12.0	-
	8	140	12.9	835	13.5	-
	9	160	16.1	845	17.0	-
	10	180	17.8	855	20.0	-
	11	200	21.0	860	22.0	-
Restrike after 2342 h (6.4 years)	1	20	0.71	542	0.0	2.0
	2	30	1.48	748	0.0	4.0
	3	60	2.59	945	0.5	4.5
	4	80	4.42	1023	2.5	3.5
	5	100	6.67	984	4.0	4.0

According to Smith (1960), *soil quake* is defined as the maximum elastic soil deformation. Therefore, a reduction in *toe quake* means a gain in tip stiffness. This behaviour was more pronounced between the first and the second tests, when tip resistance gain was 22% (from 337 to 412 kN). Among the other events (second, third and fourth tests), the reduction of its elastic limit was attenuated, as it also was for the set, reflecting in closer tip resistance values, specifically: 412, 402 and 399 kN, respectively. The decrease of stiffness gain and the small decreasing tendency of tip resistance observed in the last three tests suggests a stabilization behaviour at the tip.

Viscous forces which are function of velocity also resist pile penetration (PDI, 2006). Damping factors (*shaft* and *toe damping*) represent the dynamic component of the

soil's resistance. The results from CAPWAP analysis for *shaft damping* (J_s) and *toe damping* (J_b) did not show a clear behaviour (e.g. Paikowski & Chernauskas, 1996), the same happening with the *shaft quake* (e.g. Alves *et al.*, 2009). The model that was best adjusted to the signals was Smith's damping, for both moments: before and after the full mobilization of the pile tip resistance. This model yields good results in soils with high values of *toe quake*.

The Case Method *damping factor* (J_c) values, obtained by correlation with results from CAPWAP analysis, exhibited a small dispersion, as can be seen in Table 3 (last column). The mean values were equal to 0.61, 0.64, 0.56 and 0.64 for the first, second, third and fourth tests, respectively.

Table 2 - Predicted pile load capacity from semi empirical methods (Kormann *et al.*, 2000).

Author	Field test	Ultimate load capacity (kN)		
		Shaft	Tip	Total
Aoki & Velloso (1975)*	CPT	530	250	780
Aoki & Velloso (1985, 1996)*	CPT	700	333	1033
Philipponnat (1979)**	CPT	748	208	956
Bustamante & Ganeselli (1982)**	CPT	375	192	567
Aoki & Velloso (1975)*	SPT	390	230	620
Aoki & Velloso (1985, 1996)*	SPT	520	300	820
Décourt & Quaresma (1978)**	SPT	455	218	673
Amaral <i>et al.</i> (1999)	SPT	578	292	870
Mean	-	537	253	790
Standard deviation	-	135	50	163

apud* Cintra & Aoki (1999) *apud* Décourt (1996).

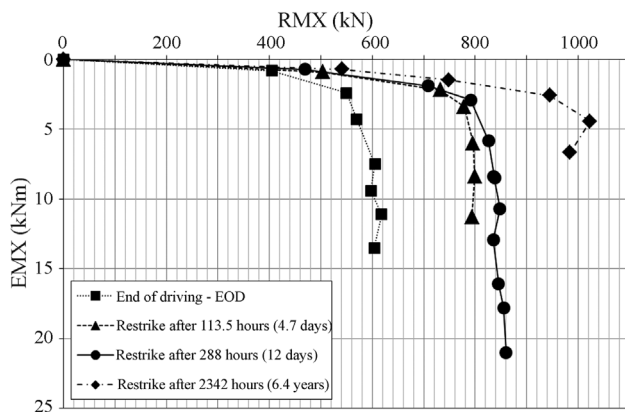


Figure 5 - RMX vs. EMX curves.

Results from the analysis showed a significant resistance mobilized at all four dynamic load test events. Blows related with higher total resistance (RMX) from Table 1 (fifth column), were selected and analyzed using the CAPWAP program (Table 3), and did not accuse an increase in mobilized load capacity within the same event.

At the first test, the full mobilized resistance occurred at blows 6 and 7, because of the higher and constant values obtained, such as 615 and 618 kN, with mean value equal to 616 kN. At the second test, the full resistance was mobilized at blows 4, 5 and 6, with values equal to 784, 750 and 767 kN and mean value equal to 767 kN. From these two tests an increase around 24.5% in total pile capacity along time (113.5 h = 4.7 days) can be noted. At the third test, blows 4 to 8 were considered as achieving the full mobilized resistance, having values equal to 824, 819, 820, 825 and 833 kN, with mean value equal to 824 kN for total pile capacity. Comparing the first test with this third test, the increase in total pile capacity along time (228 h = 12 days) was equal to 33.8%. At the fourth test, the blows considered

were numbers 4 and 5, with values equal to 966 and 925 kN and average value equal to 945 kN for total pile capacity. Comparing one more time the first test with this fourth test, the increase of total pile capacity along time (2342 days ≈ 6.4 years) was around 53.5%.

The evolution of the total mobilized pile resistance over time can be seen in Fig. 6, where the pile shaft resistance and the mobilized tip resistance are also plotted. The plotted values are the mean of blows in which a full mobilization of resistance was considered. Figure 6 shows that the increase in total pile capacity was more expressive at the beginning (first days after pile driving), being equal to 24.5% during the first 4.7 days after EOD. Comparing the second test with the third test, the increase in total pile capacity along time was equal to 7.4% during the next 7.3 days. Then, comparing the third test with the fourth test, the increase in total pile capacity along time was equal to 14.7% during the following 2330 days ≈ 6.4 years.

The trend of the available data suggests that pile load (shaft and total) capacity was not yet stabilized along time at the moment of the last test. However, such behaviour cannot be confirmed due the significant time gap (in excess of 6 years) between the third and the fourth restrike.

Analyzing the increase of the resistance between tests, it can be seen that it is important to wait a minimum time before the installation of the pile to provide better information relating to the maximum available load capacity.

Although, ASTM D4945 (2012) doesn't mention a specific waiting time, it recognizes that one of the factors that may affect the axial static capacity estimated from dynamic tests include the elapsed time since initial installation. Moreover, it states that if the test results are used for static capacity computations, dynamic measurements should (also) be performed during restrikes of the deep foundation, after waiting a period of time following the ini-

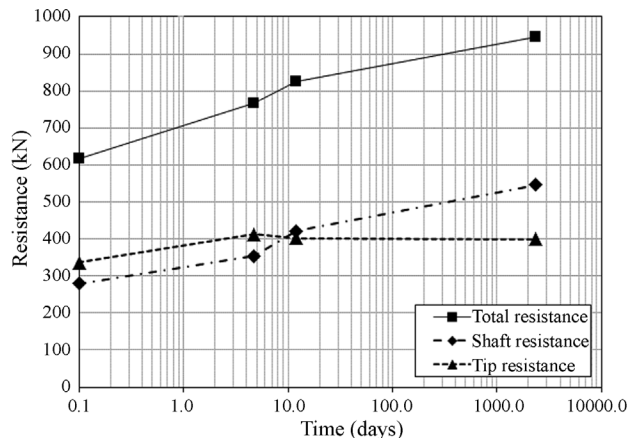
Table 3 - Results from CAPWAP analysis.

Test	Blow	Shaft resistance (kN)	Tip resistance (kN)	Total mobilized resistance (kN)	J_s (s/m)	J_t (s/m)	Q_s (mm)	Q_t (mm)	J_c
1	4	218	336	554	0.476	0.567	0.90	11.16	0.76
	5	276	294	570	0.429	0.35	2.26	12.57	0.67
	6	284	331	615	0.334	0.399	1.31	15.54	0.53
	7	275	343	618	0.081	0.561	1.57	19.74	0.48
2	4	336	448	784	0.732	0.385	1.00	5.34	0.60
	5	403	347	750	0.54	0.367	1.00	8.40	0.68
	6	325	443	767	0.531	0.170	1.00	11.3	0.66
3	4	472	352	824	0.703	0.128	0.87	4.87	0.52
	5	438	381	819	0.432	0.247	1.00	8.40	0.60
	6	466	354	820	0.365	0.239	0.97	8.41	0.62
	7	366	459	825	0.494	0.208	1.00	10.76	0.56
	8	369	464	833	0.359	0.280	1.00	12.57	0.53
4	4	566	400	966	1.019	0.499	2.04	2.50	0.64
	5	526	399	925	0.490	0.528	2.47	4.75	0.65

tial installation sufficient to allow pore water pressure and soil strength changes to occur.

Pile Driving Contractors Association (2007) suggests the following minimum often used times between end of drive and restrrike test: 1 day for piles in clean sands, 2 days for piles in silty sands, 3 to 5 days for piles in sandy silts, 7 days for piles in shales and 7 to 14 days for piles in silts and clays (longer times sometimes required). From the present case study, the significant increase in the load capacity until 12 days lends support to the waiting time suggested for piles in silts and clays.

In Fig. 6, the increase in total pile and shaft capacity along time showed to have an almost linear behaviour, because of the logarithmic scale used for time. Other authors found a similar behaviour in their graphic plots of field

**Figure 6** - Increasing pile capacity along time using log scale for time.

tests of piles, when performing the setup evaluation (*e.g.* Bullock *et al.*, 2005a; Fellenius, 2008; Doherty & Gavin, 2013).

3.3. Side shear role on pile setup

Assessing the shaft resistance of the pile, an increase along time in those values from 279 to 354 kN is observed between the first and the second test, and from 422 to 546 kN between the third and the fourth test. At the first test, shaft resistance corresponded to 45% of the total capacity. At the second test it corresponded to 46% and at the third test it corresponded to 51%. In the last test, shaft resistance corresponded to 58% of total capacity. Therefore, an increase in shaft resistance along time can be observed. In contrast, pile tip resistance tends to stabilize over time (Fig. 7).

According to Lee *et al.* (2010), the major component of the pile bearing capacity gain along time is the gain in shaft resistance. Ng *et al.* (2013a) visualized the effects of setup along the pile shaft and at the pile toe in cohesive soils from field tests, with setup influencing the shaft resistance more than the end bearing did. Komurka & Wagner (2003), Bullock *et al.* (2005a, b) and Attar & Fakharian (2013) also observed the increase of capacity along time, mainly in shaft resistance.

In Fig. 7, the increasing pile shaft resistance along time vs. depth is displayed. As it is possible to see, this behaviour is compatible with the geotechnical investigation data (Figs. 1 and 2) and with the driven pile record (Fig. 3), which accused greater resistance with increased depth. Other authors found a similar behaviour in their graphic

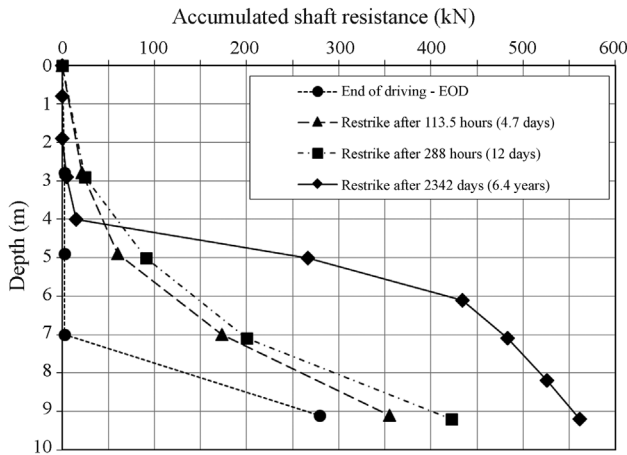


Figure 7 - Increasing pile shaft resistance along time.

plots, such as Gonçalves *et al.* (2007) and Lee *et al.* (2010).

According to Basu *et al.* (2014), based on results from one dimensional finite-element analysis (FEAs), setup factors (F_s) were observed to increase with time after pile installation and depend on both σ'_v (confining vertical effective stress) and OCR (overconsolidation ratio). F_s is defined as the ratio between the shaft resistance of the displacement pile available at any particular time t after pile installation and the shaft resistance of the pile immediately after its installation (end of driving - EOD).

Setup factors (F_s) for shaft resistance were approximately equal to 1.0, 1.3, 1.5 and 2.0 respectively for the first, second, third and fourth average data of dynamic load test results, clearly showing the setup on the pile, as shown in Fig. 8. In this picture are also plotted the normalized results for total resistance over time, with ratios equal to 1.0, 1.2, 1.3 and 1.5, respectively for the first, second, third and fourth means of dynamic load test events. Other authors found similar behaviour in their graphic plots, such as Bull-

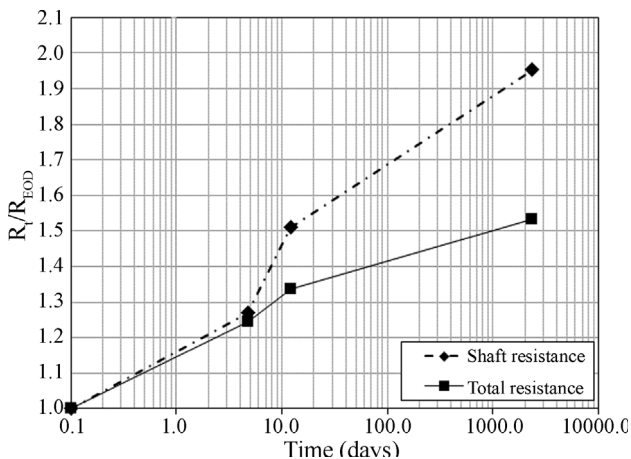


Figure 8 - Normalized total and shaft resistances along time at log scale.

ock *et al.* (2005a, b), Lee *et al.* (2010), Ng *et al.* (2013a), Attar & Fakharian (2013), Lim & Lehane (2014).

3.4. Logarithmic trend for pile setup

In agreement with Komurka & Wagner (2003), Lee *et al.* (2010), Steward & Wang (2011), Ng *et al.* (2013b), Afshin & Rayhani (2015) several empirical equations have also been proposed to quantify the magnitude of the pile setup. The most popular one was proposed by Skov & Denver (1988), who introduced a linear relationship between the logarithm of time *vs.* the pile setup. The equation is based on four case histories of dynamic and static load testing in driven piles on different types of soil, including clay, where the estimated pile capacity (R_t) at different elapsed times (t) is obtained from the pile capacity (R_{EDO}) at the end of driving - EOD (t_{EDO}).

$$\left(\frac{R_t}{R_{EDO}}\right) = A \log_{10}\left(\frac{t}{t_{EDO}}\right) + 1 \quad (1)$$

According to Attar & Fakharian (2013), in the past, setup effects were attributed to both tip and shaft resistances and the total capacity would have been considered in the relation between R_t and R_{EDO} , but recent studies have attributed the setup to shaft capacity and stated that effects on the tip are not significant (*e.g.* Bullock *et al.*, 2005a, b; Attar & Fakharian, 2013). Parameter A is the slope of the line, so the higher this value is, the more vertical is the line and the greater the gain of resistance along time also is. This parameter is closely related to the properties of the soil where the pile was installed. For instance, the soil could be clay, silty or sandy soil, the field can be layered or not, naturally or not cemented, normally consolidated or overconsolidated, with or without the presence of water level. But not only are soil properties relevant, the period of time of the pile setup observation also has an important contribution to parameter A because, at shorter periods of time, piles usu-

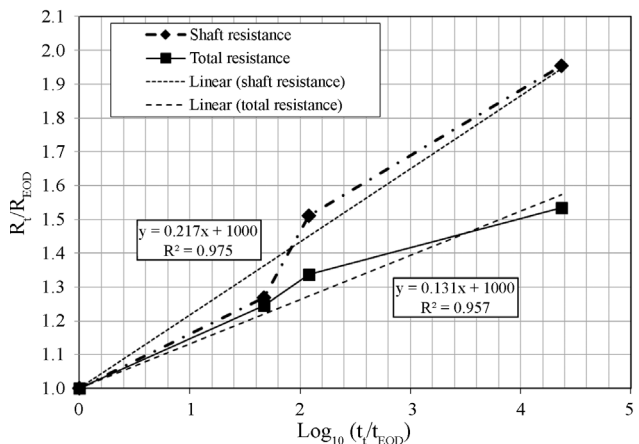


Figure 9 - Linear best fits of normalized pile resistances (R_t/R_{EDO}) as a function of normalized logarithmic time $\log_{10}(t/t_{EDO})$.

ally increase their capacity faster than at longer periods of time, therefore, parameter A changes value.

Different authors present diverse values for parameter A , ranging from 0.1 until 0.6 and different values for the time at the end of driving - EOD (t_{EDO}), ranging from 0.01 until 100 days (*e.g.* Komurka & Wagner, 2003; Bullock *et al.*, 2005a, b; Fellenius, 2008; Lee *et al.*, 2010; Steward & Wang, 2011; Doherty & Gavin, 2013; Ng *et al.*, 2013a, b; Attar & Fakharian, 2013; Afshin & Rayhani, 2015).

In this paper, it was considered $t_{EDO} = 0.1$ day, because this showed to be the best agreement of both shaft and total normalized pile capacity (R/R_{EDO}) *vs.* normalized time at $\log_{10}(t/t_{EDO})$. This was confirmed by the coefficients of determination (R^2) as shown in Fig. 9, being in the range between 0.975 and 0.957. Parameter A ranged between 0.217 and 0.131 for shaft and total pile capacity, respectively. The greater value of the parameter A of shaft capacity comparing with parameter A of total pile capacity can be explained by a likely trend to negative pore pressure generation during shear at the pile tip, normally associated to highly overconsolidated clays. This trend could imply a less pronounced increase of end bearing resistance over time.

In order to have a better idea about the driven pile setup in the Geotechnical Experimentation Site at UFPR, the mean pile setup measured during this study was compared to those proposed for piles driven in clay, according to results reported by Bullock *et al.* (2005a) and Afshin & Rayhani (2015). In comparison with previous research, the average setup presented in this study exhibits a slightly smaller rate over shorter and longer periods of time. Therefore, parameter A is smaller. Anyway, the results from this study, in a normalized capacity *vs.* time trend curve, showed to be consistent with the response observed from a wider database of pile tests in clay compiled from the literature.

The most similar results are from field tests obtained from static and dynamic load tests as well as from tests using o-cell, for example:

- i) Bullock *et al.* (2005a) performed tests in the coastal plain soils of Florida on different places. Testing sites varied widely, from shelly and silty sands to moderately plastic clays, in prestressed concrete piles ($A_{mean} = 0.22$ for pile side shear, $t_0 = 1$ day and $t_{max} = 1727$ days = 4.7 years);
- ii) Doherty & Gavin (2013), in the research field located at Belfast harbor, composed by soft clay, on driven concrete piles ($A = 0.26$ for pile side shear and 0.25 for pile total capacity, $t_0 = 100$ days and $t_{max} = 3683$ days = 10 years);
- iii) Ng *et al.* (2013a,b), on layered cohesive soil, in the state of Iowa, varying from normally consolidated to slightly overconsolidated, in steel piles ($A_{mean} = 0.11$ for pile resistance, $t_0 = 0.001$ day and $t_{max} = 36$ days);
- iv) Attar & Fakharian (2013), in layered soil deposited in marine conditions, on prestressed concrete driven pi-

les ($A = 0.32$ for shaft resistance, $t_0 = 0.01$ day and $t_{max} = 574$ days).

The parameters comprising the equation as well as the equation itself that was proposed to quantify the magnitude of the pile setup, with a linear relationship between the logarithm of time and the pile resistance, showed to be simple and consistent with the database from literature above and with results from this research for both total and shaft pile capacity.

3.5. Simulations of static load tests

The simulations of static load tests from the four dynamic load tests are displayed in Fig. 10. They were obtained from CAPWAP program. Analyzing the curves load *vs.* displacement it is possible to conclude that:

- i) As time progresses, comparing all four events, the end portion of the curves goes to the right (higher value of load), something expected given the phenomenon of setup. This behaviour is mainly due to the recovery of the lateral friction;
- ii) The rigidity of the first straight stretch (inclination) of the curves changed from the first to the last event, the changes being more pronounced when the first and the second events are analyzed. When the third and the fourth events are observed, the increase of rigidity tends to be smaller. This observation can also be associated with the increase of pile shaft resistance over time;
- iii) The rigidity of the second straight stretch (inclination) of the curves also changed from the first to the last event, the changes being more pronounced when the first and the second events are analyzed. When the third and the fourth events are observed, the increase of rigidity tends to be smaller. At this time, this observation can be associated with the mobilization of pile tip resistance and the increase stabilizes along time;
- iv) There is a clear trend of increasing the second straight stretch of the curves as the drop height of the hammer increases. Such behaviour is caused by the analyzed blows, which tend to mobilize similar total pile capacities, but as the drop height of the hammer increases (increasing the energy) the *toe quake* also increases.

3.6. Predicted *vs.* measured pile capacity

Comparing the results predicted for shaft resistance with the measured results of all four dynamic load tests, it can be concluded that the predicted results showed to be optimistic for the first (EOD) and second (4.7 days) events. In these cases, the predicted value for shaft resistance closest to the measured value refers to Bustamante & Ganeselli (1982) method from CPT. For the third event (12 days), the predicted values by Aoki & Velloso (1975) and Décourt & Quaresma (1978) methods, both from SPT, were the closest. Finally, for the fourth event (6.4 years), the closest value was predicted by Aoki & Velloso (1975) method

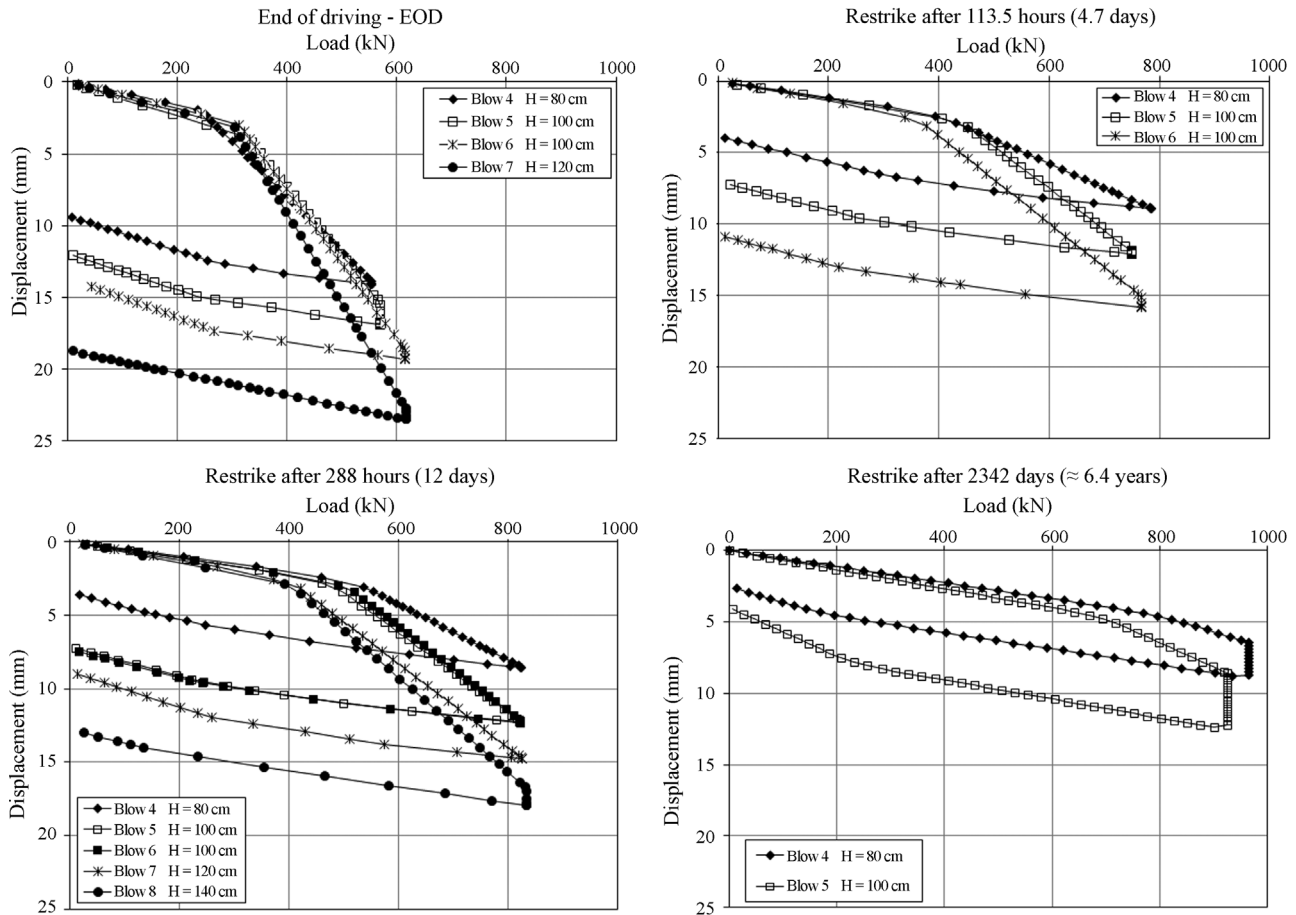


Figure 10 - Simulations of static load tests using CAPWAP program.

from CPT and Aoki & Velloso (1985, 1996) method from SPT.

For tip resistance, the predicted values were lower than the measured results in all tests. The value predicted by Aoki & Velloso (1985, 1996) method from CPT was the closest to the value measured in the first event (EOD), as well as, it was for the results of the other events, in which the tip resistance reached the stabilization.

For pile total capacity, the predicted values from Bustamante & Ganeselli (1982) method from CPT and Aoki & Velloso (1975) from SPT were closer to the measured results for the first (EOD) event. Aoki & Velloso (1975) method from CPT achieved the closest value for the second (4.7 days) event. Aoki & Velloso (1985, 1996) method from SPT reached the closest value for the third event (12 days). To close, Philipponnat (1979) from CPT data obtained the nearest value for the fourth event (6.4 years).

Since the semi empirical methods presented scattered results, the dynamic load test showed to be an useful procedure in the load capacity assessment. Additionally, it showed to be a proper tool for assessing setup. In this way, as Bullock (2008) pointed out, later restrikes tend to provide greater reliability for setup trend analysis.

4. Conclusions

This paper investigated the setup behaviour of a driven pile with the use of dynamic load tests during almost seven years. The study focused on one prestressed concrete pile, installed in a stiff clay experimentation site. It is important to note that a single precast pile element was available for testing. Thus, caution is required in any extrapolation of the procedures or results here described due the lack of a broader statistical significance. Indeed, the conclusions do not apply to other pile types than driven piles.

The results indicated that the shaft resistance increased around 95% and the tip resistance tended to remain stable during the period of testing. The total pile capacity increased approximately 53%. In addition, it could be noted that the increase in pile total capacity was more expressive at the early stages (first days after pile driving). This evidence supports the need for a minimum rest time after pile installation for the acquisition of more reliable information related to the maximum available load capacity.

A linear, normalized, capacity vs. time at logarithmic rate relationship was established to quantify the pile setup process, with t_{EDO} equal to 0.1 day and parameter A equal to 0.217 and 0.131 for shaft and total pile capacity respec-

tively, which showed to be in agreement with the literature database.

In conclusion, the positive effect of the setup when incorporated into a reliability-based framework highlights its potential benefit for the design processes of driven pile foundations.

Acknowledgments

The authors would like to show their gratitude to engineers Alexandre Chwist (Estacas Premold) and Luiz Henrique Olavo (Ensolo) for their support during the pile testing program execution.

References

- Afshin, A. & Rayhani, M.T. (2015). Evaluation of bearing capacity with time for small-scale piles driven into Leda clay. *International Journal of Geotechnical Engineering*, 9(3):307-315.
- Aoki, N. (1989). A new dynamic load test concept. Proc. 12th Int. Conf. on Soil Mechanics and Foundation Engineering, Rio de Janeiro, Brazil, v. 1, pp. 1-4.
- Aoki, N. & Alonso, U.R. (1992). Previsão e comprovação da carga admissível de estacas. Publicação EESC/USP, São Carlos, Brazil, 41 p.
- ASTM D4945 (2012). Standard test method for high-strain dynamic testing of deep foundations, American Society for Testing and Materials, Philadelphia, USA, v. 04:08.
- Attar, I.H. & Fakharian, K. (2013). Influence of soil setup on shaft resistance variations of driven piles: Case study. *International Journal of Civil Engineering, Transaction B: Geotechnical Engineering*, 11(2):113-121.
- Alves, A.M.L.; Lopes, F.R.; Randolph, M.F. & Danziger, B.R. (2009). Investigations on the dynamic behaviour of small diameter pile driven in soft clay. *Canadian Geotechnical Journal*, 46(12):1418-1430.
- Axelsson, G. (1998). Long-term increase in shaft capacity of driven piles in sand. Proc. 4th Int. Conf. on Case Histories in Geotechnical Engineering, ICCHGE, St. Louis, Missouri, Session I - Case Histories of Foundations, pp. 301-308.
- Axelsson, G. & Westin, A. (2000). Torque tests on driven rods for prediction of pile set-up. ASCE Geo-Institute Conference, Geo-Denver, New Technological and Design Developments in Deep Foundations, GSP 100, pp. 297-311.
- Basu, P.; Prezzi, M.; Salgado, R. & Chakraborty, T. (2014). Shaft resistance and setup factors for piles jacked in clay. *Journal of Geotechnical Geoenvironmental Engineering*, 140(3):04013026.
- Bullock, P.J.; Schmertmann, J.H.; McVay, M.C. & Townsend, F.C. (2005a). Side shear setup I: Test piles driven in Florida. *Journal of Geotechnical Geoenvironmental Engineering*, 131(3):292-300.
- Bullock, P.J.; Schmertmann, J.H.; McVay, M.C. & Townsend, F.C. (2005b). Side shear setup II: Results from Florida test piles. *Journal of Geotechnical Geoenvironmental Engineering*, 131(3):301-310.
- Bullock, P.J. (2008). The Easy Button for Driven Pile Setup: Dynamic Testing. From Research to Practice in Geotechnical Engineering, ASCE, Reston, VA, GSP 180, p. 471-488.
- Cintra, J.C.A.; Aoki, N.; Tsuha, C.H.C. & Giacheli, H.L. (2014). Fundações: Ensaio estáticos e Dinâmicos. Oficina de Textos, São Paulo, 144 p.
- Chamecki, P.R.; Kormann, A.C.M.; Nascimento, N.A. & Dyminski, A.S. (1998). Sítio experimental de geotecnia da UFPR - objetivos e dados preliminares. Proc. 11th Congresso Brasileiro de Mecânica dos Solos e Engenharia Geotécnica, COBRAMSEG, Brasília, Brazil, v. 2, pp. 819-826.
- Chow, F.C.; Jardine, R.J.; Naroy, J.F. & Brucy, F. (1998). Effects of time on the capacity of pipe piles in dense marine sand. *Journal Geotechnical Engineering*, 124(3):254-264.
- Doherty, P. & Gavin, K. (2013). Pile Aging in Cohesive Soils. American Society of Civil Engineers, ASCE, *Journal of Geotechnical and Environmental Engineering*, 139(9):1620-1624.
- Fellenius, B.H.; Riker, R.E.; O'Brien, A.O. & Tracy, G.R. (1989). Dynamic and static testing in a soil exhibiting set-up. American Society of Civil Engineers, ASCE, *Journal of Geotechnical Engineering*, 115(7):984-1001.
- Fellenius, B.H. (2008). Effective stress analysis and set-up for shaft capacity of piles in clay, Honoring John Schmertmann "From research to practice in geotechnical Engineering". Lair, J.E.; Crapps, D.K.; Hussein, M.H. (eds), ASCE Geotechnical Special Publication, The Geo-Institute of the American Society of Civil Engineers, GSP 180, Reston, Virginia, pp. 384-406.
- Fleming, K.; Weltman, A.; Randolph, M. & Elson, K. (2009). *Piling Engineering*. Taylor and Francis e-Library, London and New York, 398 p.
- Gerwick Jr., B.C. (1968). Prestressed concrete piles. *PCI Journal*, 13(5):66-133.
- Goble, G. & Hussein, M. (1994). Dynamic pile testing in practice. Proc. 13th Int. Conf. on Soil Mechanics and Foundation Engineering, ICSMFE, New Delhi, India, pp. 713-716.
- Gonçalves, C.; Bernardes, G.P. & Neves, L.F.S. (2007). *Estacas Pré-Fabricadas de Concreto, Teoria e Prática*. Ed. Pini, São Paulo, Brazil, 590 p.
- Hussein, M.H.; Goble, G.G.; Rausche, F. & Likins, G. (1993a). Driving long precast concrete piles. Proc. 14th Int. Cong. of the Precast Concrete Industry, Washington, D.C., 8 p.

- Hussein, M. & Likins, G. (1995). Dynamic testing of piles foundation during construction. Proc. 13th ASCE Structures Congress, Restructuring: America and Beyond, Boston, Massachusetts, USA, pp. 1350-1364.
- Hussein, M.H.; Likins, G.E. & Hannigan, P.J. (1993b). Pile evaluation by dynamic testing during restrike. Proc. 11th Southeast Asian Geotechnical Conference, SEAGS, Singapore, pp. 535-539.
- Komurka, V.E. & Wagner, A.B. (2003). Estimating soil/pile set-up. Wisconsin Highway Research Program, Report 0092-00-14, Wisconsin Department of Transportation, 58 p.
- Kormann, A.C.M. (1999). Comportamento de argilas rijas: aspectos geotécnicos da Formação Guabirotuba. Proc. Mesa Redonda Características Geotécnicas da Formação Guabirotuba, Curitiba, Brazil, pp. 119-128.
- Kormann, A.C.M. (2002). Geomechanical Behaviour of Guabirotuba Geological Formation: Field and Laboratory Tests. PhD Thesis, Departamento de Engenharia de Estruturas e Fundações, Escola Politécnica da Universidade de São Paulo, São Paulo, Brazil, 429 p.
- Kormann, A.C.M.; Chamecki, P.R.; Antoniutti Neto, A. & Russo Neto, L. (2000). Ensaio de carregamento dinâmico: Avaliações do set-up de uma estaca cravada em argila sobreadensada. Proc. Simpósio de prática de Engenharia Geotécnica da Região Sul, Geosul, Porto Alegre, Brazil, v. 1, pp. 43-51.
- Lee, W.; Kim, D.; Salgado, R. & Zaheer, M. (2010). Setup of driven piles in layered soil. *Soils and Foundations*, 50(5):585-598.
- Likins, G.; Rausche, F. & Peterman, D. (1992). Dynamic pile testing and analysis using expert system methods. Proc. 4th Int. Conf. on the Application of Stress-Wave Theory to Piles, The Hague, Netherlands, pp. 429-432.
- Lim, J.K. & Lehane, B.M. (2014). Set-up of pile shaft friction in laboratory chamber tests. *International Journal of Physical Modelling in Geotechnics*, 14(2):21-30.
- Negro, A.; Namba, M.; Dyminski, A.S.; Sanches, V.L. & Kormann, A.C.M. (2012). Twin Cities: Solos das Regiões Metropolitanas de São Paulo e Curitiba. D'Livros, São Paulo, 432 p.
- Ng, K.W.; Roling, M.; AbdelSalam, S.S.; Suleiman, M.T. & Sritharan, S. (2013a). Pile setup in cohesive soil I: Experimental investigation. *Journal of Geotechnical and Geoenvironmental Engineering*, 139(2):199-209.
- Ng, K.W.; Suleiman, M.T. & Sritharan, S. (2013b). Pile setup in cohesive soil II: Analytical quantifications and design recommendations. *Journal of Geotechnical and Geoenvironmental Engineering*, 139(2):210-222.
- Paikowski, S.G.; Birgisson, B.; Mcvay, M.; Nguyen, T.; Kuo, C.; Baecher, G.; Ayyub, B.; Stenersen, K.; O'Malley, K.; Chernauskas, L. & O'Neill, M. (2004). Load and resistance factor design (LRFD) for deep foundations. Report 507, National Cooperative Highway Research Program NCHRP, Transportation Research Board, Washington, D.C, USA, 87 p.
- Paikowski, S. & Chernauskas, L. (1996). Soil inertia and the use of pseudo viscous damping parameters. Proc. 5th Int. Conf. on the Application of Stress-Wave Theory to Piles, Orlando, Florida, Session 4 - Wave Equation Models, pp. 203-216.
- PDI, Pile Dynamics, Inc. (2003). PDA-W Users Manual. Cleveland, Ohio, USA.
- PDI, Pile Dynamics, Inc. (2006). CAPWAP Manual. Cleveland, Ohio, USA.
- Pile Driving Contractor's Association - PDCA (2007). Installation Specification for Driven Piles. PDCA Specification 103-07, www.piledrivers.org, USA.
- Rimoy, S.; Silva, M.; Jardine R.; Yang, Z.X.; Zhu, B.T. & Tsuha, C.H.C. (2015). Field and model investigations into the influence of age on axial capacity of displacement piles in silica sands. *Geotechnique*, 65(7):576-589.
- Robinson, B.; Iskander, M. (2008). Static and dynamic load tests on driven polymeric piles. Proc. Annual Congress of the Geo-Institute of ASCE, GeoCongress, New Orleans, Louisiana, USA, pp. 939-946, accessed in November 2015.
- Salamuni, E. (1998). Tectônica da Bacia Sedimentar de Curitiba (PR). PhD Thesis, Instituto de Geociências e Ciências Exatas, Universidade Estadual Paulista, Rio Claro, Brazil, 214 p.
- Salgado, R. (2008). *The Engineering of Foundations*. McGraw-Hill, New York, 896 p.
- Skov, R. & Denver, H. (1988). Time-dependence of bearing capacity of piles. Proc. 3rd Int. Conf. on the Application of Stress-Wave Theory to Piles. Fellenius, B.H. (ed), BiTech Publishers (Vancouver, BC.), Ottawa, Canada, pp. 1-10.
- Smith, E.A.L. (1960). Pile Driving Analysis by the Wave Equation. *Journal of the Soil Mechanics and Foundations Division, ASCE*, 86:35-64.
- Steward, E. & Wang, X. (2011). Predicting pile setup (Freeze): A new approach considering soil aging and pore pressure dissipation. Proc. Geo-Frontiers Conference 2011, Advances in Geotechnical Engineering, The Geo-Institute of the American Society of Civil Engineers - GSP 211, Dallas, Texas, USA, pp. 11-19.
- Tan, S.L.; Cuthbertson, J. & Kimmerling, R.E. (2004). Prediction of pile setup in non-cohesive soil, current practices and future trends in deep foundations. DiMaggio,

- J.H. & Hussein, M.H. (eds), ASCE Geotechnical Special Publication, The Geo-Institute of the American Society of Civil Engineers - GSP 125, Reston, Virginia, pp. 50-65.
- Tomlinson, M.J. (1994). Pile Design and Construction Practice. E and FN Spon, London, 411 p.
- Yan, W.M. & Yuen, K.V. (2010). Prediction of pile set-up in clays and sands. IOP Conf. Series: Materials Science and Engineering, 10(1):012104.
- York, D.L.; Brusey, W.G.; Clementesoi F.M. & Law, S.K. (1994). Setup and relaxation in glacial sand. Journal of Geotechnical Engineering, 120(9):1498-1513.

Study of the Shear Strength of a Tropical Soil with Grass Roots

M.I. Miranda Neto, C.F. Mahler

Abstract. The role of roots in shear strength has been a matter of research and also uncertainties. An investigation was conducted to identify and quantify the contribution of the roots of vetiver grass (*Chrysopogon zizanioides*) to the shear strength of soils, by means of triaxial testing. Samples were prepared from 4-inch PVC pipe molds, where tropical soil was compacted and specimens of vetiver seedlings, obtained by tillering, were grown. After 24 months of growth, from each mold of the mature vetiver grass it was possible to get at least four samples with roots inside. Similar samples of the same soil without vetiver grass were submitted to triaxial tests to determine shear strength of soil alone. Confining pressure ranging from 25 to 200 kPa was used in triaxial extension drained tests to determine a Mohr-Coulomb envelope. The shear strength parameters of soil without roots, cohesion intercept and friction angle were respectively 13 kPa and 34° , and the Mohr-Coulomb envelope of the soil with vetiver roots showed a bilinear shape with cohesion and friction angle, respectively, of 17 kPa and 59° for confining pressure below 75 kPa and 22 kPa and 33° for confining pressure above 75 kPa. So an increase in shear strength was obtained, because the roots acted to reinforce the soil mass. Triaxial compression tests were conducted in the same soil with and without roots and no significant increase in resistance was observed. The result was observed due to a vertical spread of roots, since any reinforcement in the same direction of the compressive force does not contribute to increase the strength. In conclusion, for extensional stress above 75 kPa confining pressure, the friction angle was the same as that of the soil without roots, although the intercept of cohesion was larger. Below 75 kPa, the soil showed a very large apparent friction angle due to the roots. Therefore, vetiver roots increase the shear strength in soils under extensional loadings.

Keywords: soil reinforced, soil stabilization, vetiver grass, triaxial extension test, tropical soil strength parameters, bioengineering.

1. Introduction

Many contributions have been made in recent decades to improve knowledge about the behavior of soil reinforced with metal or synthetic or natural fibers such as roots, subjected to direct shear or triaxial compression tests. One of the pioneering studies in this respect was performed by Gray & Ohashi (1983). They concluded that the main role of fibers is to increase the soil shear strength, and that a confining pressure exists below which the fiber has a tendency of be pulled out of the soil. Later, Gray & Al-Refeai (1986) indicated that rougher fibers tend to be more effective in increasing the shear strength and Maher & Gray (1990) showed that bilinear shearing envelopes of reinforced soils have a breaking point, named the critical confining pressure, below which the reinforcement tends to be pulled out.

After Gray & Ohashi (1983), other researchers (Michalowski & Zhao, 1996; Zornberg, 2002; Michalowski & Cermák, 2003; Heineck & Consoli, 2004; Gao & Zhao, 2013) have carried out theoretical studies to develop predictive models of the improvement of shear strength due to the addition of fibers in the soil. Some researchers have fo-

cused on the behavior of the addition of discrete randomly distributed synthetic fibers (Freitag, 1986; Feuerharmel, 2000; Casagrande, 2001; Casagrande & Consoli, 2002; Heineck *et al.*, 2005; Casagrande, 2005; Consoli *et al.*, 2007; Sadek *et al.*, 2010; Palacios, 2012), fibers and cement (Consoli *et al.*, 1998), or natural fibers from vetiver roots (Focks, 2006; Barbosa, 2012).

This study is another contribution to knowledge of the behavior of reinforced soil. This article examines the behavior of a tropical soil with natural inclusion of vetiver grass roots subjected to extensional forces. Since the roots' preferential direction is vertical, it is expected that soil reinforced with predominantly vertical roots subjected to triaxial compression tests should behave differently than reinforced soil under triaxial extension tests. Therefore, given that the root system is predominantly vertical, the extension test would better simulate the role of the roots in the reinforcement of the soil than compression tests since they would not be subject to buckling. In geotechnics, the axial extension would be, for example, an unloading by excavation and the lateral extension would be from passive earth pressure by jack reaction or earthquake.

Manoel Isidro de Miranda Neto, D.Sc., Associate Professor, Departamento de Engenharia Civil, Universidade Federal Fluminense, Niterói, RJ, Brazil. e-mail: manoel.isidro@gmail.com.

Claudio Fernando Mahler, D.Sc., Full Professor, Departamento de Engenharia Civil, Universidade Federal do Rio de Janeiro, Rio de Janeiro, RJ, Brazil. e-mail: mahler@coc.ufrj.br.

Submitted on May 25, 2016; Final Acceptance on March 16, 2017; Discussion open until August 31, 2017.

The main objective is to evaluate the contribution of vetiver roots on the shear strength of a tropical soil, especially through triaxial extension tests.

The use of natural fibers such as plant roots as reinforcement inclusions in soil, particularly for slope stabilization, has been proposed as an effective bioengineering method. However, solutions involving plants usually face problems such as the range of the root system, the low growth rate of the plant until the root system reaches maturity, the susceptibility of the plants to damage such as fire, drought and vandalism, and also the introduction of alien species in the environment, all of which can discourage their use in engineering projects.

Vetiver grass is well known for its tolerance to aggressive environments and rapid growth rate. Also, its roots can reach several meters and it is resistant to disease. These traits have caused its planting to be recommended as an effective method to stabilize slopes (Truong, 2000).

The bioengineering solutions for reestablishing vegetation using grasses are quite effective in erosion control, but some doubts still exist as to slope protection against sliding. Knowledge is incomplete about how much increase in shear strength is provided by the introduction of roots in the soil. In practical terms, if the shear strength parameters of a slope reinforced with roots are properly known, the increase in the safety factor can be assessed more accurately.

2. Materials and Methods

This study involved triaxial strength tests on soils with and without vetiver roots. The insertion of the roots as reinforcement in the soil was done by growing grass in tubular molds with 98 mm inner diameter and 1.0 m length, previously filled with compacted soil. Tubes containing compacted soil without grass were used as controls. Each tube was prepared with 14 layers of 6 cm soil at 23% average moisture using 11 blows of a 2 kilogram hammer at 50 cm of drop distance. Therefore, to prevent root growth the compaction energy used in the preparation of samples was $2.3 \text{ kg}\cdot\text{cm}/\text{cm}^3$, approximately half of the normal Proctor energy.

The tubular molds made it possible to extract up to four specimens to perform triaxial tests. These molds had a 5 cm layer of granular base, which functioned as a filter, buffered with a pierced end cap to allow drainage of water. The top of the mold had a free edge of about 5 cm to allow a suitable depth of the water level in irrigation of the crop. Figure 1 shows the molds with vetiver grass.

The plants were obtained by clump division. Two clumps of grass generated 20 seedlings, each one planted in a mold with compacted soil. The molded soil void ratio ranged from 0.68 to 0.79, dry unit weight ranged from 1.63 to $1.53 \text{ g}/\text{cm}^3$ and average density of solid constituents was $2.75 \text{ g}/\text{cm}^3$. This soil was collected in the alluvial fan resulting from the gully erosion into the mantle of tropical residual/colluvium soil formed by weathering from mica-schists and gneisses, constituting the geological setting from Meso/Neoproterozoic era named the Búzios complex in



Figure 1 - Vetiver grass grown in molds with age of 18 months (near the second flowering).

Rio de Janeiro, Brazil. The particle size distribution consisted of 10% gravel, 72% sand, 10% silt and 8% clay. The cation-exchange capacity was $4.45 \text{ cmol}/\text{kg}$, $\text{pH} = 5.1$ and $K_i = 2.05$ suggesting a tropical soil. In terms of mineralogy, the soil contains kaolinite, muscovite, quartz and weathered feldspar. The low amount of clay is related to the leaching processes in the alluvial fan.

The molds were watered weekly, including those without vetiver grass, and they were kept in a greenhouse until the stem of the plant exceeded one meter in height. Then the molds were left outdoors exposed to the weather, with continued weekly watering. The vetiver grass was planted in October 2011 and the first flowering occurred in July 2012, indicating that the plants had reached maturity. The first triaxial test was carried out when the specimens were a little over two years old, and were repeated from January to December 2014.

The specimens for triaxial tests were extracted from the base to top of the mold, keeping the plants alive for further withdrawal of samples. Figure 2 shows the sampling sequence. The tests were performed on the same day of sampling so that the roots had some vitality when tested. At the end of the test, the roots were exhumed and their general condition, mass and moisture were measured along with the amount of roots with diameter greater than 0.4 mm. The cross sectional root area was obtained by computing all roots greater than 0.4 mm in diameter, which accounted for more than 90% of the total root mass. The fiber area ratio was defined as the ratio of fiber total cross-sectional area and sample cross-sectional area.

The drained triaxial compression tests were performed on specimens measuring 98 mm in diameter and height of approximately 18 cm. The degree of saturation was checked by pore pressure parameter, B , corresponding to 0.95, obtained by backpressures of 600 kPa. For confining pressure of 25 kPa the maximum incremental back pressure was 25 kPa to avoid over consolidation during the process. For the remaining confining pressures (50, 75,

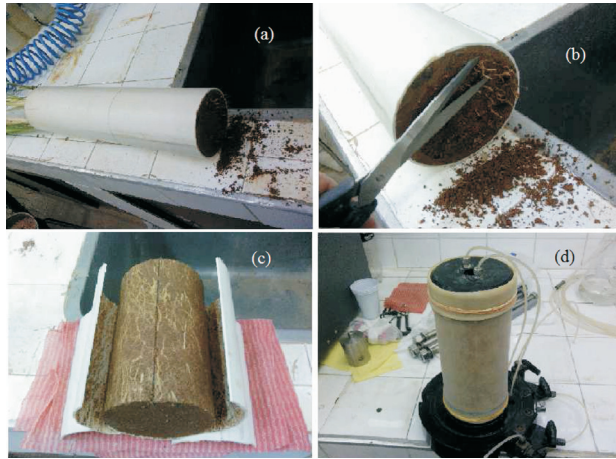


Figure 2 - The sampling: (a) cutting the sample; (b) trimming the roots left out; (c) removing the PVC layer; (d) assembling the sample in the triaxial cell.

100, 150 and 200 kPa), the counter pressure increments were 40 kPa.

The hydrostatic consolidation pressures applied were 25, 50, 75, 100, 150 or 200 kPa, depending on the stress level of the test. The shear phase consisted in applying axial loading maintaining pressure in the triaxial cell until rupture, normally characterized by no increment in deviator stress and in volume change with axial deformation. The velocity of loading was controlled by strain at a rate of 0.17%/min.

Attempts to run triaxial extension drained loading tests failed. In this test, after the hydrostatic consolidation, the loading is applied by increasing the confining pressure and maintaining the axial stress. This stress path aims to simulate the jack reaction of an earth support system. The back-pressures were high, about 600 kPa, to ensure high degree of saturation, and the long stress path was interrupted before rupture due to reaching the maximum pressure of the triaxial cell. For this reason, triaxial extension drained unloading tests in the shear phase were performed.

In the triaxial extension drained unloading test, the saturation and consolidation phase were similar to compression tests. The shear phase was run maintaining the confining pressure and reducing the axial load until failure. The sample stretched as a process of extension by excavation. The speed of unloading was initially controlled by the axial stress, at the ratio of -0.2 kPa/min until the strain rate reached -0.02%/min. From there on, the unloading control was by strain ratio of -0.02%/min until failure. The negative sign means axial discharge or extensional displacement. These lower rates in the triaxial extension unloading tests were obtained experimentally and prevented the top porous stone from detaching from the sample during the shear phase.

3. Results and Discussion

In this work, 31 triaxial extension drained unloading tests were carried out: 10 tests on samples without roots and 21 tests on samples with roots (two of the samples with roots were discarded after statistical analysis). Details of statistical treatment can be found in Miranda Neto (2015).

Also, 21 drained compression triaxial tests were performed: 12 tests on samples without roots and 9 on samples with roots. Figures 3 and 4 show respectively stress-strain curves for the extension tests on samples with roots and without roots.

In the triaxial extension tests, the major principal effective stress (σ'_1) is the effective confining stress (σ'_b), the axial strain by stretching (ϵ_a) is negative and the effective axial stress (σ'_v) is the minor principal effective stress (σ'_3).

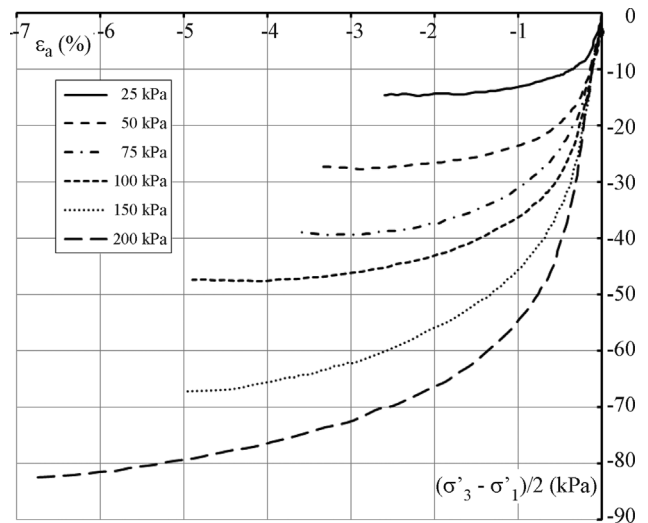


Figure 3 - Stress-strain curves of soil with roots for confining stress from 25 to 200 kPa.

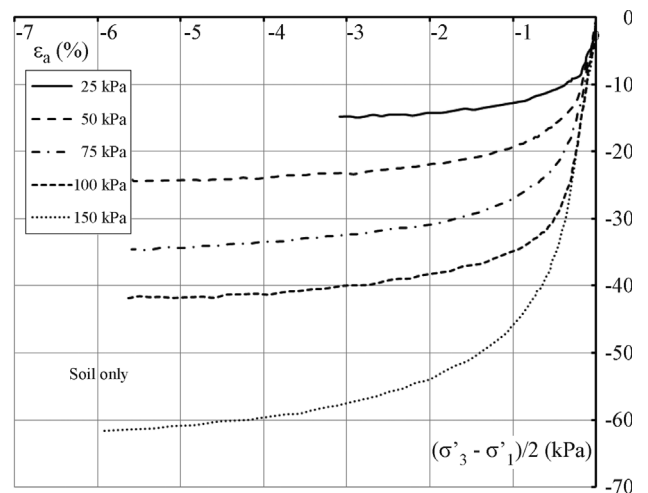


Figure 4 - Stress-strain curves of soil only for confining stress from 25 to 150 kPa.

The deviator stress (σ'_d) is negative both in the loading and unloading extension tests.

The comparison of the Figs. 3 and 4 for the same shear stress shows that the soil without roots deformed more than the soil with roots. On the other hand, for the same strain, for example 2%, the soil with roots exhibited shear strength greater than the soil alone. The exception was for the confining pressure of 25 kPa, when both soils had similar behavior.

Furthermore, for the soil with roots, when the confining pressure increased, the strain at failure became larger. The soil under low confining pressure had brittle behavior and the soil at high confining stress had ductile behavior. This behavior is similar to that of loose and dense sands described by Lee & Seed (1967), due to the critical confining pressure and critical void ratio.

The samples of soil with roots had void ratio after consolidation phase ranging between 0.69 and 0.78. This is not reason enough to determine such different behavior between samples. Nevertheless, the tests at higher confining pressures were conducted on samples with smaller void ratios, and to avoid the dilatancy effect on shear strength, the samples tested at low confining pressures had higher void ratios.

For soil without roots, with the exception of the sample tested at confining pressure of 25 kPa, whose strain at failure was 2.5%, the rupture fell between 5 and 6% of axial strain.

Figure 5 shows that only the samples tested at confining pressure below 75 kPa exhibited a smooth dilatant behavior at shear, despite higher void ratios than samples tested at confining pressure above 75 kPa.

The data from the triaxial extension drained unloading tests performed on soil samples without roots are represented in the p-q diagram of Fig. 6. Figure 7 shows the results for the soil tests with roots.

Figure 6 establishes a Mohr-Coulomb strength envelope with -12.5 kPa for cohesion intercept and -34.6° for internal friction angle in the soil without roots.

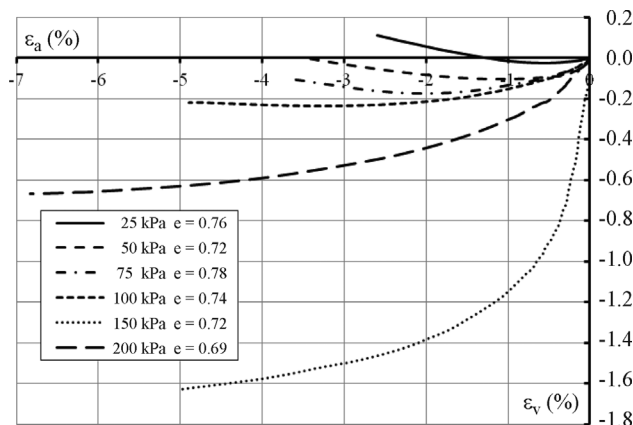


Figure 5 - Volumetric changes of soil with roots for confining stress from 25 to 200 kPa.

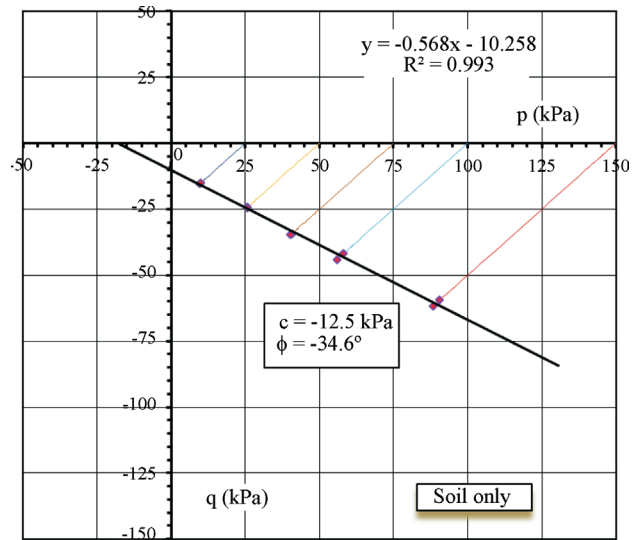


Figure 6 - Mohr-Coulomb envelope in p-q diagram for soil only.

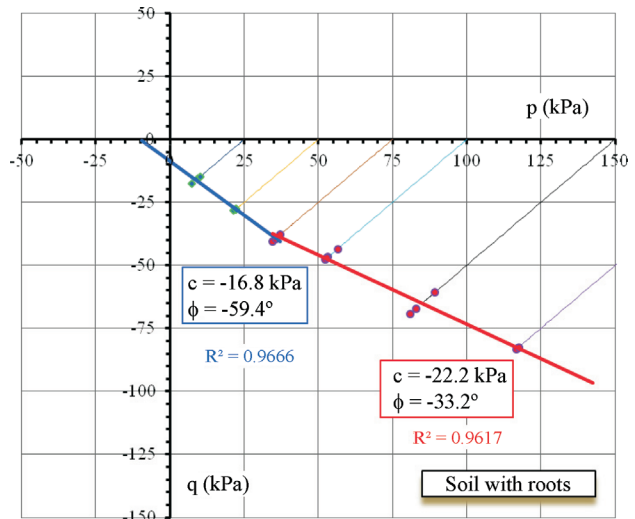


Figure 7 - Mohr-Coulomb envelope in p-q diagram for soil reinforced with roots.

In the p-q diagram of Fig. 7, the triaxial extension drained unloading tests performed on samples of soil with roots showed that above 75 kPa of confining pressure, a Mohr-Coulomb strength envelope could be modeled with similar slope to the soil without roots and with linear coefficient of -22.2 kPa, which corresponds to an extrapolation of the envelope for zero confining pressure, called cohesion intercept.

Below 75 kPa of confining pressure, an initial segment of the envelope could be modeled with the results of tests performed at confining pressures of 25, 50 and 75 kPa. This fitted branch could provide the shear strength parameters, internal friction angle of -59.4° and cohesion intercept of -16.8 kPa. Therefore, the envelope for the soil with roots was modeled as bilinear, with change of slope at the confining pressure of 75 kPa.

The bilinear envelope was reported long ago as a characteristic of reinforced soil (Gray & Ohashi, 1983, Gray & Al-Refeai, 1986 and Maher & Gray, 1990). Gray & Ohashi (1983), by performing direct shear testing on reinforced sands, concluded that the fibers under low confining pressure tend to be pulled out and the soil exhibits a higher friction angle. Above a threshold stress, the internal friction angle of the soil is not affected by the fiber and the envelope has the same internal friction angle for both the soil alone and reinforced soil.

For confining pressure above 75 kPa, the friction angle of soil reinforced with roots was the same as soil without reinforcement, although in modeling the Mohr-Coulomb envelope, the cohesion parameter, which corresponds to the linear coefficient, was different from one sample to another. In both cases, the cohesion was here taken as a cohesion intercept and not a cementation or real cohesion. This does not mean that the fibers give cohesion to the soil. There may be some aggregation, but the envelope model presented a greater intercept of cohesion for confining pressure above 75 kPa.

Also in the initial portion of the envelope, the soil with roots presented a friction angle greater than that of the soil alone. The cohesion intercept of -16.8 kPa for the reinforced soil was slightly different from the value of -12.5 kPa for soil alone. This difference, although small, might be due to a cohesive woof formed by the roots.

Miranda Neto (2015) showed that the turning point in the Mohr-Coulomb envelope for extension tests in soil with roots occurs at normal stress at failure $\sigma_N = 5.2$ kPa and shear strength $\tau = -25.6$ kPa. For confining pressures ($\sigma'_1 = \sigma'_2 = \sigma'_3$) of 25, 50 and 75 kPa, the respective minor main effective stresses ($\sigma'_v = \sigma'_3$) are negative and represent a plausible stress state in the triaxial test, but are not feasible in situ, for example, in case of slope analysis and stabilization. Figure 8 illustrates that the stress state where the minor effective principal stress (vertical) is zero corresponds to a major effective principal stress (confining pressure) of 82.2 kPa at failure and a shear strength of -34.2 kPa. The vertical effective stress equal to zero in a geostatic stress is the ground surface. Therefore, in this

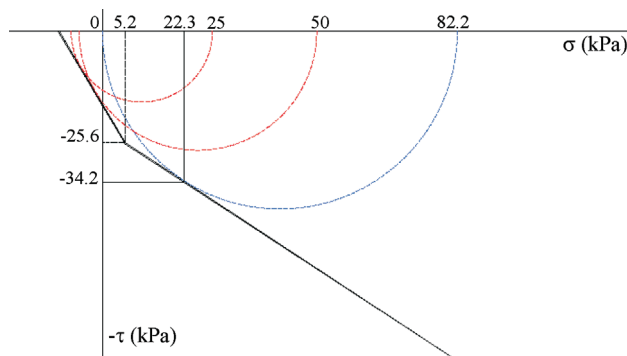


Figure 8 - Mohr-Coulomb envelope in $\tau - \sigma$ space for extension test with roots.

case, the occurrence of the first branch of the envelope is not feasible.

Complementing this study of shear envelope, were also performed triaxial compression drained tests on samples of soil with roots and without roots at confining stresses ranging from 25 to 150 kPa. The results are shown in Fig. 9.

There were no significant variations observed in the triaxial compression drained tests for the samples either with or without roots. The adjustments of the envelopes resulted in sufficiently straight lines to discard the bilinear model for this compression case. This can be explained by the predominantly vertical architecture of the root system, as seen in Fig. 10 (d). The samples with roots in the axial direction, the same direction as the compressive stress deviation ($\sigma'_1 - \sigma'_3$), did not show effective participation of roots in shear strength. Even though the stress state in the triaxial cell induced a shear plane inclined with respect to the preferred direction of the roots, the soil showed similar shear strength with and without roots in the compression tests.

In these triaxial compression tests, the peripheral roots forced the rubber membrane and buckled it even against the confining pressure in the triaxial cell, as seen in Fig. 10 (b). Wu *et al.* (1988) concluded: “In compression, the roots failed by buckling”. This phenomenon seems to have occurred in these triaxial compression tests.

Figure 10 (a) illustrates a sample of soil without roots in extension for 200 kPa confining pressure, showing stretching and a set of failure planes; (b) illustrates a specimen subjected to triaxial compression with roots showing buckling; (c) shows general aspects of the roots taken from a specimen; and (d) shows a mold with partially removed soil showing the root system architecture.

Note in Fig. 10 (a) that the planes of failure for samples submitted to extension testing are close to orientation of slip lines for Rankine passive state (Lambe & Whitman,

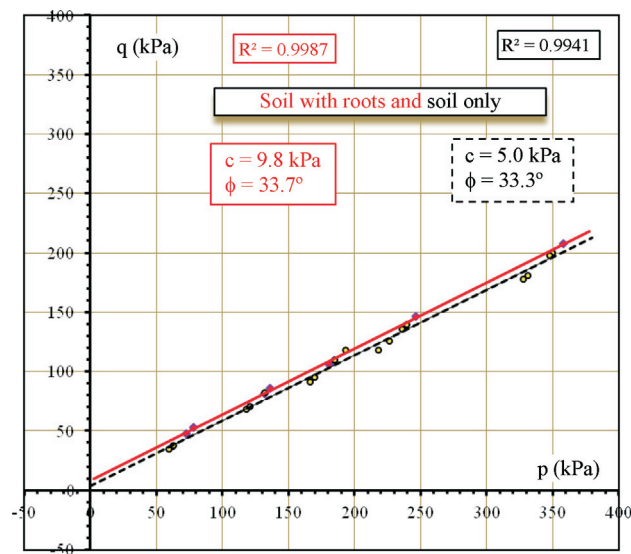


Figure 9 - Mohr-Coulomb envelope in $p-q$ diagram for triaxial drained compression tests.

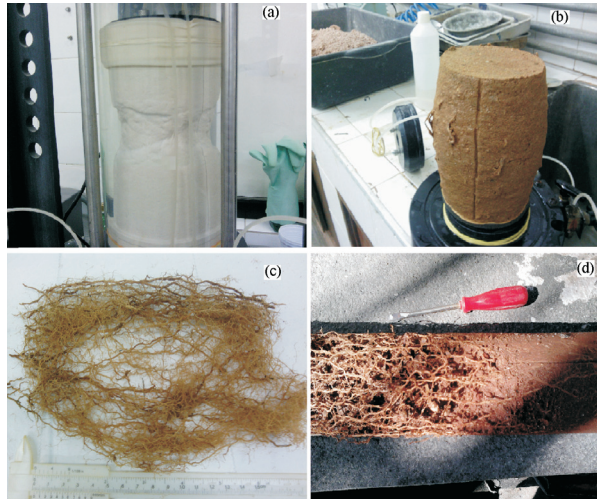


Figure 10 - (a) sample of soil at failure; (b) buckling of the roots; (c) roots of one sample; (d) root system architecture.

1969). In triaxial compression tests, these planes are steeper. The planes of failure are not orthogonal to the preferential direction of the roots.

Figure 10 (c) shows the roots from a sample subjected to extension testing at confining pressure above 75 kPa. There is no evidence that the roots were broken. Gray & Ohashi (1983) considered that the reinforcement does not break because it is more extensible than the soil: “Inclusions have rupture strains larger than the maximum tensile strains in the soil without inclusions.” Therefore, assuming that the roots are more extensible than the soil, these roots cannot rupture regardless of their ultimate strength or the imposed load (Gray & Ohashi, 1983).

The fiber area ratio of the samples with roots ranged from 0.28% to 0.74%, close to the fiber area ratios tested by

Gray & Ohashi (1983). Most tests in this study were run at fiber area ratio of 0.45%.

Since the fiber area rates were similar for most samples, it was not possible to analyze in this respect the most brittle behavior of the samples at confining pressures up to 75 kPa, especially for 50 and 75 kPa, which showed less strain at failure for soil with roots than soils without roots. This is a matter for more detailed research, due to issues related with the dilatancy effects at low confining stress (Lee & Seed, 1967) and the fiber aspect ratio (Maher & Gray, 1990) or fiber content (Gray & Al-Refeai, 1986).

Using the strength parameters obtained in this study, Miranda Neto (2015) performed a stability analysis by slice method on a naked slope and a slope using vetiver grass and verified that the gain in the safety factor for circular surface was of the order of 16%.

Table 1 shows an individual gain in shear strength for some levels in effective normal stress at failure (σ'_N) for extension test while Table 2 shows the same gain in shear strength for compression testing. There is a reduction in the gain with the increase of the tension level for extension testing.

4. Conclusions

Triaxial drained tests were performed on soil samples with roots and without roots of vetiver grass, grown naturally in molds. Test results showed that vetiver roots can increase shear strength of the soil used in this study and the following conclusions emerged.

The vetiver roots increased the shear strength of the soil for extension unloading up to 30% near ground surface and decreased with depth until less than 7% close to the extremity of the root system.

For compression loading, the increase in shear strength was less than 24% near the ground surface and decreased to less than 8% close to the end of the root system.

Table 1 - Gain in shear strength by stress level in extension test.

σ'_N (kPa)	Soil with roots		Soil only		τ_{root} (kPa)	τ_{soil} (kPa)	τ_{root}/τ_{soil} (%)
	c (kPa)	ϕ°	c (kPa)	ϕ°			
25	-22.2	-33.2	-12.5	-34.6	-38.5	-29.7	30
50	-22.2	-33.2	-12.5	-34.6	-54.9	-47.0	17
75	-22.2	-33.2	-12.5	-34.6	-71.3	-64.2	11
100	-22.2	-33.2	-12.5	-34.6	-87.6	-81.5	7.5

Table 2 - Gain in shear strength by stress level in compression test.

σ'_N (kPa)	Soil with roots		Soil only		τ_{root} (kPa)	τ_{soil} (kPa)	τ_{root}/τ_{soil} (%)
	c (kPa)	ϕ°	c (kPa)	ϕ°			
25	9.8	33.7	5.0	33.3	26.5	21.4	24
50	9.8	33.7	5.0	33.3	43.1	37.8	14
75	9.8	33.7	5.0	33.3	59.8	54.3	10
100	9.8	33.7	5.0	33.3	76.5	70.7	8

The contribution of vetiver roots in this soil for extension unloading increased the cohesion intercept for confining stress above 75 kPa. Below 75 kPa, despite an increase in frictional angle, no effective contribution is possible because it is not a feasible stress state.

The vetiver roots in soil acted as extensible reinforcements.

Since the length of these roots is at most 4 m, the effective improvement caused by the roots only applies to the topsoil. Nevertheless, the improvement of topsoil can cause an increase in overall slope stability of 16%.

Acknowledgments

The authors thank the continued support of FAPERJ, CAPES and CNPq.

References

- Barbosa, M.C.R. (2012). Study on Application of Vetiver Grass in the Improvement of the Shear Strength Parameters of Slope Soils. PhD Thesis, Federal University of Ouro Preto, Ouro Preto, 128 p. (In Portuguese).
- Casagrande, M.D.T. (2001). Study on Behavior of a Reinforced Soil with Polypropylene Fibers Aiming at the Use as Base of Shallow Foundations. MSc Dissertation, Federal University of Rio Grande do Sul, Porto Alegre, 94 p. (In Portuguese).
- Casagrande, M.D.T. (2005). Performance of Soils Reinforced with Fibers Submitted to Large Strains. PhD Thesis, Federal University of Rio Grande do Sul, Porto Alegre, 219 p. (In Portuguese).
- Casagrande, M.D.T. & Consoli, N.C. (2002). Study on behavior of a silt sandy soil reinforced with polypropylene fibers. *Soils and Rocks*, 25(3):223-230.
- Consoli, N.C.; Prietto, P.D.M. & Ulbrich, L.A. (1998). Influence of fiber and cement addition on behavior of sandy soil. *Journal of Geotechnical and Geoenvironmental Engineering*, ASCE 124(12):1211-1214.
- Consoli, N.C.; Heineck, K.S.; Casagrande, M.D.T. & Coop, M.R. (2007). Shear strength behavior of fiber-reinforced sand considering triaxial tests under distinct stress paths. *Journal of Geotechnical and Geoenvironmental Engineering*, ASCE 133(11):1466-1469.
- Feurharmel, M.R. (2000). Behavior of Soils Reinforced with Polypropylene Fibers. MSc Dissertation, Federal University of Rio Grande do Sul, Porto Alegre, 131 p. (In Portuguese).
- Focks, D.J.J. (2006). Vetiver Grass as Bank Protection Against Vessel-Induced Loads. MSc Dissertation, Delft University of Technology, Faculty of Civil Engineering and Geosciences, Delft, 95 p.
- Freitag, D.R. (1986). Soil randomly reinforced with fiber. *Journal of Geotechnical and Geoenvironmental Engineering*, ASCE 112(8):823-826.
- Gao, Z. & Zhao, J. (2013). Evaluation on failure of fiber-reinforced sand. *Journal of Geotechnical and Geoenvironmental Engineering*, ASCE 139(1):95-106.
- Gray, D.H. & Ohashi, H. (1983). Mechanics of fiber reinforcement in sand. *Journal of Geotechnical and Geoenvironmental Engineering*, ASCE 109(3):335-353.
- Gray, D.H. & Al-Refeai, T. (1986). Behavior of fabric vs. fiber reinforced sand. *Journal of Geotechnical and Geoenvironmental Engineering*, ASCE 112(8):804-820.
- Heineck, K.S. & Consoli, N.C. (2004). Discussion to discrete framework for limit equilibrium analysis of fibre-reinforced soil. *Geotechnique*, ICE 54(1):72-73.
- Heineck, K.S.; Coop, M.R. & Consoli, N.C. (2005). Effect of microreinforcement of soils from very small to large strains. *Journal of Geotechnical and Geoenvironmental Engineering*, ASCE 131(8):1024-1033.
- Lambe, T.W. & Whitman, R.V. (1969). *Soil Mechanics*. John Wiley & Sons, New York, 165 p.
- Lee, K.L. & Seed, H.B. (1967). Drained strength characteristics of sands. *Journal of the Soil Mechanics and Foundations Division*, ASCE 93(6):117-141.
- Maher, M.H. & Gray, D.H. (1990). Static response of sand reinforced with randomly distributed fibers. *Journal of Geotechnical and Geoenvironmental Engineering*, ASCE 116(11):1661-1677.
- Michalowski, R.L. & Zhao, A. (1996). Failure of fiber-reinforced granular soils. *Journal of Geotechnical and Geoenvironmental Engineering*, ASCE 122(3):226-234.
- Michalowski, R.L. & Cermák, J. (2003). Triaxial compression of sand reinforced with fibers. *Journal of Geotechnical and Geoenvironmental Engineering*, ASCE 129(2):125-136.
- Miranda Neto, M.I. (2015). Contribution of Vetiver Grass Roots in Shear Strength of Sandy Soil. PhD Thesis, COPPE/PEC Federal University of Rio de Janeiro, Rio de Janeiro, 225 p. (In Portuguese).
- Palacios, M.A.P. (2012). Behavior of Sand Reinforced with Polypropylene Fiber Submitted to Triaxial Extension Tests. Master Dissertation, Pontifical Catholic University of Rio de Janeiro, Rio de Janeiro, 101 p. (In Portuguese).
- Sadek, S.; Najjar, S.S. & Freiha, F. (2010). Shear strength of fiber-reinforced sands. *Journal of Geotechnical and Geoenvironmental Engineering*, ASCE 136(3):490-499.
- Truong, P. (2000). The Global Impact of Vetiver Grass Technology on the Environment. Proceedings of the Second International Conference on Vetiver, Office of the Royal Development Projects Board, Bangkok, pp. 48-61.
- Wu, T.H.; McOmber, R.M.; Erb, R.T. & Beal, P.E. (1988). Study of soil-root interaction. *Journal of Geotechnical and Geoenvironmental Engineering*, ASCE 114(12):1351-1375.
- Zornberg, J.G. (2002). Discrete framework for limit equilibrium analysis of fibre-reinforced soil. *Geotechnique*, ICE 52(8):593-604.

Cavity Expansion Analysis to Predict Side Shear Set-Up in Clayey Soils

P.C.R. Silva, F. Massad

Abstract. In this study, fifty driven piles located in the Santos Coastal Plain (“Baixada Santista”), Brazil, have been dynamically tested at various times after installation, indicating gain of capacity over time. The average side shear resistance, related to a low-OCR clayey layer – known as SFL soil, was evaluated over time, indicating side shear set-up within a relatively narrow range of values (between 2.0 and 2.5) approximately 20 days after installation. The cavity expansion theory, which considers an ideal cohesive soil, has been used to predict the effective radial stress over time, considering two main parameters: undrained shear strength and horizontal coefficient of consolidation. Finally, the average of measured pile shaft capacities were compared to the unit shear resistances predicted by the β Method (effective stress method). The theoretical values of side shear set-up are fairly similar to the results of the analyzed load tests, which seems to support the viability of the presented method.

Keywords: driven piles, dynamic load test, pile set-up, clayey soils, numerical analysis.

1. Introduction

In the design of deep foundations, there are still some poorly understood phenomena, which are not therefore properly considered when calculating foundations, such as time-dependent effects that alter the load capacity of driven piles over time. In some cases, it is possible to observe a decrease in pile resistance after driving, known as relaxation, and in other cases the opposite effect is noticed, causing an increase in soil resistance over time, known as set-up or freeze. Its incorporation into pile design can offer substantial benefits, resulting in significant economic gain.

A reliable prediction of the set-up is only possible when pile tests are carried out beforehand in order to verify capacity gain over time. The tests must be performed for many days, while set-up occurs, generating an increase in terms of both cost and time for the construction. Consequently, a reliable and cost-effective method of predicting the long-term set-up magnitude based on numerical analyses would be very advantageous. The purpose of this paper is to evaluate the ability of the Cavity Expansion Analysis to predict the side shear set-up of driven piles in clayey soils.

This paper presents a brief summary of pile set-up and some methods for predicting the set-up phenomenon. In addition, it describes a method for predicting pile set-up using the Cavity Expansion Analysis and presents a Brazilian case, comparing load tests conducted on 50 piles and the results of numerical analyses.

2. Background

The increase in load capacity over time has been documented in several studies, including the ones by Yang (1956), Seed & Reese (1955), Housel (1958), McClelland *et al.* (1969), Flaate (1972), Thorburn & Rigden (1980), McManis *et al.* (1989), Skov & Denver (1988), Fellenius *et al.* (1989) and many others. The results of these studies, carried out predominantly in clayey soils, were shown in Titi & Wathugala (1999), as can be seen in Fig. 1.

Studies by Komurka *et al.* (2003) indicate that set-up is directly related to shaft resistance, while Chow *et al.* (1998) indicate that the loss of pile capacity (relaxation) is more influenced by toe resistance. Therefore, it can be concluded that friction piles have greater set-up than end-bearing piles.

Two concepts are used to define set-up, as described below:

- set-up: obtained by the ratio between total load capacity after some time and load capacity at the end of driving;
- side shear set-up: obtained by the ratio between shaft resistance after some time and shaft resistance at the end of driving.

Set-up values can vary widely due to the characteristics of each soil and pile material. However, it is observed that values above 2 are relatively common and maximum values are around 10. Long *et al.* (1999) analyzed the results of 80 load tests conducted on piles comprised of several materials driven in different soil types (sand, silt and clay). It was observed that set-up can occur in all cases, although this phenomenon is more pronounced in clayey soils. Bilfinger (2010) states that set-up mechanisms can be

Pedro Cavalheiro Ribeiro da Silva, MSc. Student, Escola Politécnica, Universidade de São Paulo, Av. Prof. Almeida Prado 83, 05508-070 Cidade Universitária, São Paulo, SP, Brazil. e-mail: pcavalheiro1@gmail.com.

Faiçal Massad, PhD, Full Professor, Escola Politécnica, Universidade de São Paulo, Av. Prof. Almeida Prado 83, 05508-070 Cidade Universitária, São Paulo, SP, Brazil. e-mail: faissal@usp.br.

Submitted on July 25, 2016; Final Acceptance on March 13, 2017; Discussion open until August 31, 2017.

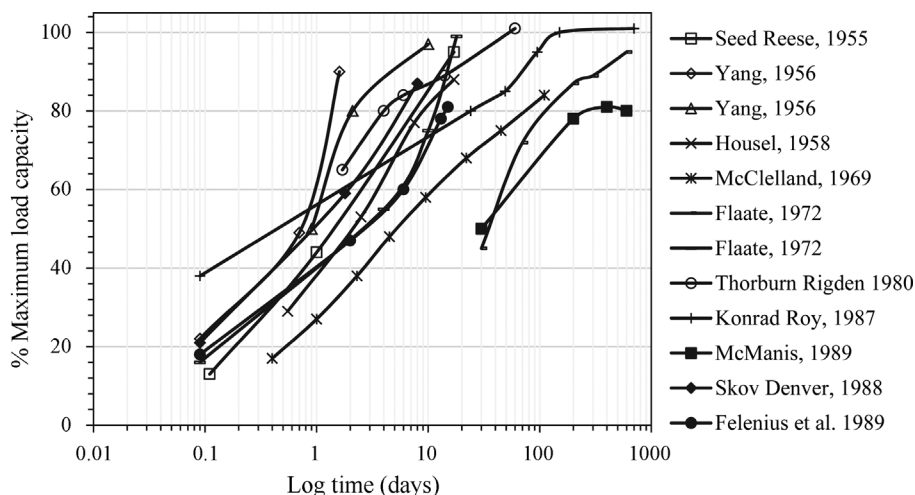


Figure 1 - Pile load capacity vs. time (Titi *et al.*, 1999).

divided into two main groups, *i.e.*, the mechanisms associated with pore pressure variations and those that are related to different phenomena, such as aging and creep.

In the case of clayey soils, as a pile is driven, the soil displacement along the shaft is predominantly radial (Komurka *et al.*, 2003). Randolph & Wroth (1979) state that, in clay, the soil around the shaft is remolded up to 20 radius from the pile axis and significant excess pore pressure is generated, thus causing a reduction in the effective stress and, consequently, facilitating the driving process. At the end of driving, the excess pore water pressure begins to dissipate, allowing the soil around the pile to reconsolidate. During reconsolidation, the soil undergoes a gradual increase in resistance, hence pile load capacity increases.

For soils with low OCR, at the end of driving, the excess pore pressure generated in the soil-pile interface is between 3 and 6 times the undrained shear resistance of the soil (Randolph & Wroth, 1979). However, in the case of soils with high OCR, the excess pore pressure can be null or negative (Coop & Wroth, 1989; Bond & Jardine, 1995). The time to dissipate the excess pore pressure is proportional to the square of the radius of the pile and inversely proportional to the horizontal coefficient of consolidation of the soil (Soderberg, 1961). Consequently, piles with a larger diameter take longer to set up than the ones with a smaller diameter (Long *et al.*, 1999) and excess pore water pressure dissipates slower for a group of piles than for a single pile (Camp & Parmar, 1999).

At the end of driving, total radial stress around the pile is higher than the initial horizontal stress, having been observed values between 6 and 11 times the undrained shear resistance (Earth Technology Corporation, 1986; Lehane & Jardine, 1994; Paikowsky & Hart, 2000). These studies also show reductions in total radial stress during consolidation, indicating that the total radial stress after consolidation is about 40% lower than the total stress observed at the end of driving.

The most popular methods to predict set-up in driven piles are actually based on empirical methods, correlations with in-situ tests or previous studies on test piles.

2.1. Empirical methods to predict pile set-up

Most of the studies regarding set-up are based on the results of load tests used to formulate methods for predicting the gain of load capacity as a function of time. Typical set-up values for different soil types were presented by Rausche *et al.* (1996). For instance, for clays these authors recommends set-up of 2.0, for silty 1.5 and for sand 1.0.

The most popular relation between load capacity and time was initially presented by Skov & Denver (1988), according to whom the increase in the total resistance of the pile is considered proportional to the log of time, as shown in Eq. 1.

$$\frac{Q_t}{Q_0} = 1 + A \cdot \log(t/t_0) \quad (1)$$

where Q_t = axial capacity at time t after driving, Q_0 = axial capacity at time t_0 , A = constant, depending on the soil type and t_0 = an empirical initial time value.

Komurka *et al.* (2003) presented pile load capacity as a function of time divided in 3 phases. During phase 1, because of the highly disturbed state of the soil, the rate of variation in load capacity is not constant with the logarithm of time, taking place a short period after driving (see Fig. 2). Phase 2 begins when the dissipation rate of excess pore water pressure becomes constant (linear) with the log of time, occurring until the total dissipation of excess pore pressure. Phase 3 is set after primary consolidation ends. In this phase, set-up rate is independent of effective stress when load capacity gain occurs due to aging. During this phase, the increase in resistance remains linear with the logarithm of time, but with lower rates than the ones observed in phase 2.

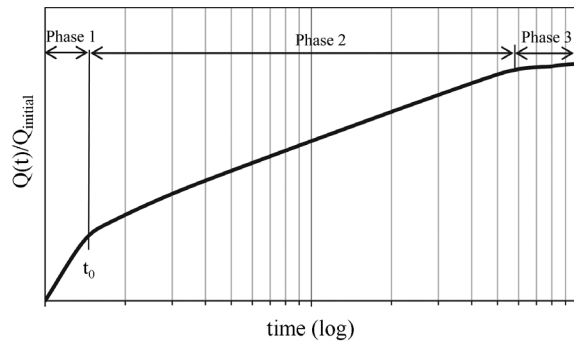


Figure 2 - Set-up development with the logarithm of time (Korurka *et al.*, 2003).

It is important to note that t_0 refers to the time when set-up becomes linear with the logarithm of time. Korurka *et al.* (2003) state that the duration of the logarithmically nonlinear dissipation rate of excess pore water pressure depends on the properties of both the soil (type, permeability and sensitivity) and the pile (type, permeability and size).

The t_0 values recommended in several studies are presented according to soil type and pile characteristics, varying between 0.01 day (Long *et al.*, 1999; Svinkin & Skov, 2000), 1.0 day (Axelsson, 1988; Bullock, 1999; McVay *et al.*, 1999) and 2.0 days (Camp & Parmar, 1999). Studies indicate that the larger the diameter of the pile, the greater the value of t_0 (Camp & Parmar, 1999).

Paikowsky *et al.* (1996), when evaluating the results of dynamic load tests in different piles, concluded that parameters “A” and t_0 must be obtained for each situation, considering that both depend on the characteristics of the soil as well as those of the pile. In practice, parameter “A” either can be predicted using field tests or can be obtained empirically. Table 1 presents some values for parameter “A” and the corresponding t_0 , obtained in several studies.

2.2. Methods for predicting set-up with in-situ tests

For an exploration-phase field test to be valuable for evaluating set-up, the test must have a significant side shear component, as well as the ability to separate side shear from end bearing (Bullock, 1999). Several studies have been

Table 1 - Summary of time t_0 and parameter “A” obtained in several studies.

Author(s)	t_0 (days)	Parameter “A”	
		min	max
Svinkin & Skov (2002)	0.1	1.60	3.50
Axelsson (1998)	1.0	0.20	0.80
Bullock (1999)	1.0	0.10	0.80
Bilfinger (2010)	1.0	0.14	0.44
Skov & Denver (1988)	1.0	0.20	0.60
Camp & Parmar (1999)	2.0	0.37	1.31

conducted looking for correlations between geotechnical in-situ tests and set-up, including torque measurement in SPT tests (Bullock & Schmertmann, 2003), analyses of torque tests on driven rods (Axelsson, 1998; Axelsson & Westin, 2000) and uplift measurement in SPT tests (Rausche *et al.*, 1996), among others.

Bullock & Schmertmann (2003) evaluated several results of standard penetration test with torque tests (SPT-T test) performed in different soil types, divided into two groups (clay and sand). During the test, both torque and rotation angle were recorded. The tests can measure both peak and residual torque and can be performed at various times after driving. The results show that in clayey soils the maximum torque tends to increase over time, while in sandy soils the maximum torque does not present considerable variations over time.

Similar studies conducted with the SPT sampler were developed by Axelsson (1998) and Axelsson & Westin (2000) in noncohesive soils. During the studies, torque measures applied to several small-diameter rods in different periods of time after driving were recorded. The tests with small-diameter rods have indicated an increase in resistance of approximately 30%, while static load tests performed on piles embedded into the same site indicated an increase in resistance of approximately 40% in comparison with the initial resistance. Axelsson (2002) found that with staged testing the increase in peak torque after some time is considerably higher than the increase in residual torque.

Rausche *et al.* (1996) evaluated SPT-T and uplift measurement in SPT tests in order to predict “damping” and “quake” parameters for dynamic analyses on piles. Uplift tests carried out 10, 25 and 70 min after the end of pile driving indicate that the development of uplift strength is linear with the logarithm of time, as well as with pile shaft resistance. The values obtained for the uplift tests were equivalent to approximately 80% of the maximum torque.

2.3. Test piles to predict set-up

The results of dynamic and/or static load tests conducted in different periods after the end of driving on test piles are currently the most effective way to predict set-up due to the uncertainties surrounding theoretical and empirical methods.

The procedure proposed by Bullock (2008) suggests performing dynamic load tests at the end of pile driving and some time after that, in order to calibrate resistance variation over time. By considering this method, it is important to determine the exact time when the tests are carried out, as it is known that in the early hours after driving variation in pile capacity is more significant. According to Bullock (2008), it is possible to predict the set-up factor by performing dynamic load tests 15 min, 60 min and 1 day after the end of driving, with the exception of sandy soils, in which larger periods are required to observe the effects of aging. However, the same author recommends performing load

tests after longer periods to confirm the rate and magnitude of set-up.

3. Numerical Simulation Procedure

In the present study, set-up is evaluated by considering the cylindrical cavity expansion theory, since field studies indicate that soil displacements around the pile during pile driving can be considered exclusively radial (Korurka *et al.*, 2003).

Isolated piles are usually evaluated using axisymmetric models, according to which structures are circular with symmetrical cross-section and uniform loads around the central axis (y-axis), where deformation and stress are equal in all radial directions. Fig. 3 presents a schematic example of an axisymmetric model, in which the x-axis represents the radial direction and the y-axis corresponds to the axial line of symmetry.

In applications such as driven pile modeling, the driving process is usually simulated using the cylindrical cavity expansion theory with the initial radius equal to zero. In practice, the numerical analysis must begin with a cylindrical cavity with radius different from zero to avoid infinite stress that would appear in case an initial cavity with null radius was considered. Carter *et al.* (1979) defined some relations between the radius of the cylindrical cavity (model) and that of the pile, leading to satisfactory results when comparing field data to numerical analyses. The study suggests that to simulate pile driving it is necessary to consider a cavity expansion model with initial radius (a_0) defined by:

$$a_0 = \frac{r_0}{\sqrt{3}} \tag{2}$$

where a_0 : initial radius of the cylindrical cavity and r_0 : pile radius.

The final radius (a_f) is equivalent to 2 times a_0 . This relationship is indicated in Fig. 4, which schematically

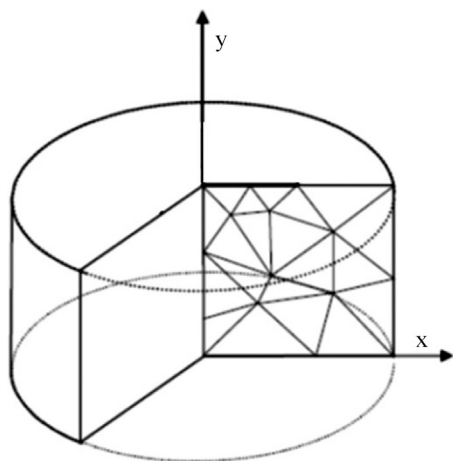


Figure 3 - Example of an axisymmetric problem (modified from Brinkgreve *et al.*, 2014).

presents the cavity radius considered in the model, comparing it to the pile radius (r_0). It is important to note that the initial and final cavity radii are equivalent to 0.58 and 1.15 times r_0 , respectively.

Figure 5 shows the cylindrical cavity expansion model adopted in the numerical analysis developed on the Plaxis software. It is important to highlight that the analyses were performed with a unit height model, in order to speed up calculations. The model parameters were thus defined considering a “slice” from the center of the soil layer analyzed; therefore, the results are average values.

Using the numerical analysis, it is possible to predict the excess pore pressure and radial stress around the pile shaft over time. By considering the stress obtained in the numerical analysis, the variation in unit shaft resistance (τ) can be predicted with the β method (Burland, 1973), also known as effective stress method, defined by:

$$\tau_f = \sigma'_r \cdot \tan \delta \tag{3}$$

where τ : unit shaft resistance, σ'_r : radial effective stress on the pile shaft and δ : friction angle between pile and soil.

It is important to note that effective radial stress, σ'_r , is proportional to the initial effective vertical stress, σ'_{v0} , defined by the equation:

$$\sigma'_r = K \sigma'_{v0} \tag{4}$$

It is also important to highlight that coefficient K , representing the ratio between radial stress and the initial vertical stress, is different from K_0 , which represents the in situ horizontal stress ratio, especially in the case of driven piles whose horizontal stress acting on the pile shaft is usually higher than the initial horizontal stress of the soil.

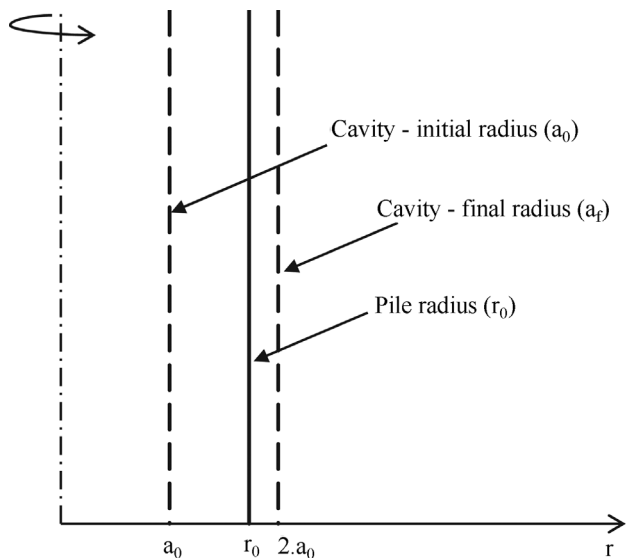


Figure 4 - Cylindrical cavity expansion model for evaluating driven piles.

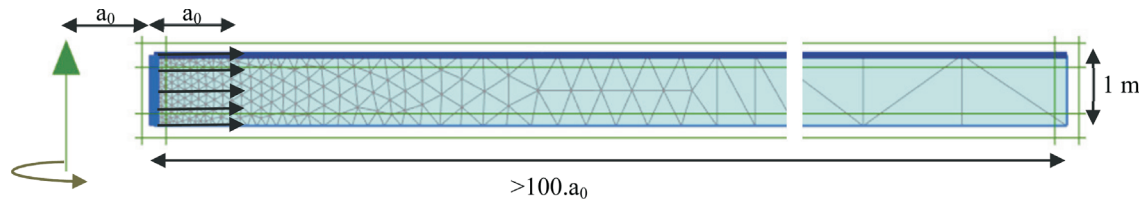


Figure 5 - Numerical model adopted to simulate cavity expansion in an axisymmetric one-dimensional model.

4. Case History in Santos Coastal Plain

4.1. Site overview

The test site is located in the Brazilian Southeast coast, specifically in the Santos Coastal Plain, around 80 km east of the city of São Paulo. The tests were conducted during the construction of a port terminal, comprising a pier around 1,100 m long, supported by approximately 2,300 prestressed concrete piles, with external diameter of 80 cm and wall thickness of 15 cm.

4.2. Subsurface conditions

The Santos Coastal Plain is characterized by a succession of sedimentary layers extending between the mountains and the ocean. These sediments were deposited during the last 100,000 years at different sedimentation cycles and with occasional erosion. Studies indicate that during periods of glaciation, there was significant drawdown in the water level (about 130 m), influencing the origin and history of the stress of the soil deposited in this area, causing an increase in effective stress and drying the soil layers closer to the surface. After the end of glaciation, sea level rose again, experiencing new sedimentation cycles (Massad, 2009). Another important phenomenon that influenced soil characteristics in the region are temporary depositions of high sand dunes.

Soil investigation consisted in several SPTs, 2 CPTUs and 7 Vane Tests. The main layers of sedimentary soil, composed predominantly of clayey materials and deposited in different periods, are described below:

- Mangrove (0 to -5 m): surface layer, with null N_{SPT} values, which is still in the formative phase.
- Fluvio-Lagoon Sediments (SFL) (-5 to -25 m): deposited after the sea level rose again, with small OCR (between 1.0 and 3.0) and N_{SPT} values around 0 to 5 blows/30 cm.
- Transitional Clays (AT) (-25 to -40 m): materials of geological origin characterized by high OCR due to the increase in effective stress as a consequence of sea level drawdown, with N_{SPT} values ranging from 5 to 25 blows/30 cm.

Interspersed with the argillaceous materials there are sandy lenses and, under these horizons, it is usual to find residual soil, up to 10 m thick, resting on the rock mass.

Figure 6 presents the undrained shear resistance (s_u) vs. depth, obtained in 2 CPTUs and 7 Vane Tests performed in the area. CPTU values were obtained by the known ex-

pression derived from the theory of cylindrical cavity expansion:

$$s_u = \frac{q_t - \sigma_{v_0}}{N_{KT}} \quad (5)$$

where N_{KT} is an empirical factor usually varying in the range of 10-13 in the Santos Coastal Plain (Massad, 2009). In this paper, a value of 11.5 was adopted in consonance with VT results (see Fig. 6).

Six CPTU pore pressure dissipation tests, shown in Fig. 7, were carried out at different depths, allowing to predict the horizontal coefficient of consolidation (c_h). Considering the method by Houlsby and Teh (1988), the values obtained for c_h were between 5.10^{-3} and 50.10^{-3} cm²/s.

The results indicate a value of excess pore water pressure (Δu) generated on the cone shaft at the end of driving between approximately 4 and 6 times s_u .

The cavity expansion analysis was carried out considering exclusively the SFL layer (-5 to -25 m), with Mohr-Coulomb model (linear elastic perfectly plastic behavior) and Hardening Soil Model, that accounts for stress-dependency of stiffness moduli. The average geotechnical parameters, around the -15.0 m level, are presented in Table 2 and Table 3.

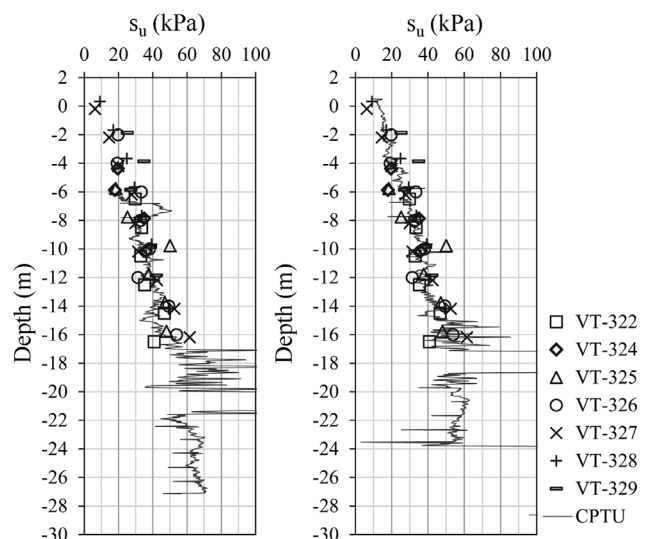


Figure 6 - Undrained shear resistance (s_u) obtained through CPTU-325, CPTU-326 and Vane Test results, both with Bjerrum's (1973) correction ($\mu = 0.7$).

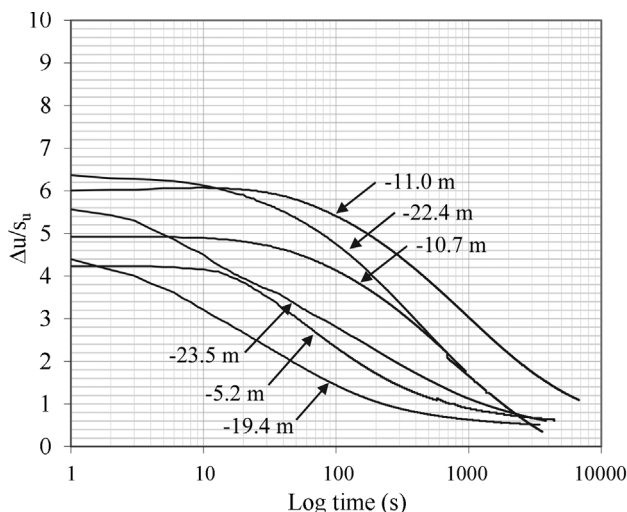


Figure 7 - CPTU pore pressure dissipation tests, normalized by s_u .

4.3. Load tests

To evaluate set-up, 62 dynamic load tests with increasing energy were carried out in 50 piles, shown in Fig. 8, with an 80 cm diameter and driven lengths ranging from 28 to 57 m. All load tests were performed with a Juntan HHK 16A hammer, weighing 160 kN, with increasing falling heights ranging from 0.20 to 1.20 m.

Figure 9 presents the maximum load capacities, obtained through CAPWAP analyses considering the highest energy blow of each pile and performed in some cases at the end of driving (EOD) and in other cases after some time elapsed (1 to 87 days).

The dynamic load tests, performed at different intervals of time from the end of driving until up to 87 days, resulted in total resistance ranging from 3,570 to 11,030 kN. A tendency of resistance gaining over time can be noticed. However, the relation between resistance and time is not well defined.

Figure 10 shows the average unit shaft resistance (τ) of the SFL layer found in the CAPWAP analysis between -5.0 and -25.0 m deep. It is possible to note that the SFL material is the main focus of the analysis, since this layer is composed predominantly of clayey material with low OCR values, which means that its set-up should be more significant than that of sandy layers (sand lenses and residual soil) or clayey soils (“AT” soil) with high OCR.

In this case, the average unit shaft resistance at the end of driving resulted in a range of values from 0 to 12 kPa, while results obtained after some time reached up to 42 kPa. It is important to note that the results from Pier 2 indicated lower values than the results from other areas, despite the fact that the geotechnical investigations did not point to any significant variation in the soil in this location. It is thus possible to assume that some variation may have occurred during driving or even when processing the CAPWAP analysis, resulting in lower capacities than expected. Therefore, for theoretical analyses, data obtained in this area (Pier 2) will be disregarded.

5. Numerical Simulation Results

Numerical simulation analyses were carried out, considering Mohr-Coulomb and Hardening-Soil models, to predict variation in pore water pressure and radial stress around an 80 cm prestressed pile over time. It is important

Table 2 - Geotechnical parameters of the SFL soil (-15.0 m) – Moh-Coulomb.

γ (kN/m ³)	E (MPa)	K_0	ν	s_u (kPa)	c_h (10 ⁻³ cm ² /s)	k_h (10 ⁻⁵ m/h)
15	10	0.86	0.25	40 to 60	5 to 50	1.8 to 18

Table 3 - Geotechnical parameters of the SFL soil (-15.0 m) – Hardening Soil.

γ (kN/m ³)	s_u (kPa)	E_{50} (MPa)	E_{oad} (MPa)	E_{ur} (MPa)	ν_{ur}	c_h (E-3 cm ² /s)	k_h (E-6 m/h)
15	40 to 60	10	10	30	0.2	5 a 50	1.8 a 18

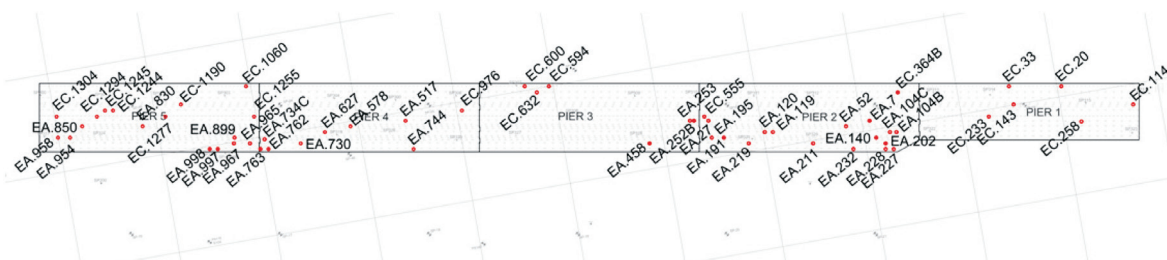


Figure 8 - Pier plant, indicating the piles tested.

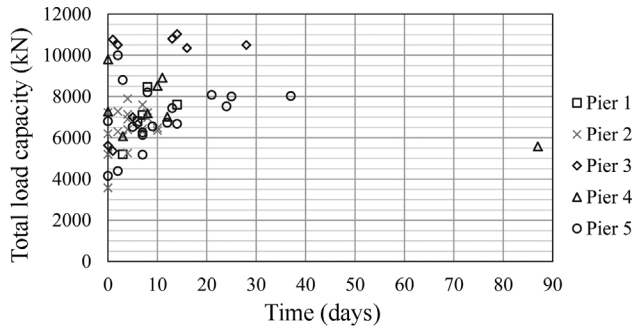


Figure 9 - Total load capacity vs. time from 62 CAPWAP analyses.

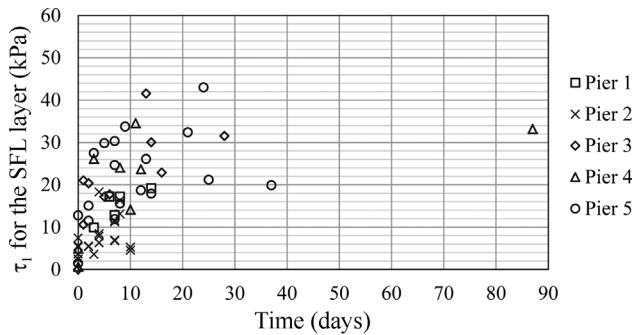


Figure 10 - Average unit shaft resistance in the SFL layer (-5 to -25 m) vs. time.

to say that the results obtained with Hardening-soil model will not be presented, as they were almost the same as the results considering the Mohr-Coulomb model. The cylindrical cavity expansion model is shown in Fig. 5.

5.1. Excess pore pressure (Δu)

Variations in pore water pressure, resulting from cylindrical cavity expansion adopting Mohr-Coulomb model, are presented as a function of time in Figs. 11 and 12. It is worth remembering that numerical analyses were performed considering s_u values between 40 kPa (Fig. 11) and 60 kPa (Fig. 12) and c_h values between $5 \cdot 10^{-3}$ and $50 \cdot 10^{-3} \text{ cm}^2/\text{s}$.

The results indicate maximum values of excess pore water pressure (Δu) generated in the soil-pile interface around 180 and 240 kPa for soils with undrained shear resistance (s_u) of 40 and 60 kPa, respectively. These results are equivalent to approximately 4.0 to 4.5 times s_u , in consonance with the CPTU dissipation tests (see Fig. 7).

5.2. Total radial stress (σ_r)

As previously mentioned, pile driving generates excess in both pore water pressure and total radial stress around the pile. Variations in total radial stress around the pile, due to cavity expansion, are presented in Figs. 13 ($s_u = 40 \text{ kPa}$) and 14 ($s_u = 60 \text{ kPa}$).

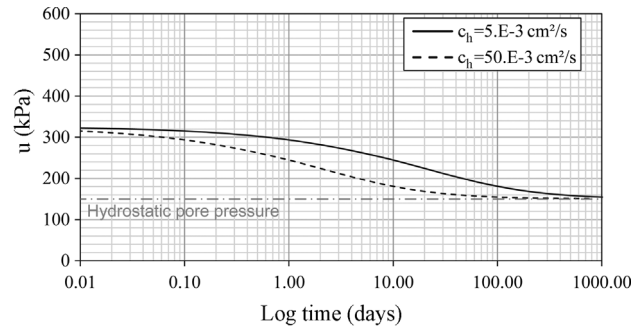


Figure 11 - Pore water pressure (u) from cavity expansion analyses – $s_u = 40 \text{ kPa}$.

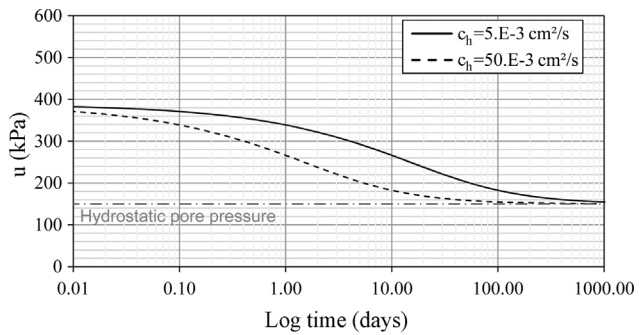


Figure 12 - Pore water pressure (u) from cavity expansion analyses – $s_u = 60 \text{ kPa}$.

The results indicate an increase in total radial stress (σ_r) between 220 and 300 kPa at the end of driving. After full consolidation, total radial stress is reduced to about 75% of the radial stress at the end of driving, ranging from 170 to 240 kPa. Both ranges are for soils with undrained shear resistance (s_u) equal to 40 and 60 kPa, respectively.

It is worth noting that at the end of driving, predicted σ_r is between 2.0 and 2.3 times the initial radial stress (σ_{r0}), and after the total stress reduction predicted σ_r varies between 1.8 and 2.1 times σ_{r0} .

5.3. Effective radial stress (σ'_r)

Figures 15 and 16 present the effective radial stress acting on the pile shaft over time for undrained shear resistance of 40 kPa (Fig. 15) and 60 kPa (Fig. 16).

During the analyzed period, between the end of driving and after full consolidation, an increase in effective radial stress of about 120 and 170 kPa was observed for undrained shear resistance of 40 and 60 kPa, respectively.

The ratio between effective radial stress after cavity expansion (σ'_r) and effective vertical stress at rest (σ'_{v0}) is defined by:

$$K = \frac{\sigma'_r}{\sigma'_{v0}} = \frac{\sigma'_{r0}}{\sigma'_{v0}} \cdot \frac{\sigma'_r}{\sigma'_{r0}} = \frac{1}{K_0} \cdot \frac{\sigma'_r}{\sigma'_{r0}} \quad (6)$$

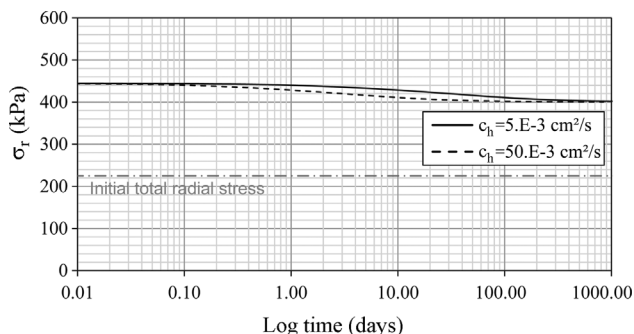


Figure 13 - Total radial stress (σ_r) from cavity expansion analyses – $s_u = 40$ kPa.

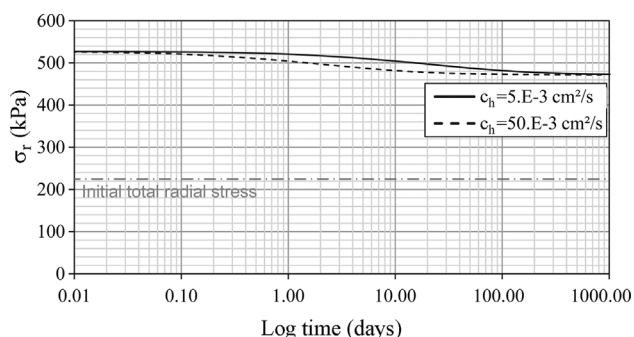


Figure 14 - Total radial stress (σ_r) from cavity expansion analyses – $s_u = 60$ kPa.

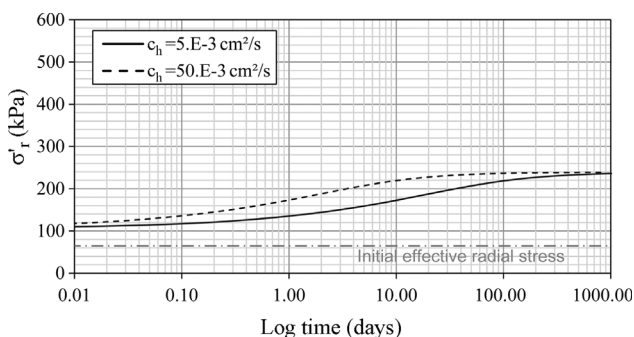


Figure 15 - Effective radial stress (σ'_r) from cavity expansion analyses – $s_u = 40$ kPa.

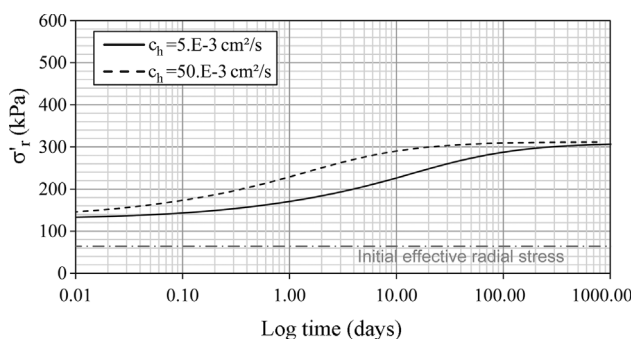


Figure 16 - Effective radial stress (σ'_r) from cavity expansion analyses – $s_u = 60$ kPa.

The values of K shortly after driving vary between 1.6 and 2.0, and after full consolidation these values are between 3.2 and 4.1. For the numerical analysis, an average value of 3.6 was considered. In these computations a value of $K_0 = 0,86$ was assumed, as shown in Table 2.

6. Evaluation of Side Shear Set-Up

To evaluate the ultimate value of the unit shaft resistance ($\tau_{l,ult}$), the following expression was used:

$$\tau_{l,ult} = \tan \delta \cdot \sigma'_r \quad (\text{with } \sigma'_r = K \cdot \sigma'_{v_0}) \quad (7)$$

According to Burland (1973) the proportionality between σ'_r and σ'_{v_0} is a simplifying assumption and, in his words, “it represents a simple and logical starting point”.

Parameter δ , representing the friction angle between the pile and the soil, depends on the characteristics of both the soil and the pile material and can be set through laboratory tests, although most of the studies on this topic are related to sandy soils, so little information on pile driving in clay is available.

The product $K \cdot \tan(\delta)$ was defined by Burland (1973) as coefficient β , resulting in:

$$\tau_{l,ult} = \beta \cdot \sigma'_{v_0} \quad (8)$$

Several studies indicate values of β ranging from 0.25 to 0.30 for driven piles in clays with low OCR. Thus, considering $K = 3.6$ and $\beta = 0.3$ leads to $\tan(\delta)$ equals approximately to 0.08. Note that this figure implies a value of δ roughly equals to 5° , which may seem low. However, Atkinson (1993) cites that δ lies generally between the residual friction angle (ϕ'_r) and the peak friction angle (ϕ'_p). Laboratory tests performed on SFL clays in the overconsolidated range of stress lead to ϕ'_p from 6° to 8° (Massad, 2016), with a non zero cohesion. The same material, when tested above preconsolidation stress, results in ϕ'_p around 15° and 25° with zero cohesion (Massad, 2009). In this context and taking into account the sensitivity of the SFL clays, ranging from 3 to 5, indicating a low value for ϕ'_r , it can be assumed that $\delta = 5^\circ$ is within the range of expected values.

Taking into account effective radial stress as a function of time (Figs. 15 and 16), obtained using numerical modeling, and considering $\tan(\delta)$ equals to 0.08 in Eq. 7, the values predicted for unit shaft resistance as a function of time are shown in Fig. 17.

The average unit shaft resistance acting on the SFL layer varies between 10.7 and 13.1 kPa at the end of driving and 23.1 and 31.2 kPa after full consolidation, considering s_u equal to 40 and 60 kPa, respectively. These results are consistent with static load tests performed on floating piles around this area, according to data presented by Massad (2009).

Despite of the scattering of τ_p , there is a trend of results within a relatively narrow range of values. In addition,

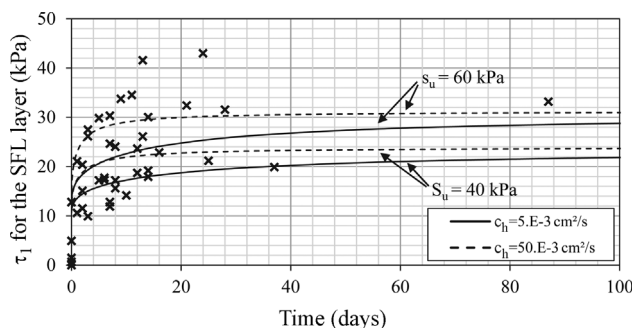


Figure 17 - Unit shaft resistance for the SFL layer over time from CAPWAP and numerical analyses.

side shear set-up ranges from 2.0 to 2.5 approximately 20 days after driving.

It is important to note that for the 80 cm prestressed piles, the time for 90% of the total set-up is approximately 6 and 70 days, related to horizontal coefficients of consolidation (c_h) of 50.10^{-3} and 5.10^{-3} cm^2/s , respectively. The results of the numerical analyses indicate that after 1 day of pile driving, about 50% to 70% of the total pile capacity gain predicted was observed.

Finally, it is possible to conclude that the methodology proposed to predict side shear set-up by considering cavity expansion analyses and β method is in consonance with field results obtained from CAPWAP analyses.

7. Conclusions

Literature review indicated that:

- increases in pile load capacity over time can occur in any kind of soil or pile material, although pile set-up is more pronounced in normally consolidated clays;
- set-up is more influenced by shaft capacity than by toe resistance; and
- changes in pore water pressure and total radial stress after the end of driving are the main mechanisms responsible for set-up in clayey soils.

The unit shear resistance of the case history SFL layer obtained from the dynamic load tests ranged from 0 to 12 kPa at the end of driving ($t = 0$ day) and a maximum of 42 kPa a certain time after driving.

A method based on the cavity expansion theory has been presented to predict side shear set-up of driven piles. Based on the comparisons between observed and predicted results for side shear set-up in low-OCR clay soils of the case history, known as SFL clay, the following conclusions can be drawn:

Predictions of unit shaft friction using the cavity expansion theory and application of effective stress analyses (β method) indicate that:

- the average unit side friction acting on the SFL layer varies between 10.7 and 13.1 kPa at the end of driving and between 23.1 and 31.2 kPa after full consolidation. The latter figures are in consonance with the results of dy-

namic load tests and consistent with static load tests performed on floating piles in Santos Coastal Plain;

- the predicted side shear set-up found in cavity expansion analyses varies between 2.0 and 2.5 for the SFL layer, in consonance with the results of dynamic load tests;
- the time required for 90% of the set-up to take place is approximately equal to 6 and 70 days for c_h between 5.10^{-3} and 50.10^{-3} cm^2/s , respectively; and
- the numerical analysis indicated that one day after the end of driving, about 50% and 70% of the total set-up predicted occurred, for values of c_h between 5.10^{-3} and 50.10^{-3} cm^2/s , respectively.

The applied method proved a valuable tool for estimating pile set-up as it is cost- and time-efficient. Moreover, the results showed good correlation between the side shear set-up evaluated through cavity expansion analyses and load tests on driven piles.

Acknowledgments

The authors would like to thank the Polytechnic School of the University of São Paulo (EPUSP) for supporting this research, as well as the company Andrade Gutierrez, Eng. Werner Bilfinger and Eng. Paulo Alberto Neme, for providing the necessary information for the analysis carried out in this article.

References

- Atkinson, J.H. (1993). *An Introduction to the Mechanics of Soils and Foundations: Through Critical State Soil Mechanics*. McGraw-Hill Book Co., Berkshire, UK.
- Axelsson, G. (1998). Long-term set-up of driven piles in non-cohesive soils evaluated from dynamic tests on penetration rods. *Proceedings of the First International Conference on Site Characterization*, v. 2, pp. 895-900.
- Axelsson, G. & Westin, A. (2000). Torque tests on driven rods for prediction of pile set-up. *New Technological and Design Developments in Deep Foundations*, pp. 297-311.
- Axelsson, G. (2002). A Conceptual Model of Pile Set-up for Driven Piles in Non-Cohesive Soil. *Deep Foundations Congress, Geotechnical Special Publication, No 116, Volume 1, ASCE, Reston, Va.*, pp. 64-79.
- Bilfinger, W. (2010). Set-up em estacas cravadas. *V Congresso Luso-Brasileiro de Geotecnia, Gramado*, v. 1, pp. 9-29.
- Bjerrum, L. (1973). Problems of soil mechanics and construction on soft clays: state of the art report. *Proceedings 8th ICSMFE, Moscow*, pp. 1-53.
- Bond, A.J. & Jardine, R.J. (1995). Shaft capacity of displacement piles in a high OCR clay. *Geotechnique*, 45(1):3-23.
- Brinkgreve, R.B.J., *et al.* (2014). *Plaxis Reference Manual*. Plaxis bv., The Netherlands

- Bullock, P.J. (1999). Pile Friction Freeze: A Field and Laboratory Study, Volume 1. Ph.D. Dissertation, University of Florida.
- Bullock, P.J. (2008). The easy button for driven pile setup dynamic testing. From research to practice in geotechnical engineering. ASCE. Reston, VA, GSP 180, pp. 471-488.
- Bullock, P.J. & Schmertmann, J.H. (2003). Determining the effect of stage testing on the dimensionless pile side shear setup factor. Research Report BC354, RPWO#27, Florida Department of Transportation.
- Burland, J.P. (1973). Shaft friction of piles in clay—a simple fundamental approach. *Ground Engineering* 6:30-42.
- Camp III, W.M. & Parmar, H.S. (1999). Characterization of pile capacity with time in the cooper marl: A study of the applicability of a past approach to predict long term pile capacity. *Transportation Research Record*, 1663:16-24.
- CAPWAP (Case Pile Wave Analysis Program), 2006 version. By PDI - Pile Dynamics Inc.. 2006. Software for Windows.
- Carter, J.P.; Randolph, M.F. & Wroth, C.P. (1979). Stress and pore pressure changes in clay during and after the expansion of a cylindrical cavity. *International Journal for Analytical and Numerical Methods in Geomechanics*, 3(4):305-322.
- Chow, F.C.; Jardine, R.J.; Bruzy, F. & Nauroy, J.F. (1998). Effects of time on capacity of pipe piles in dense marine sand. *Journal of Geotechnical and Geoenvironmental Engineering*, 124(3):254-264.
- Coop, M.R. & Wroth, C.P. (1989). Field studies of an instrumented model pile in clay. *Geotechnique*, 39:679-696.
- Earth Technology Corporation (1986). Final report: some aspects of the fundamental behavior of axially loaded piles in clay soils. Earth Technology Corporation, San Bernardino.
- Fellenius, B.; Riker, R.; O'Brien, A. & Tracy, G. (1989). Dynamic and static testing in soil exhibiting set-up. *J. Geotech. Engrg.*, 115(7):984-1001.
- Flaate, K. (1972). Effects of pile driving in clays. *Canadian Geotechnical Journal*, 9(1):81-88.
- Houlsby, G.T. & Teh, C.I. (1988). Analysis of the piezocone in clay. *Proceedings of the International Symposium on Penetration Testing*. Rotterdam, Netherlands, v. 1, pp. 777-783.
- Housel, W.S. (1958). Procedures for testing soils. ASTM, p. 360.
- Komurka, V.; Wagner, A.B. & Edil, T.B. (2003). Estimating soil/pile set-up. Wisconsin Highway Research Program #0092-00-14.
- Konrad, J.M. & Roy, M. (1987). Bearing capacity of friction piles in marine clay. *Geotechnique* 37(2):163-175.
- Lehane, B. M. & Jardine, R.J. (1994). Displacement-pile behaviour in a soft marine clay. *Canadian Geotechnical Journal*, v. 31, ISSN: 0008-3674, pp. 181-191.
- Long, J.H.; Kerrigan, J.A. & Wysockey, M.H. (1999). Measured time effects for axial capacity of driven piling. *Transportation Research Record* 1663, paper n. 99-1183, pp. 8-15.
- Massad, F. (2009). Solos Marinheiros da Baixada Santista: Características e Propriedades Geotécnicas. Oficina de Textos, São Paulo.
- Massad, F. (2016). Personal communication.
- McClelland, B.; Focht, J.A. & Emrich, W.J. (1969). Problems in design and installation of offshore piles. *Journal of Soil Mechanics Foundation Division*, 95:1491-1514.
- Mcmanis, K.L.; Folse, M.D. & Elias, J.S. (1989). Determining pile bearing capacity by some means other than the engineering news formula. Federal Highway Administration Report n. FHWA/LA-89/234.
- McVay, M.C.; Schmertmann, J.; Townsend, F. & Bullock, P. (1999). Pile friction freeze: a field and laboratory study. Florida Department of Transportation, v. 1, pp. 192-195.
- Paikowsky, S.G. & Hart, L.J. (2000). Development and field testing of multiple deployment model pile (MDMP). Federal Highway Administration Publication n. FHWA-RD-99/194.
- Paikowsky, S.G.; Labelle, V. & Hourani, N.M. (1996). Dynamic analyses and time dependent pile capacity. *Proceedings of the 5th International Conference on the Application of Stress-Wave Theory to Piles*, Orlando FL, pp. 325-339.
- Plaxis Introductory 2D, Introductory 2014 version. By Plaxis Corporation, 2014. Software for Windows.
- Randolph, M.F. & Wroth, C.P. (1979). An analytical solution for the consolidation around a driven pile. *Intl. J. Numer. and Anal. Methods in Geomech.*, 3(2):217-229.
- Rausche, F.; Thendean, G.; Abou-matar, H.; Likins, G. & Goble, G. (1996). Determination of pile drivability and capacity from penetration tests. FHWA.
- Seed, H.B. & Reese, L.C. (1955). The action of soft clay along friction piles. *Proceedings, ASCE*, v. 81, paper n. 842.
- Skov, R. & Denver, H. (1988). Time-dependence of bearing capacity of piles. *Proc. 3rd International Conference on Application of Stress-Wave Theory to Piles*, Canada, pp. 1-10.
- Soderberg, L.O. (1961). Consolidation theory applied to foundation pile time effects. *Geotechnique*, 12(3):217-225.
- Svinkin, M.R. & Skov, R. (2000). Set-up effect of cohesive soils in pile capacity. *Proceedings of the 6th International Conference on Application of Stress Waves to Piles*, São Paulo, Brazil, Balkema, pp. 107-111.

- Thorburn, S. & Rigden, W.J. (1980). A practical study of pile behavior. Proc. 12th Annual Offshore Technology Conf., Houston.
- Titi, H.H. & Wathugala, G.W. (1999). Numerical procedure for predicting pile capacity - setup/freeze. Transportation Research Record 1663, paper n. 99-0942, pp. 25-32.
- Yang, N.C. (1956). Redriving characteristics of piles. Journal of the Soil Mechanics and Foundations Division, v. 82, paper n. 1026, SM 3, ASCE.

List of symbols

A : Constant, depending on the soil type
 a_0 : Initial radius of the cylindrical cavity
 c_h : Horizontal coefficient of consolidation
 δ : Friction angle between pile and soil
 ϕ'_r : Soil residual friction angle
 ϕ'_p : Soil peak friction angle
 Δu : Excess porewater pressure
 E : Young's modulus
 γ : Unit weight

K : Ratio between radial stress and the initial vertical stress
 K_0 : In situ horizontal stress ratio
 N_{KT} : Factor relating corrected cone end resistance and undrained shear strength
 ν : Poisson's ratio
 q_i : Cone resistance
 Q_0 : Axial capacity at time t_0
 $Q_{initial}$: Axial capacity at the end of driving
 Q_t : Axial capacity at time t after driving
 r_0 : Pile radius
 σ'_r : Effective radial stress on the pile shaft
 σ_r : Total radial stress
 σ'_{r0} : Effective radial stress at rest, before driving
 σ_{r0} : Total radial stress at rest, before driving
 s_u : Undrained shear resistance
 σ_{v0} : Initial total vertical stress
 σ'_{v0} : Initial effective vertical stress
 t_0 : Empirical initial time value
 τ_{ult} : Ultimate unit shaft resistance
 τ_s : Unit shaft resistance

Statistical Modeling of Municipal Solid Waste Settlement from a Lysimeter

C.L. Araújo Neto, B.M.A. Nóbrega, R.B.A. Sousa, M.C. Melo, W. Paiva, V.E.D. Monteiro

Abstract. The sanitary landfill settlement prediction is an important tool for an integrated waste management system once it allows the evaluation of the sanitary landfill useful life and assists in the development of planning actions. Several settlement models have been used as an attempt to estimate the waste volume reduction over time. However, there are few models that consider the waste biodegradation processes. The objective of this paper is to build a simple linear regression model to determine the settlements that took place over time in a lysimeter filled with municipal solid waste from the city of Campina Grande, State of Paraíba, Brazil. The lysimeter was built in the Environmental Geotechnics Group's experimental field which is located at the Federal University of Campina Grande's main campus. For the settlement model development, the municipal solid waste settlement from a lysimeter was monitored during 1309 days. It was observed that in the interquartile range, data exhibited a trend of linearity, so this monitoring time was selected in order to develop the model. Through the tests carried out, it can be considered that the developed model presents significant statistical parameters to estimate the waste settlement. Such model can be applied for the estimation of settlement from sanitary landfills with similar features to the ones used in this model.

Keywords: linear regression, experimental cell, sanitary landfill, statistical analysis, Brazil, waste displacement.

1. Introduction

Waste settlement monitoring is one of the most important steps during the sanitary landfill's operation phase. The settlement, also known as waste body displacement, not only affects the geotechnical and environmental aspects of a sanitary landfill but also maximizes its useful life. However, during the sanitary landfill's project implementation phase, this parameter is not taken into account. Only meteorological, social and geographical parameters are usually considered.

Sanitary landfill settlement is a direct consequence of compression, particles rearrangement and biodegradation of municipal solid waste (MSW). According to Qian *et al.* (2002), the total settlement of a sanitary landfill may vary from 25% to 50% of its initial height. When settlement is predicted, many problems can be minimized, such as damage to the liquid and gas collection system, cracks in the soil cover layer and instability of MSW mass (Durmusoglu *et al.*, 2005 ; Ouvry and Page, 2005; Melo, 2003).

The primary settlement occurs due to loads imposed over the waste mass such as the waste self-weight and the cover layer weight, which influence the compaction pro-

cess. The secondary settlement takes place through the MSW decomposition process that can occur for many years until the organic matter biodegradation is completed (Babu & Lakshmikanthan, 2015; Hettiarachchi *et al.*, 2009). According to Farias (2014), the study of waste settlement mechanism is complex but can it be simplified with the use of lysimeter that simulates the behavior of a full scale landfill cell.

Bareither & Kwak (2015) instrumented a steel made lysimeter (8.2 m height, 2.4 m diameter) to monitor settlement at various depths in the waste column. Such system consisted of steel plates attached to steel rods that extended from the bottom to the top of the lysimeter. Rafizul *et al.* (2014) conducted experiments in a lysimeter made of PVC pipe with height and inner diameter of 1.8 m and 2 m, respectively. Several settlement models, as the ones developed by Sowers (1973), Zimmerman *et al.* (1977), Simões (2000) and Babu *et al.* (2010), have been used as an attempt to estimate the waste volume reduction over time. However, not all models consider the waste biodegradation processes (El-Fadel & Khoury, 2000).

Cláudio Luis de Araújo Neto, PhD. Student, Departamento de Engenharia Civil, Universidade Federal de Campina Grande, Campina Grande, PB, Brazil. e-mail: claudioluisneto@gmail.com.

Breno Moura de Araújo Nóbrega, Undergraduate Student, Departamento de Engenharia Civil, Universidade Federal de Campina Grande, Campina Grande, PB, Brazil. e-mail: breno.moura.n@gmail.com.

Raul Batista Araujo de Sousa, Undergraduate Student, Departamento de Engenharia Civil, Universidade Federal de Campina Grande, Campina Grande, PB, Brazil. e-mail: raulbatista01@gmail.com.

Márcio Camargo de Melo, PhD., Associate Professor, Departamento de Engenharia Agrícola, Universidade Federal de Campina Grande, Campina Grande, PB, Brazil. email: melomc90@gmail.com.

William de Paiva, PhD., Associate Professor, Departamento de Engenharia Sanitária e Ambiental, Universidade Estadual da Paraíba, Campina Grande, PB, Brazil. e-mail: wili123@ig.com.br.

Veruschka Escarião Dessoles Monteiro, PhD., Associate Professor, Departamento de Engenharia Civil, Universidade Federal de Campina Grande, Campina Grande, PB, Brazil. e-mail: veruschkamonteiro@hotmail.com.

Submitted on August 18, 2016; Final Acceptance on March 13, 2017; Discussion open until August 31, 2017.

Hachich (2000) states that models are intended to explain reality, predict behavior and support decisions. The efficiency of a model is directly related to its purpose. To explain the reality, models must incorporate all parameters that influence the studied variable. Nonetheless, models should preferably be simple and depend on easily obtainable parameters (Boskov, 2006).

This study aims to develop a simple linear regression model in order to determine the settlement occurring over time in a lysimeter filled with municipal solid waste.

2. Methodology

2.1. Construction and instrumentation of the lysimeter

The lysimeter (Fig. 1) was constructed in the Environmental Geotechnics Group's experimental field which is located at the Federal University of Campina Grande's main campus, city of Campina Grande, Brazil. The lysimeter was built with solid bricks masonry and had an internal diameter, height and volume of 2.0 m, 3.5 m and 11 m³, respectively. The lysimeter's cylindrical shape tends to facilitate waste arrangement and compaction, lateral pressure distribution and prevention of preferential leachate paths. Also, this shape reduces the contact between waste and inner wall's surface. The structure was built on a concrete base. The bottom and cover layer was made with a low-permeability soil (permeability coefficient: 10⁻⁶ m.s⁻¹).

The lysimeter had a drainage system composed of a 0.04 m diameter PVC pipe that was drilled and placed on the compacted soil layer. A crushed stone layer was spread over the soil to induce the leachate flow. Besides that, the lysimeter was equipped with gases drainage system, piezo-



Figure 1 - Lysimeter.

meter for liquid level measurement, magnetic and circular steel plates for depth and surface settlement measurement as well as thermocouples for temperature measurement over depth (Fig. 2).

2.2. Sampling and collection of MSW

In order to obtain a representative sample of the waste from the city of Campina Grande, a planning process was carried out through statistical inference. This statistical investigation presents a confidence level of 95,5% and a maximum error of 5%.

The statistical planning considered the city's population, area and the amount of waste produced per person based on data from the Brazilian Institute of Statistical Geography (IBGE in Portuguese abbreviation). The sample's size was determined through Eq. 1:

$$n = \frac{Z^2 \sigma^2 N}{e^2(N-1) + Z^2 \sigma^2} \quad (1)$$

where Z = abscissa of the standard normal distribution, σ = standard deviation of population, N = population size, e = sampling error and n = sample size.

A value of $Z = 2.00$ was considered, which means a confidence level of $(1 - \alpha) = 0,955$. For the standard deviation of population, a predetermined value was used though amplitude approximation. The amplitude represented the difference between the higher (1.5 kg) and lower (1.0 kg) waste amount produced by one person in Campina Grande, so the amounts were 532.623 and 355.082 kg, respectively. This way, the standard deviation of population was about 44.385. The population size is equivalent to the number of neighborhoods in the city, which was 50 according to IBGE's database. The admitted sampling error was 5%.

The sample size calculated in Eq. 1 corresponded to the number of neighborhoods, where the MSW would be collected. The obtained value was $n = 12$. Then, the city was divided into 4 different zones (north, south, east and west). After, a stratified sampling was carried out proportionally to the number of neighborhoods in each zone. Finally, the neighborhoods were randomly chosen (Table 1).

The waste samples were collected from commercial and domestic buildings and were not previously segregated. From the total collected waste amount, about 7,800 kg were destined to the lysimeter filling process and approximately 600 kg were used in the physical characterization (gravimetric composition), which was conducted based on LIPOR's (2000) methodology - adapted by Leite (2008) and Pereira *et al.* (2010).

2.3. Lysimeter's filling and monitoring processes

The collected waste was homogenized and quartered (according to ABNT NBR 10007, 2004). Then, four buckets (volume of 0.006 m³) were filled with waste samples

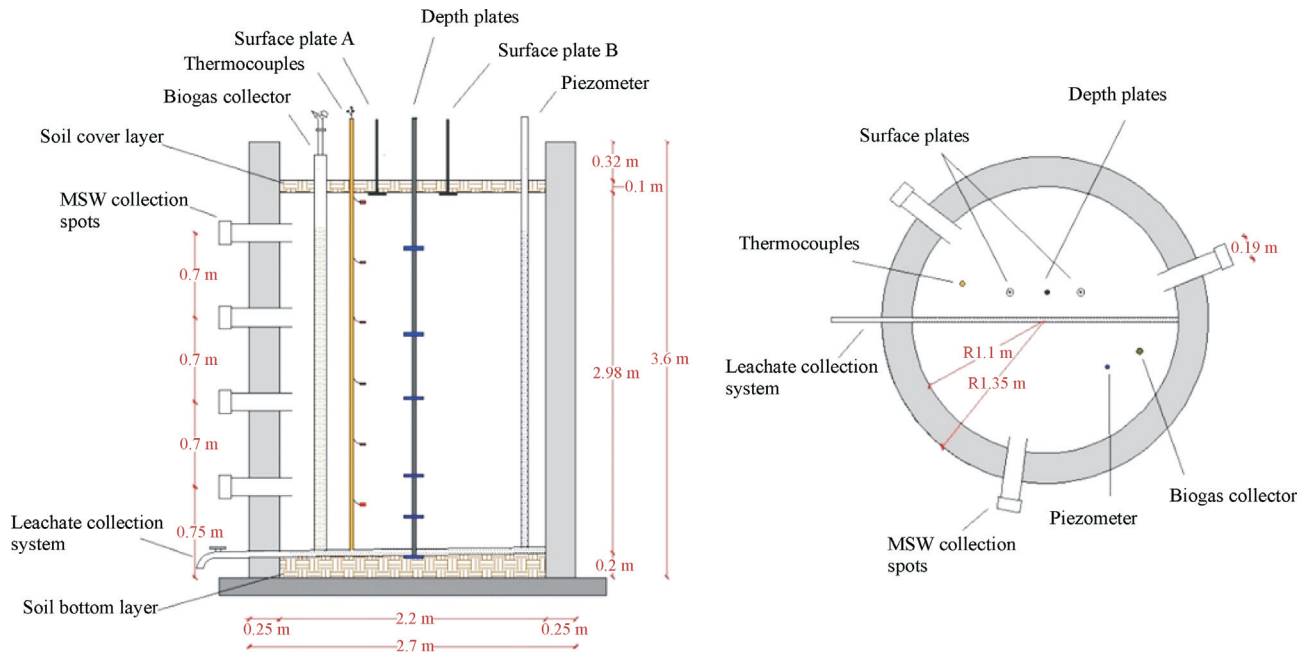


Figure 2 - Schematic view of the lysimeter.

Table 1 - Amount of MSW collected in the selected neighborhoods from Campina Grande.

Zone	Neighborhood	Collected MSW (kg)
North	Conceição	271.13
	Nações	110.85
	Palmeira	448.66
South	Estação Velha	261.20
	Jardim Paulistano	632.84
	São José	311.41
	Velame	475.90
East	José Pinheiro	1,270.24
	Nova Brasília	739.97
West	Dinâmica	431.95
	Malvinas	3,052.04
	Quarenta	393.87
Total		8,400.06

and dumped into the lysimeter (Fig. 3a) followed by manual compaction (Fig. 3b) that was performed by using a weight and a number of blows that produced a compaction energy proportionally similar to the one generated by a compaction vehicle in sanitary landfill sites. The referred steps (buckets filling, waste deposition into lysimeter, and compaction) were repeated until the predetermined waste body height was achieved.

The surface waste settlement was monitored according to the procedures described by Leite (2008), Melo

(2011) and Farias (2014), with necessary adaptations to this specific study. To obtain this parameter, vertical displacements of the metal plates were measured. These plates had a diameter of 0.15 m and were attached to a 0.6 m height rod (Fig. 4b). The two plates were installed after the lysimeter filling phase and were located between the top waste layer and the soil cover layer. The surface settlement measurements were carried out by stretching a nylon string, setting it on the edge of the lysimeter wall, and then measuring the vertical distance between the string and the top of the rods (Figs. 4c and 4d).

2.4. Statistical treatment of data and settlement model elaboration

The settlement monitoring lasted four years. After this time, the lysimeter's settlement became practically stabilized. Thus, the model considered the database from the monitoring period.

The statistical modeling process consisted of a linear model development using simple linear regression. To achieve this, the waste settlement behavior was observed over time by means of a scatter diagram. Because of data variability, only data in the interquartile range was selected for the model development. According to Paiva (2009), interquartile range represents dispersion measures that are insensitive to disturbing observations. This range is used for outlier's identification and is determined by the Eqs. 1 and 2.

$$L_i = Q_1 - 1.5A_{int} \quad (2)$$

$$L_s = Q_3 + 1.5A_{int} \quad (3)$$



Figure 3 - a- waste disposal into the lysimeter and d -Waste mass compaction.

with

$$A_{int} = Q_3 - Q_1 \quad (4)$$

where L_i = lower critical limit; L_s = upper critical limit, Q_1 = first quartile, Q_3 = third quartile and A_{int} = interquartile distance.

The normality of the dependent variable (settlement) was verified by the Kolmogorov-Smirnov test, proposed by Massey Jr. (1951). The assumption of data normality is essential for performing statistical inferences and when there is a small sample, it is necessary to carry out tests to check normality.

The correlation coefficient, proposed by Pearson (1896), was determined to check the degree of association between variables of settlement and time. According to Borges (2003), perfect correlation means a result equal to 1; very strong correlation is for values between 0.99 and 0.80; strong correlation is for values between 0.79 and 0.60; weak correlation ranges from 0.59 to 0.40; very weak correlation has values from 0.39 to 0.20; valueless correlation is for 0.19 to 0.001 values, and zero correlation is when the result is equal to 0. To determine if a particular correlation occurred due to either a random sampling error or because of chance, a Student's t-test, developed by Gosset (1908), was applied.

To establish a simple model that describes the relationship between two variables normally distributed (settlement and time), a simple linear regression was performed as described by Galton (1886). Thus, it was used a simple linear regression equation (Eq. 5), in which for each monitoring time, a respective settlement value could be calculated.

$$\hat{y} = a + bx + \varepsilon \quad (5)$$

where \hat{y} = estimated settlement value (dependent variable), x = time (independent variable), a = linear coefficient, b = angular coefficient and ε = statistical residual.

After choosing the equations to model the behavior of waste settlement over time, the coefficient of determination (R^2) was analyzed. Such coefficient measures the relationship between two quantitative variables and ranges from 0% to 100%. The higher the value for R^2 , the greater is the dependence of a variable in relation to another or the better the model fit in relation to the monitored parameters. However, errors may occur and variables may not show any relationship of cause and effect between them.

The residual analysis was performed using the tests of Durbin & Watson (1950) to verify the independence, and Breusch & Pagan (1979) to verify the residual homoscedasticity. According to Fernandes *et al.* (2014), if any of these assumptions is not met, the model is not suitable and

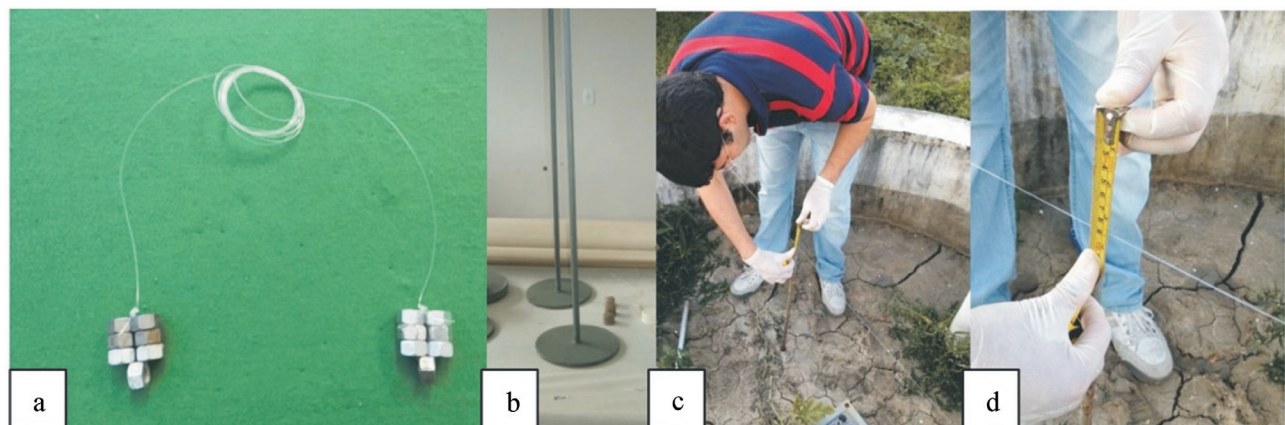


Figure 4 - a- Nylon string; b - Metal surface plates; c and d - Surface settlement-measurement.

the obtained deviation has to be corrected or considered in the model.

3. Results

3.1. Gravimetric composition of MSW

Figure 5 shows that 47% of the MSW is composed of putrescible materials. This high amount of organic matter (OM) can influence waste mass settlement when the environment provides favorable conditions for the biodegradation of OM. The percentage of recyclable materials, such as plastic, papers and cardboards, metals and glass, in the total waste composition is shown as well.

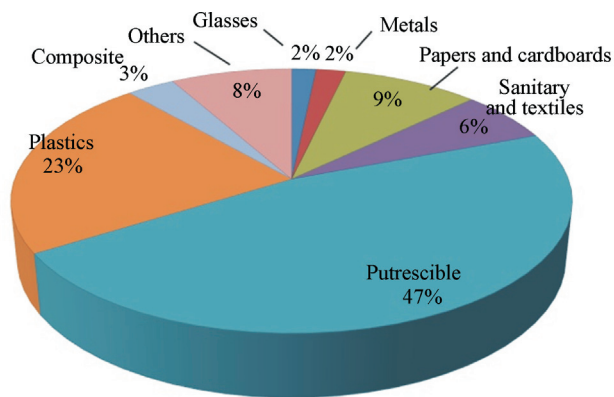


Figure 5 - Gravimetric composition of the MSW from Campina Grande.

3.2. Settlement model

Figure 6 presents the dispersion diagram of the studied variables, which shows an association between the values of settlement and time. Initially, there is no linear relationship between the variables. However, from day 19, the monitored data presented a positive linear trend. In other words, as time increased, the values of settlement concomitantly increased. Before day 19, the settlement had a nonlinear trend, which is mainly due to volume reduction caused by mechanical processes (rearrangement of the particles and compaction due to waste's self-weight) that occur in the waste mass during the lysimeter filling process.

According to Hettiarachchi *et al.* (2009) and Dixon & Jones (2005), waste settlement takes place due to mechanical and biological processes. The initial settlement phase, which is usually 30 days long, is characterized by the predominance of compressibility and mechanical processes. The final settlement phase is mostly due to biological processes. These features may reduce or increase the degree of

linear dependence between the variables of time and settlement.

When settlement occurs due to the predominance of mechanical processes, there is a quick waste mass deformation and a non-linear settlement behavior over time. However, when biodegradation processes are present, waste settlement tends to be linear over time, which is probably due to the organic matter biostabilization constant. The interquartile range and its critical limits (Table 2) were determined with the purpose of removing outliers and selecting a range in which the settlements values present a linear behavior over time.

As the interquartile range indicates, the model had to be developed with settlement values above 0.3068 m and less than 0.7368 m. However, before modeling, the normal-

Table 2 - Settlement variability.

Variable	1st quartile	3rd quartile	Mean	Median	Lower critical limit	Upper critical limit
Settlement (m)	0.4485	0.5950	0.5608	0.5430	0.3068	0.7368

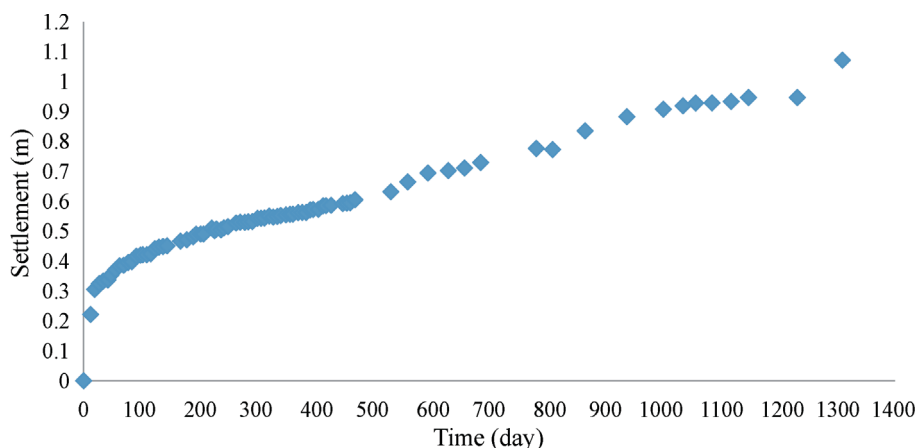


Figure 6 - Dispersion diagram of waste settlement over time.

ity of settlement data was analyzed through the Kolmogorov - Smirnov test (Table 3).

Considering a significance level (α) of 0.05 and a number of observations (n) of 67, it can be seen in Table 3 that $D_{calculated}$ is less than the $D_{tabulated}$. Thus, there was no evidence to reject the normality assumption. Also, research data followed a normal distribution since the p-value is greater than 0.05 (null hypothesis). Tables 2 and 3 only analyzed the response variable (settlement) because time is an independent variable, not requiring such studies since its variation does not depend on settlement.

The selected range for determining the linear regression model presented a correlation coefficient of 0.98, which indicates that settlement and time are directly related. In other words, there is a strong linear correlation between these variables, but this correlation may have occurred by chance. Because of that, a Student's t-test was carried out to verify if the association between the variables is real. With a significance level of 0.05 and a degree of freedom of 65, the $t_{calculated} = 39.4$ was higher than the $t_{critical} = 1.10$, meaning that the correlation is statistically significant.

The linear regression was determined with $R^2 = 0.97$, indicating that 97% of the settlement variability can be explained by the model during the considered time range. Through Table 4, it is verified that p-value was lower than 0.05, so the regression has statistical significance. Also, as indicated by the angular coefficient of the linear regression equation, for each additional day, it is expected that the waste mass presents a settlement of 0.00055 m.

Equation 6 was used to perform predictions about the settlement that occurred in the lysimeter over the time range between 19 and 809 days.

$$y = 359.9 + 0.55x \quad (6)$$

where y = settlement (mm) and x = time (day).

According to Eq. 6, it is expected to occur a deformation of 0.805 m in the waste mass until day 809. Because of that, there will be a gain of available spaces that might be used to storage more waste. This way, such space saving could maximize the sanitary landfill useful life.

According to Table 4, the upper and lower equations can be determined, with 95% of confidence (Eqs. 7 and 8),

from the developed model, which means that the observed data is within this range.

$$\text{Lower: } y = 332.9 + 0.52x \quad (7)$$

$$\text{Upper: } y = 366.6 + 0.58x \quad (8)$$

where: y = settlement (mm) and x = time (day).

Figure 7 shows the model's trend lines and the settlement values from the lysimeter monitoring.

To investigate the suitability of the regression model and validate it, a statistical residual analysis was conducted through the regression diagnosis. The Goldfeld-Quandt test (Table 5) was used to test the null hypothesis in which the errors variances are equal (homoscedasticity) and the alternative hypothesis in which the errors variances are a multiplicative function of the variable.

As it is seen in Table 5, the statistical residual has homoscedasticity since the p-value is greater than the significance level of 0.05. Thus, the standard errors of the estimators obtained by the method of least squares are consistent and statistical inference is valid, so it is possible to conclude that the estimators of the linear regression equation are appropriate.

To verify if the residual is independent, the Durbin-Watson test (Table 6) was performed. Such test had the statistical residual dependence as null hypothesis and statistical residual independence as alternative hypothesis.

According to Table 6, $0 \leq DW \leq DL$ and the p-value was less than 0.05, which means that the null hypothesis can be rejected. Therefore, it is possible to affirm, with a confidence level of 95%, that the residuals are independent and have a positive correlation.

4. Conclusion

The developed model considered significant statistical parameters to estimate waste settlement. Such model can be applied for estimating settlement values from sanitary landfills with similar features to the ones used in this model.

The lysimeter's total waste settlement was about 1.1 m during a monitoring time of 1300 days. The settlement prediction through the developed model is only indicated for an amount of time longer than 19 days and less than 809 days. However, this fact does not disqualify the proposed model since adjustment difficulties for models like this one are typical during the initial period.

To obtain a model that reflects the initial monitoring time, other variables such as waste density, cover layer and

Table 3 - Normality test.

Variable	p-value	$D_{calculated}$	$D_{tabulated}$
Settlement	0.099	0.099	0.167

Table 4 - Linear regression.

	Coefficient	p-value	Lower limit	Upper limit
Linear (Intersection)	359.9	1.05×10^{-67}	351.3	358.6
Angular (Time)	0.55	7.4×10^{-50}	0.52	0.57

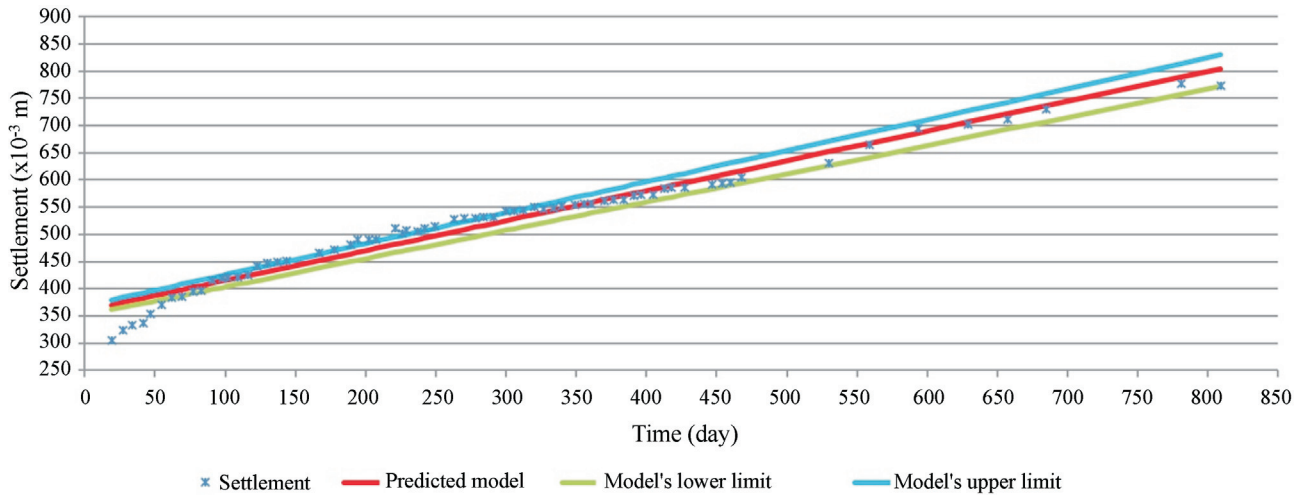


Figure 7 - Dispersion of the predicted settlement values adjusted by the models.

Table 5 - Goldfeld-Quandt test.

Variable	GQ	p-value
Time	0.42	0.98

Table 6 - Durbin-Watson test

DW	DL	DU	p-value
0.126	1.573	1.634	0.42×10^{-34}

external loads must be incorporated into modeling, or another model should be developed with a combination of linear and nonlinear regression.

References

ABNT (2004). NBR 10007: Resíduos Sólidos - Amostragem de Resíduos. Rio de Janeiro, Brazil, 21 p.

Babu Sivakumar, G.L.; Reddy, K.R.; Chouskey, S.K. & Kulkarni, H.S. (2010) Prediction of Long-term Municipal Solid Waste Landfill Settlement Using Constitutive Model. Practice Periodical of Hazardous, Toxic, and Radioactive Waste Management, 14(3):139-150.

Babu, G.S. & Lakshmikanthan, P. (2015). Estimation of the components of municipal solid waste settlement. Waste Management & Research, 33(1):30-38.

Bareither, C.A. & Kwak, S. (2015) Assessment of municipal solid waste settlement models based on field-scale data analysis. Waste Management, 42:101-117.

Borges, B.L.M. (2003). Simplificando a Estatística: Coleção de Textos e Exercícios Didáticos. EDUEP, Campina Grande.

Boscov, M.E.G. (2006). Desafios geotécnicos no projeto e construção de aterros de resíduos. Proc. XIII Congresso Brasileiro de Mecânica dos Solos e Engenharia Geotécnica, COBRAMSEG, Curitiba, v. 4, pp. 1-30.

Breusch, T.S. & Pagan, A.R. (1979). A simple test for heteroscedasticity and random coefficient variation. *Econometrica. Journal of the Econometric Society*, 47(5):1287-1294.

Dixon, N. & Jones, D.R.V. (2005). Engineering properties of municipal solid waste. *Geotextiles and Geomembranes*, 23(3):205-233.

Durbin, J. & Watson, G.S. (1950). Testing for serial correlation in least squares regression: I. *Biometrika*, 37(3/4):409-428.

Durmusoglu, E.; Corapcioglu, M.Y. & Tuncay, K. (2005). Landfill settlement with decomposition and gas generation. *Journal of Environmental Engineering*, 131(9):1311-1321.

El-Fadel, M. & Houry, R. (2000). Modeling settlement in MSW landfills: a critical review. *Critical Reviews in Environmental Science and technology*, 30(3):327-361.

Farias, R.M.S (2014). Estudo de recalques em aterros de resíduos sólidos urbanos: Uma abordagem experimental e estatística. MSc Thesis, Universidade Federal de Campina Grande, Campina Grande.

Fernandes, T.J.; Pereira, A.A.; Muniz, J.A. & Savian, T.V. (2014). Seleção de modelos não lineares para a descrição das curvas de crescimento do fruto do cafeeiro. *Coffee Science*, 9(2):207-215.

Galton, F. (1886). Regression towards mediocrity in hereditary stature. *The Journal of the Anthropological Institute of Great Britain and Ireland*, 15:246-263.

Gosset, W.S. (1908). The probable error of a mean. 1st ed. *Biometrika*, v.6, pp.1-25.

Hachich, W. (2000). Modelos em Engenharia Geotécnica. Prova de notório saber, Concurso de Titular, Escola Politécnica da USP, São Paulo.

Hettiarachchi, H.; Meegoda, J. & Hettiaratchi, P. (2009). Effects of gas and moisture on modeling of bioreactor landfill settlement. *Waste Management*, 29(3):1018-1025.

- IBGE (2010). Instituto Brasileiro de Geografia e Estatística. Contagem Populacional, 2010.
- Leite, H.E.A.S. (2008). Estudo do Comportamento de Aterros de RSU em um Biorreator em Escala Experimental na Cidade de Campina Grande - Paraíba. MSc Thesis, Universidade Federal de Campina Grande - UFCG, Campina Grande.
- LIPOR (2000). Serviço Intermunicipalizado de Gestão de Resíduos do Grande Porto. Caderno Técnico.
- Massey Jr, F.J. (1951). The Kolmogorov-Smirnov test for goodness of fit. *Journal of the American Statistical Association*, 46(253):68-78.
- Melo, M.C. (2003). Uma Análise de Recalques Associada à Biodegradação no Aterro de Resíduos Sólidos da Muri-beca. MSc Thesis, Universidade Federal de Pernambuco, Recife .
- Melo, M.C. (2011). Estudo da Matéria Orgânica nos Recalques de Resíduos Sólidos Urbanos Aterrados. PhD Dissertation, Universidade Federal de Campina Grande, Campina Grande.
- Ouvry, J.F. & Page, B. (2005). Settlement of waste packaged in chaffs in a domestic waste disposal. Proc. International workshop on hydro-physico-mechanics of landfills, Grenoble University I, France.
- Paiva, W. (2009). Aplicação da Estatística Para Descrever um Comportamento de um Solo Expansivo. PhD Dissertation, Universidade Federal de Pernambuco, Recife.
- Pearson, K. (1896). Regression, heredity, and panmixia. *Philosophical Transactions of the Royal Society of London*, 187:253-318.
- Pereira, F.T.G.; Leite, H.E.A.; Garcez, L.R.; Araujo, E.P.; Melo, M.C. & Monteiro, V.E.D. (2010). Composição Gravimétrica dos Resíduos Sólidos Urbanos da Cidade de Campina Grande-PB. Proc. 2º Simpósio Nordeste de Resíduos Sólidos, SINRES, Campina Grande-PB.
- Qian X.D.; Koerner R.M. & Gray D.H. (2002) *Geotechnical Aspects of Landfill Design and Construction*. Englewood Cliffs, NJ: Prentice-Hall.
- Rafizul, I.M.; Subbir, Y. & Alamgir, M. (2014). Lysimeter Studies for Leachate Characterization Generated from Municipal Solid Waste in Pilot Scale Landfill of Bangladesh. *The Journal of Solid Waste Technology and Management*, 40(4), 311-326.
- Simões, G.F. (2000). Modelo para Avaliação de Recalques em Aterros de Disposição de Resíduos Sólidos Urbanos. PhD Dissertation, Programa de Pós-Graduação em Engenharia Civil, Pontifícia Universidade Católica do Rio de Janeiro, Rio de Janeiro, 136 p.
- Sowers, G.F. (1973). Settlement of waste disposal fills. Proc. Eighth International Conference on Soil Mechanics and Foundation Engineering's, Moscow, v. 2, pp. 207-210.
- Zimmerman, R.E.; Chen, W.W.H. & Franklin, A.G. (1977). Mathematical model for solid waste settlement. Proc. Conf. on Geotechnical Practice for Disposal of Solid Waste Materials, Ann Arbor, Michigan, USA, pp. 210-226.

Appendix: Table A1 - Experimental readings of each plate.

Time (days)	Surface plate A (m)	Surface plate B (m)	Mean (m)	Time (days)	Surface plate A (m)	Surface plate B (m)	Mean (m)
0	0.00	0.00	0.00	320	0.56	0.54	0.55
12	0.22	0.23	0.22	327	0.55	0.55	0.55
19	0.30	0.31	0.31	334	0.55	0.55	0.55
27	0.32	0.33	0.32	340	0.55	0.55	0.55
34	0.33	0.34	0.33	349	0.56	0.55	0.55
42	0.34	0.34	0.34	356	0.56	0.55	0.56
47	0.35	0.36	0.35	361	0.56	0.55	0.56
55	0.37	0.37	0.37	370	0.56	0.56	0.56
62	0.38	0.39	0.38	377	0.56	0.56	0.56
69	0.38	0.39	0.39	384	0.57	0.56	0.56
77	0.39	0.40	0.40	391	0.57	0.57	0.57
83	0.39	0.40	0.40	396	0.57	0.57	0.57
91	0.41	0.42	0.42	405	0.58	0.57	0.57
98	0.42	0.42	0.42	413	0.59	0.58	0.58
102	0.42	0.42	0.42	418	0.59	0.58	0.59
109	0.42	0.42	0.42	427	0.59	0.58	0.59
116	0.43	0.42	0.42	447	0.60	0.59	0.59
123	0.44	0.45	0.44	454	0.60	0.59	0.59
130	0.44	0.45	0.45	460	0.60	0.59	0.60
137	0.45	0.45	0.45	468	0.61	0.60	0.61
144	0.45	0.45	0.45	530	0.64	0.62	0.63
167	0.47	0.47	0.47	559	0.67	0.66	0.66
178	0.47	0.47	0.47	594	0.70	0.69	0.69
189	0.48	0.49	0.48	629	0.70	0.70	0.70
194	0.49	0.49	0.49	657	0.72	0.70	0.71
202	0.49	0.49	0.49	685	0.73	0.73	0.73
207	0.49	0.49	0.49	781	0.78	0.78	0.78
221	0.51	0.51	0.51	809	0.78	0.78	0.78
226	0.50	0.50	0.50	865	0.84	0.83	0.84
229	0.51	0.51	0.51	916	0.86	0.85	0.86
237	0.50	0.51	0.50	937	0.89	0.87	0.88
242	0.51	0.51	0.51	1000	0.91	0.90	0.91
249	0.52	0.52	0.52	1034	0.92	0.92	0.92
256	0.52	0.52	0.52	1056	0.92	0.94	0.93
263	0.53	0.53	0.53	1084	0.92	0.94	0.93
270	0.53	0.53	0.53	1117	0.93	0.94	0.93
278	0.53	0.53	0.53	1147	0.95	0.94	0.95
284	0.53	0.53	0.53	1231	0.96	0.94	0.95
291	0.53	0.53	0.53	1309	1.11	1.04	1.07
300	0.54	0.54	0.54				
306	0.55	0.54	0.54				
312	0.54	0.55	0.54				

An Evaluation of the Shaft Resistance of Piles Embedded in Gneissic Rock

E.L. Juvencio, F.R. Lopes, A.L.L.S. Nunes

Abstract. In the design of piles drilled in rock, the following questions arise: (i) at what point of the soil/weathered rock/sound rock profile should the pile socket be designed; (ii) is the contribution of residual soil to be disregarded; (iii) how much consideration should be given to the pile boring method (rotary or hammering). Furthermore, usual design methods consider only the side shear capacity of the socket, which is evaluated through empirical expressions that require the uniaxial compressive strength of the intact rock (q_u or UCS). And, quite often in practice, a comprehensive test program is not available, and only boring logs are available. This paper examines data from a BRT (Bus Rapid Transit) project in Rio de Janeiro, with 8 bridges, in which some 30 dynamic tests were performed on piles partly embedded in residual soil and partly in rock - a gneiss. These tests produced profiles of mobilized side shear. For the evaluation of the mobilized side shear, a series of laboratory tests were performed on rock samples with different RQDs, taken from borings at the pile sites. A relation between q_u (uniaxial compressive strength of the intact rock) and RQD could be established for gneissic rocks of Rio. Values of mobilized side shear are compared to q_u derived from the RQD correlation. Finally, an expression for the prediction of mobilized pile shaft capacity is put forward.

Keywords: pile foundations in rocks, bearing capacity of piles, skin friction, dynamic tests on piles.

1. Introduction

Pile foundations drilled in rock are required for heavy structures and/or when rock occurs at relatively shallow depths. Although a straightforward solution, the design engineer often faces questions such as (i) at what point of the soil/weathered rock/sound rock profile should the pile socket be designed; (ii) is the contribution of residual soil to be disregarded; (iii) how to proceed in the - not uncommon - situation in which only boring data, such as rock classification and RQD, is available; (iv) how much consideration should be given to the boring method. The last question arises from the fact that most common boring methods are either (a) water assisted (“wet”) rotary drilling or (b) compressed-air assisted (“dry”) down-the-hole hammer drilling.

Usual design methods consider only the shaft capacity of the rock socket - through side shear or skin resistance - which is evaluated through empirical expressions. Such expressions have as starting point the uniaxial compressive strength of the intact rock (q_u or UCS). However, it is not uncommon in practice that a laboratory test program, which covers the extension of the work, is not available and design has to be based on boring data (rock classification and RQD).

Several bridges had to be built for a BRT project in Rio de Janeiro, and most of the foundations were piles in rock. In the Rio de Janeiro region, the usual rock is gneiss, with occasional granite occurrences. The city is known for its rock outcrops, and, in most of the flatter areas, rock is found under a cover of weathered material, usually a few meters thick. In this project, as usual in the city, piles were embedded partly in residual soil and partly in rock. As part of the quality control of the project, 30 dynamic pile tests were performed.

The dynamic tests produced a profile of mobilized side shear for each pile. For the evaluation of the mobilized side shear (as a function of the uniaxial compressive strength), a series of laboratory tests were performed on rock samples with different RQDs, taken from borings at the pile sites. A relation between uniaxial compressive strength of the intact rock (q_u) and RQD could be established for gneissic rocks in the Rio de Janeiro region. Values of mobilized side shear are compared with the uniaxial compressive strengths of the intact rock (q_u) derived from the RQD correlation. Finally, an expression for the prediction of mobilized pile shaft capacity is put forward.

2. Current Rock Socket Design Methods

A rock-socketed pile, with its main resistance components, can be seen in Figure 1. In design practice, if perfect

Erisvaldo L. Juvencio, DSc., Consulting Engineer, Fundação Oswaldo Cruz, Rio de Janeiro, RJ, Brazil. email: erisvaldo.lima@gmail.com.
Francisco R. Lopes, PhD., Full Professor, COPPE, Universidade Federal do Rio de Janeiro, Rio de Janeiro, RJ, Brazil. email: flopes@coc.ufrj.br.
Anna Laura L.S. Nunes, PhD., Associate Professor, COPPE, Universidade Federal do Rio de Janeiro, Rio de Janeiro, RJ, Brazil. email: alaura@coc.ufrj.br.
Submitted on September 2, 2016; Final Acceptance on March 13, 2017; Discussion open until August 31, 2017.

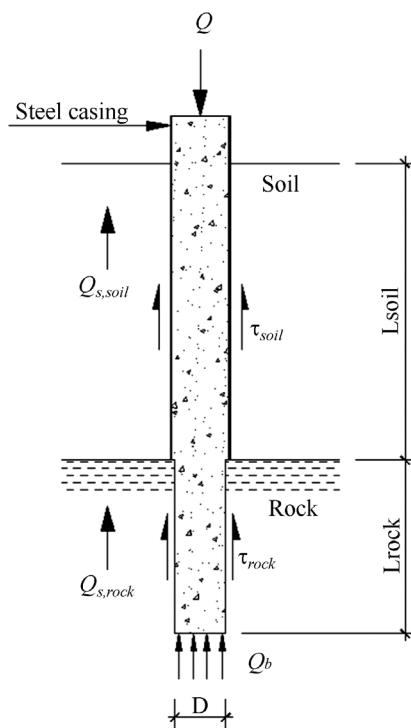


Figure 1 - A rock-socketed pile, with its main resistance components.

clearing of the bottom of the borehole is not ensured, pile base contribution (Q_b) is not considered. Furthermore, since the displacement necessary for full mobilization of the pile shaft shear resistance in rock (τ_{rock}) is much smaller than that for the overlying soil (τ_{soil}), soil contribution ($Q_{s,soil}$) is considered with restriction. Therefore, rock-socketed piles derive most of their bearing capacity from the shaft shear resistance in rock ($Q_{s,rock}$).

According to Goodman (1989), when concrete is poured against a drilled rock surface, it develops a strong bond, which can carry shear stresses up to the shear strength of rock or of the concrete, whichever is smaller.

Most design methods derive from a comparison of the rock compressive strength (q_u) measured in laboratory tests with the pile shaft shear resistance (τ_{max}) observed in field or model tests. Laboratory tests are performed on rock specimens that are homogeneous and have no joints and, therefore, some correction has to be made to extend the laboratory measured strength to the strength of the rock mass.

The pile/rock interface (or side shear) resistance is usually predicted from the rock compressive strength through an expression such as:

$$\tau_{ult} = \alpha q_u^\beta \quad (\text{usually in MPa}) \quad (1)$$

Eq. 1 can be expressed in normalized form by dividing both unit side shear resistance and compressive strength by atmospheric pressure ($p_{atm} = 0.1013$ MPa):

$$\frac{\tau_{ult}}{p_{atm}} = \alpha' \left(\frac{q_u}{p_{atm}} \right)^{\beta'} \quad (\text{unit independent}) \quad (2)$$

where α (and α') and β (and β') are empirical factors, while q_u is the uniaxial compressive strength of the *intact rock*.

When using Eq. 1 in MPa, values for α in the range 0.2-0.8 (upper limit for very rough or grooved boring surfaces) and for β in the range 0.6-0.8 have been suggested by Horvath (1978), Meigh & Wolski (1979), Pells *et al.* (1980), Rowe & Armitage (1987), Zhang (1997), Zhang & Einstein (1998). In the case of Eq. 2, values for α' in the range 0.8-2.5 (upper limit for very rough or grooved surfaces) and β' in the range 1.0-2.5 have been suggested by Rosenberg & Journeaux (1976), Horvath & Kenney (1979), Mcvay *et al.* (1992).

As mentioned earlier in this item, the pile shaft shear resistance is limited by the shear resistance of the concrete, which can be estimated as:

$$\tau_{conc} = 0.1 f_{ck} \quad (3)$$

where f_{ck} is the characteristic (compressive) strength of the concrete.

The above expression is based on laboratory tests of concrete joints conducted at the Federal University of Rio de Janeiro. The strength envelope indicated that the shear strength at a concrete joint under no compressive stress is very close to the tensile strength of the concrete. In the upper part of the pile, normal stresses are low and the assumption of these conditions for the whole shaft is on the safe side.

3. BRT Project in Rio de Janeiro

A new BRT (Bus Rapid Transit) line, named Transcarioca, connects the borough of Barra da Tijuca to Rio de Janeiro International Airport (Maestro Tom Jobim). As it approaches the airport, a series of 6 bridges/viaducts were required, as shown in Fig. 2. Figures 3 and 4 show OAE-02/03 and OAE-06 in perspective.

The region, as typical of Rio de Janeiro, presents gneisses at relatively shallow depths. Therefore, foundations for most bridge columns were cast-in-place piles excavated through soil and penetrating rock.

With the aim of both quality control and of acquiring a better knowledge of rock-socketed pile behaviour, 30 (high strain) dynamic load tests were carried out.

Piles partly embedded in rock are commonly installed by driving a steel casing down to the top of the bedrock and then boring the socket. The pile is completed by placing the

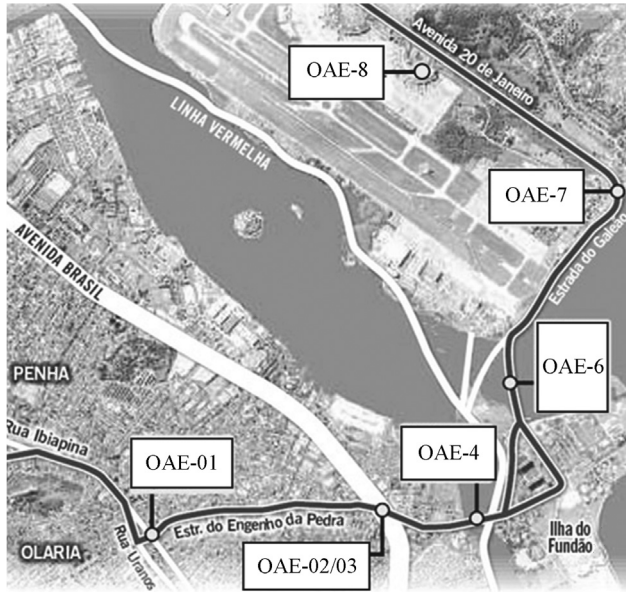


Figure 2 - Location of bridges of the BRT Project close to Rio de Janeiro International Airport.



Figure 3 - OAE 2/3 (Pedro Ernesto Viaduct).



Figure 4 - OAE 6 (Pereira Passos Bridge).

reinforcement (usually a “cage”) and pouring a self-compacting concrete. The steel casing is driven by a hammer or forced down by a rotary equipment that has a pull-down force and the interior of the casing is cleared from soil (usually washed or removed by auger) before introducing the boring tool. Boring methods usually fall in two categories: (a) rotary drilling, with rock debris removed by water circulation (sometimes referred to as “wet” or Wirth drilling), and (b) use of down-the-hole (DTH) hammer, with debris removed by compressed-air (“dry” boring). The steel casing is usually lost and becomes part of the pile (as in this work) but, in some situations, the casing can be retrieved with the help of a vibrator.

Piles types for the BRT Project, their service (or working) loads and rock drilling equipment can be seen in Table 1.

The “dry” hammer boring proved much more efficient than the “wet” rotary drilling. Since compressed-air lifting of rock debris is restricted to a limited depth (typically 15 m), “dry” hammer boring was used on land and the “wet” rotary drilling on water.

Figures 5 to 7 show equipment used in boring rock sockets.

Dynamic tests were carried out according to Brazilian standard NBR 13208 (2007), which follows ASTM D4945 (2012). As a standard test procedure in Brazil, pile (soil/rock) resistances were measured at various blows, with increasing energy in order to evaluate the proximity of the ultimate resistance. Data acquisition equipment was Pile Dynamics Inc. made Pile Driving Analyzer (PDA), and data were processed by (a) the CASE Method (using program PDI-CURVES) for all blows and (b) CAPWAP (CAse Pile Wave Analysis Program) for the blow with the highest energy.



Figure 5 - Rotary equipment for rock drilling, with rock bit diameter 70 cm, sitting on top of an already impact driven steel casing, diameter 80 cm.

Table 1 - Characteristics of the BRT Project piles.

Bridges	Service Load (kN)	Steel casing diameter	Rock sockets diameter	Equipment used for rock drilling
OAE 1	2000	50 cm	39 cm (15")	DTH hammer
OAE 2/3	4000	80 cm	70 cm	DTH hammer
OAE 4 and 7	4000	80 cm	70 cm	Wirth drilling
OAE 6	2500	80 cm	70 cm	Wirth drilling
OAE 8	1600	50 cm	39 cm (15")	DTH hammer



Figure 6 - Equipment used to drive (by turning and pushing down) a steel casing, diameter 50 cm, and then lower a DTH hammer, 39 cm diameter.



Figure 7 - Equipment used to drive (by turning and pushing down) a steel casing, diameter 80 cm, and then lower a DTH hammer, 70 cm diameter.

Blows for pile diameter 50 cm (socket diam. 39 cm) were delivered by a 40 kN weight, falling from heights that varied from 15 cm to 75 cm. For pile diameter 80 cm (socket diam. 70 cm), a 61.2 kN weight, falling from 15 cm to 160 cm, was used. In the case of the 80 cm pile, the hammer is somewhat lighter than what would be desirable

(Rausche *et al.*, 2006, suggest a ram weight of at least 1% of the test load for piles in rock). It should be mentioned that the dynamic tests were hired by the Contractor without interference from the authors.

3.1. Criteria followed in the definition of pile length in the design stage

In the definition of pile length in the Design Stage, the following criteria were followed:

- (i) the pile socket was considered starting at the point where, in a mixed boring, percussion driving (SPT procedure) was not possible and had to change to rotary driving; at this point material classification conventionally changes from *residual soil* to *weathered rock*;
- (ii) the contribution of residual soil to pile capacity was disregarded (only the rock socket was considered);
- (iii) in the lack of laboratory tests, rock resistance was estimated from boring data, available at each bridge column, basically rock classification and RQD.

The rock - always a gneiss - unconfined compression resistance (q_u) was estimated as:

$$q_u = 5 + 0.4RQD \quad (q_u \text{ in MPa, } RQD \text{ in } \%) \quad (4)$$

This relation, adopted by the design firm, was intended to be on the safe side for use in preliminary design, and indicates a maximum q_u of 45 MPa for 100% RQD.

For the design of the lengths of the pile sockets, Eq. 2 was used with $\alpha' = 0.3$ and $\beta' = 0.7$ (values in the center of the literature's range). This led to rock socket lengths in the range 4 – 8 m (6 m being the typical length), adopted in the initial Design Stage. As in usual design practice, pile point resistance was not considered.

4. An Investigation into the Gneiss Resistance as Related to RQD

There is an argument as to whether RQD is an indication of the degree of rock fracturing only or is also an indication of rock weathering. In the case of the Rio de Janeiro gneiss, which is not a much fractured rock, RQD has a direct relation with weathering. Thus, a correlation between RQD and the uniaxial compressive strength (q_u) - obtained from the large pieces of the sample - was sought.

In order to establish a relation between the uniaxial compressive strength of the Rio de Janeiro gneiss and RQD, a set of samples was taken from boring with 4 RQD intervals, as if representing a rock weathering profile (as proposed by Deere, 1969). Figure 8 shows the set of selected samples, all obtained by rotary coring with NX double tube barrels (diameter 54.7 mm).

Rock samples (diameter 54.7 mm and height 109.4 mm) were cut and trimmed to ASTM D4543 (2001) specifications, and subject to axial compression in a Shimadzu testing machine, Model UH-F 1000 kN (Fig. 9a), of the Structures Laboratory of COPPE (Graduate School of Engineering), Federal University of Rio de Janeiro. Loading rate was 0.1 mm/min and vertical displacements were measured with a LVDT system, as shown in Fig. 9b.

Typical failure modes can be seen in Fig. 10.

4.1. Test results and analysis

The results of laboratory tests are summarized in Table 2 (samples obtained from the BRT Project), which presents individual results (5 specimens) and average

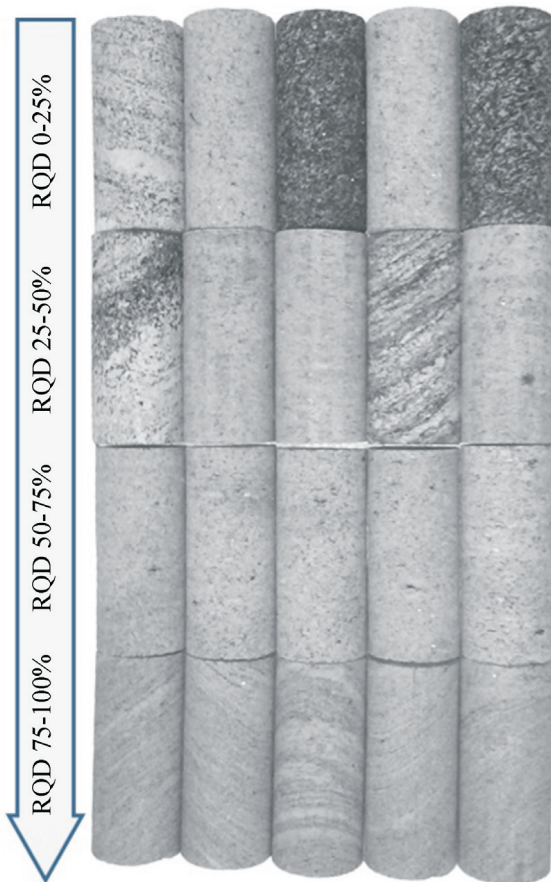


Figure 8 - Idealized rock profile with a set of 5 samples for each RQD interval.

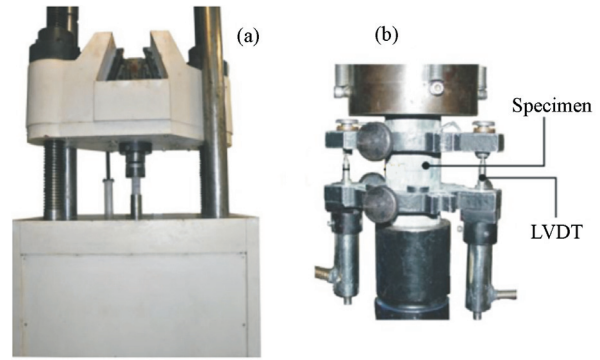


Figure 9 - (a) A Shimadzu 1000 kN testing machine and (b) test setup.

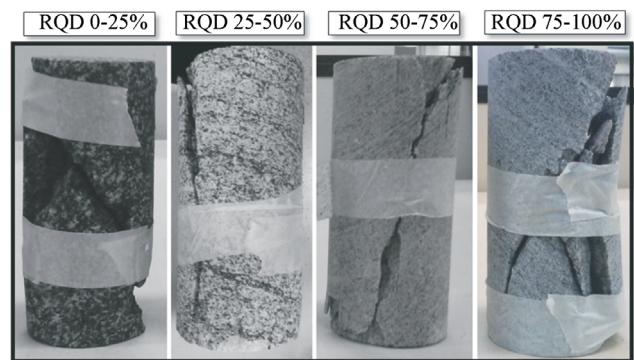


Figure 10 - Rock specimens after failure.

compressive strength, together with average RQD values for each set.

Test results of Table 2 (average values) are plotted in Fig. 11, which also displays a straight trend line and the line from the Design Stage Eq. 4. As can be seen in this figure, the Design Stage relation is well on the safe side.

The authors had access to a set of boring logs and laboratory test results also performed on gneiss in the Rio de Janeiro region. The Harbour of Rio de Janeiro is undergoing improvement works, more precisely at the cruiser's terminal (Pier Maua). At this location, rotary borings were conducted by Geodrill, and 13 samples, of various RQDs, were tested at the Rio de Janeiro State University (UERJ). Table 3 presents the results of individual tests.

Test results from both sets of data (Tables 2 and 3) are plotted in Fig. 12, also with a trend line. From this figure, it can be concluded that an *average relation* - close to the trend line - would be:

$$q_u = 5 + 0.8RQD \quad (q_u \text{ in MPa, } RQD \text{ in } \%) \quad (5)$$

In projects for which a comprehensive investigation, that includes laboratory tests, is not available for design, the authors suggest a safer equation:

$$q_u = 5 + 0.6RQD \quad (q_u \text{ in MPa, } RQD \text{ in } \%) \quad (6)$$

Table 2 - Values of RQD and q_u , BRT Project (5 specimens tested per RQD interval).

Rock description	RQD interval (%)	Average RQD (%)	q_u for each specimen (MPa)					Average q_u (MPa)
			Spec 1	Spec 2	Spec 3	Spec 4	Spec 5	
Gneiss (biotite gneiss) highly weathered and highly fractured	0-25	12.5	20.0	19.1	10.2	8.8	12.0	14.0
Gneiss (biotite gneiss) weathered and slightly fractured	25-50	33.5	36.6	25.7	43.3	37.8	32.1	35.1
Gneiss (biotite gneiss) moderately weathered and slightly fractured	50-75	62.5	39.3	55.4	87.0	75.2	72.2	65.8
Gneiss (biotite gneiss), sound and slightly fractured	75-100	87.5	79.3	85.4	87.4	97.3	97.2	89.3

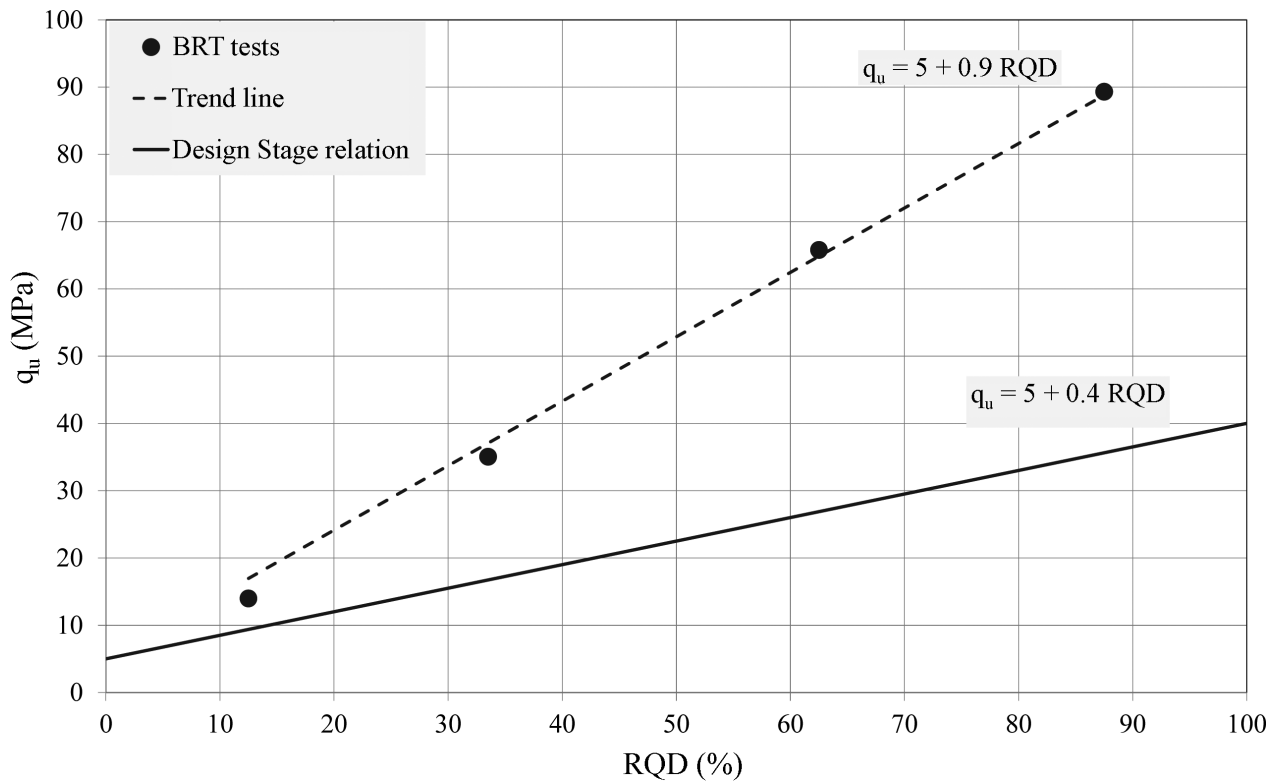


Figure 11 - Relation q_u vs. RQD from laboratory tests for the BRT Project (tests at the Federal University of Rio de Janeiro) and line from the Design Stage equation.

also shown in Fig. 12 - as *current proposal*.

5. Mobilized Side Shear and an Evaluation of Current Design Methods

An evaluation of the mobilized side shear of the pile was carried out by the analysis of the results of the 30 (high-strain) dynamic load tests (ASTM standard D4945). The blows with the highest energy were analyzed with CAPWAP, which can produce the mobilized side shear distribution with depth. Although subject to some discussion as to the uniqueness of its results (*e.g.*, Danziger *et al.*, 1996), CAPWAP results are accepted in practice, for both

distinguishing base and shaft loads and for the assessment of side shear distribution.

Boring logs - with SPT (in soil) and RQD (in rock) - were drawn alongside with the mobilized side shear revealed in CAPWAP analyses. All 30 ground and side shear profiles can be seen in Juvencio (2015), and a set of 5 typical profiles are shown in Figs. 13 to 17. In these figures, the following situations can be distinguished:

- i) the soil overlying the rock is weak, and side shear is developed only along the rock socket: Fig. 13;
- ii) soil and rock quality varies with depth, and side shear is very variable down to the pile tip: Fig. 14;

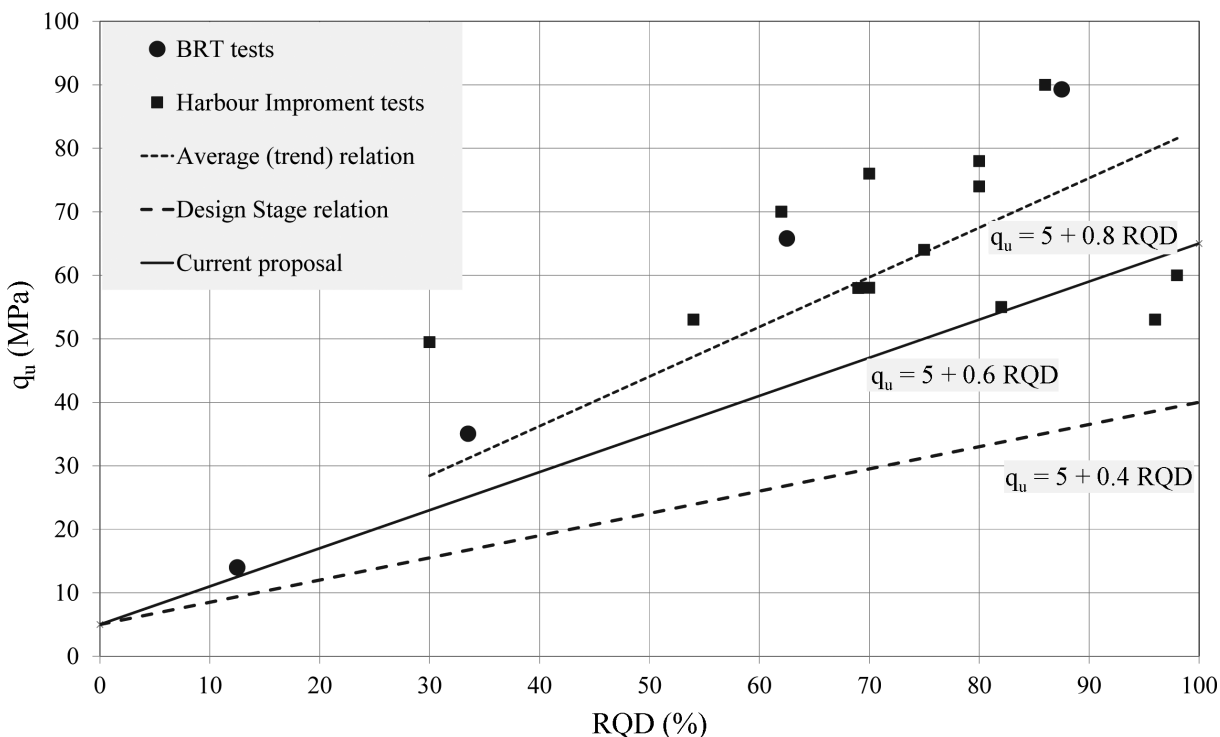


Figure 12 - Relation q_u vs. RQD from laboratory tests for the BRT Project (tests at Federal University of Rio de Janeiro) and for the Harbour Improvement (tests at Rio de Janeiro State University), including Design Stage relation, and current proposal.

Table 3 - Values of RQD and q_u , Rio de Janeiro Harbour Improvement (individual test results) Source: Geodrill / Rio de Janeiro State University.

Rock description	Sample no.	RQD (%)	q_u (MPa)
Gneiss, texture medium	01	69	58.0
	02	75	64.0
	03	86	90.0
	04	70	76.0
	05	62	70.0
	06	98	60.0
	07	70	58.0
	08	30	49.5
	09	80	78.0
	10	80	74.0
	11	82	55.0
	12	54	53.0
	13	96	53.0

iii) there is a good quality residual soil over the rock, and side shear is developed along both materials with an almost linear variation: Fig. 15;

iv) there is a good quality soil over the rock, and a little relatively low side shear is developed in the rock socket: Fig. 16;

v) the rock socket is too long, and the side shear decays along the socket to an almost null value: Fig. 17.

Figure 17 is in agreement with remarks by Wyllie (1999) that, in high quality rocks, load is carried by the upper portion of the socket. Wyllie suggests that this early transfer of shear stresses is favored by the fact that the rock has a higher Young's modulus (E_r) than the concrete. In the case of the Rio de Janeiro gneissic rock, when RQD was higher than 75%, E_r exceeded 45 GPa. On the other hand, the Young's modulus of the concrete is 30 - 35 GPa. In the case of Fig. 17, the rock had a RQD of 78%.

Figure 18 presents typical maximum displacement (DMX in Pile Dynamics software notation) vs. mobilized pile (total) resistance, in a series of blows with increasing energy, for two piles. This plot gives an indication of how close the test came to reach the pile maximum resistance (or capacity). Figure 18a, with results of pile E111, Block 16, Bridge OAE 8, presents a straight line (with maximum displacement of approximately 2 mm), which indicates that the maximum mobilized load was far from failure. Figure 18b, with results of pile E04, Support 2, Bridge OAE 6, presents a somewhat curved line (with a maximum displacement of approximately 5 mm), which indicates that the mobilized load was high. It should be noted that all tests mobilized loads that were at least twice the service load.

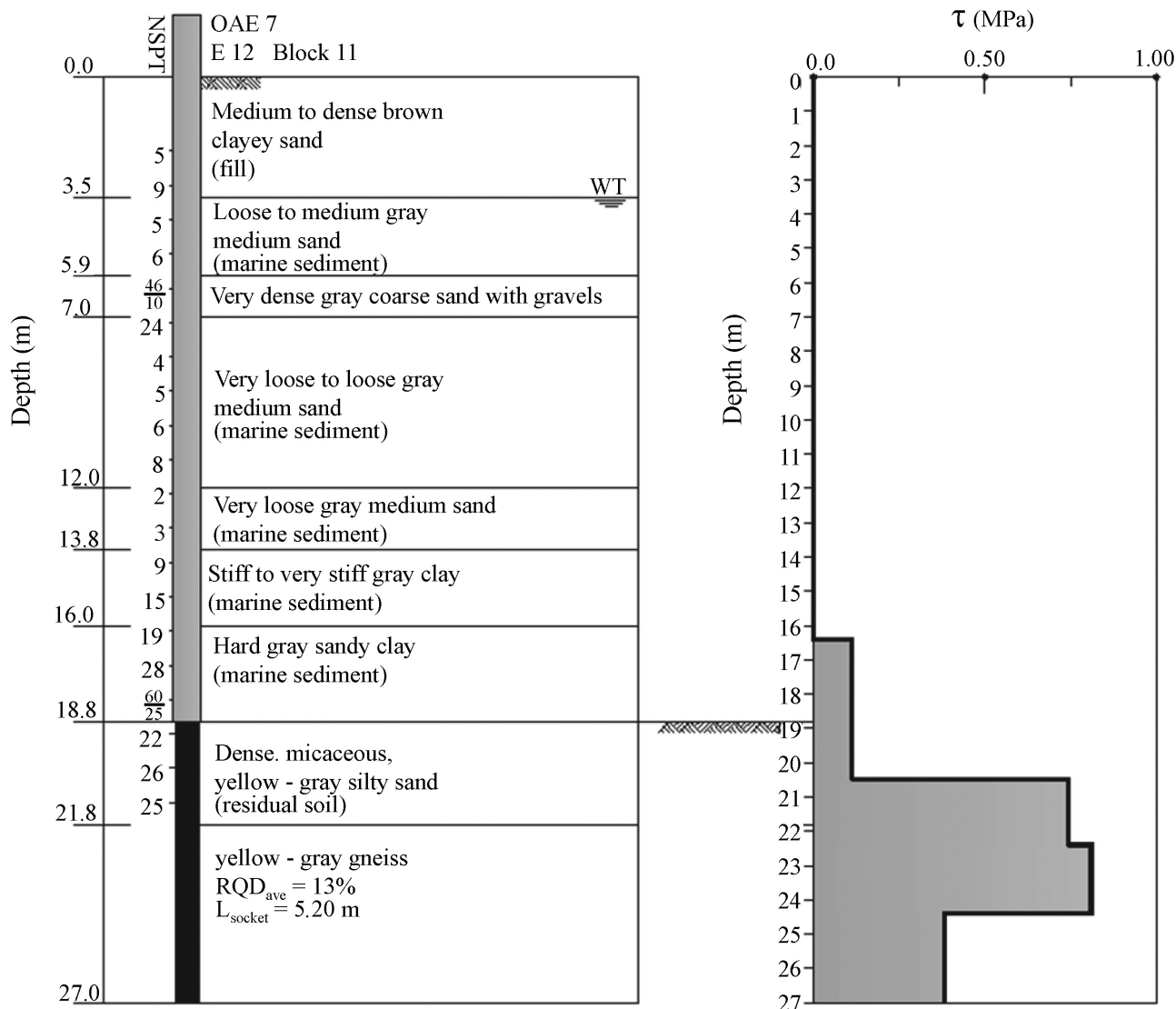


Figure 13 - Ground profile and mobilized shear stresses - OAE 7, Block 11, E12.

Table 4 presents pile dimensions, average RQD along the rock socket and average mobilized shear stress at the socket from dynamic tests.

Figure 19 (data from Table 4) presents a plot of the average mobilized shear stress obtained in dynamic tests against the average q_u estimated from average RQD along the pile socket with Eq. (6).

This figure indicates that mobilized shear stress values were lower than the side shear resistances predicted by the more commonly used methods, such as Horvath (1978), Williams & Pells (1981) (where $\tau_{ult} = \alpha_1 \beta_1 q_u$ and $\alpha_1 = 0.5q_u^{-0.5}$, and $\beta_1 = 0.6$; $\tau_{ult} = 0.5 \times 0.6q_u^{0.5}$) and Rowe & Armitage (1987). This can be explained by the fact that maximum shear resistance was not reached, mainly due to limited energy in the dynamic tests. Another contributing factor is that the above mentioned methods were developed

for sedimentary rocks, the maximum resistances of which are more easily reached in tests.

Figure 19 also shows that the boring method - either wet drilling, represented by circles, or dry hammering, represented by squares - seems to have little effect on the mobilized shear stress.

6. A Proposal for the Evaluation of Side Resistance of Pile Sockets in Gneiss

Since failure was not reached, the use of the data from the previous section (basically *average mobilized side shear*) to estimate the side shear capacity of a pile would be clearly on the safe side. For a more reasonable prediction of pile capacity it would be better to correlate the *maximum mobilized side shear* obtained at each pile segment in the

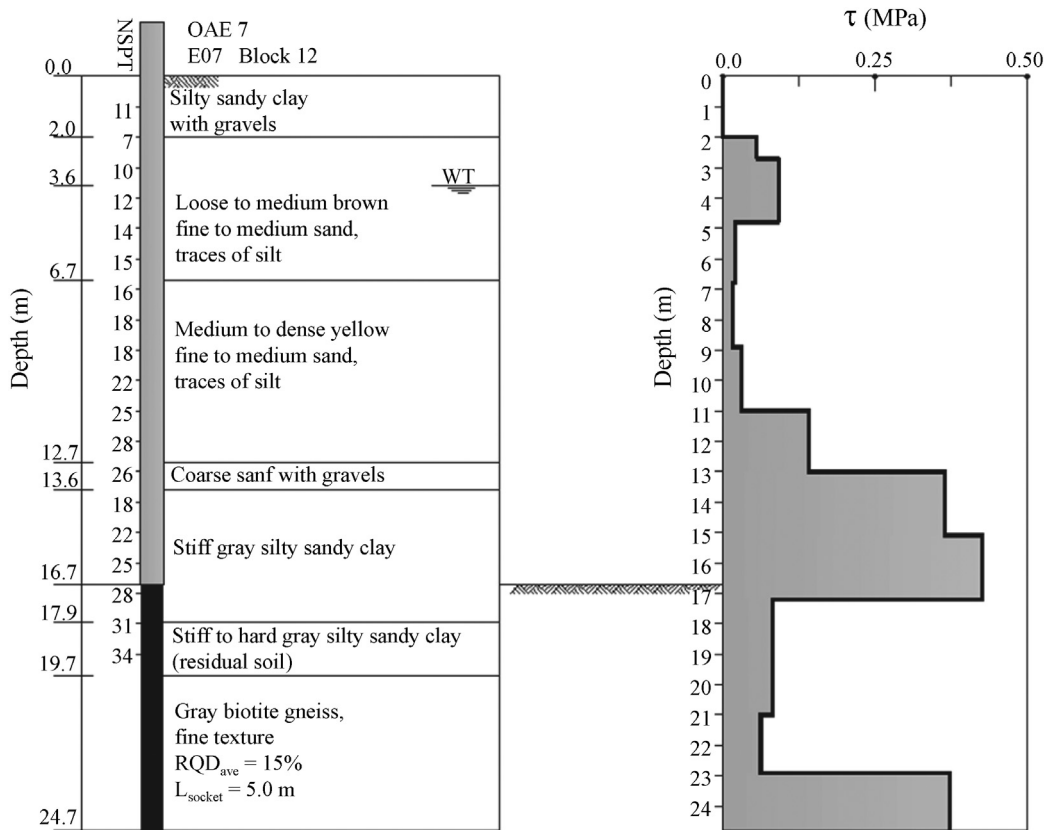


Figure 14 - Ground profile and mobilized shear stresses - OAE 7, Block 12, E07.

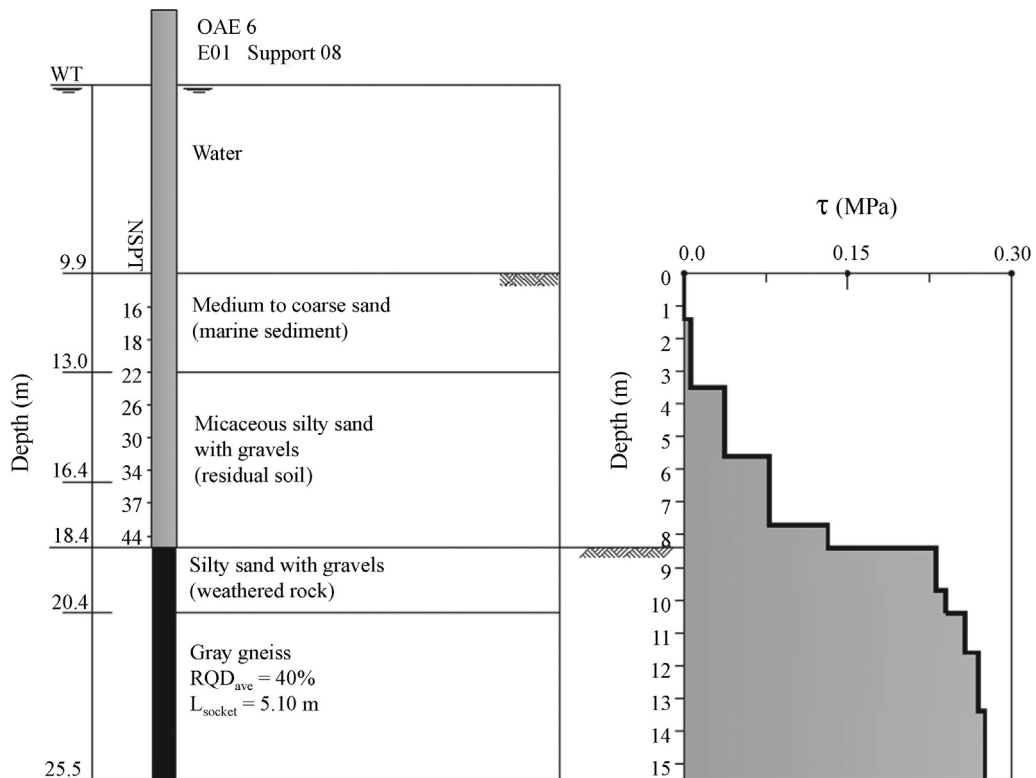


Figure 15 - Ground profile and mobilized shear stresses - OAE 6, Support 08, E01.

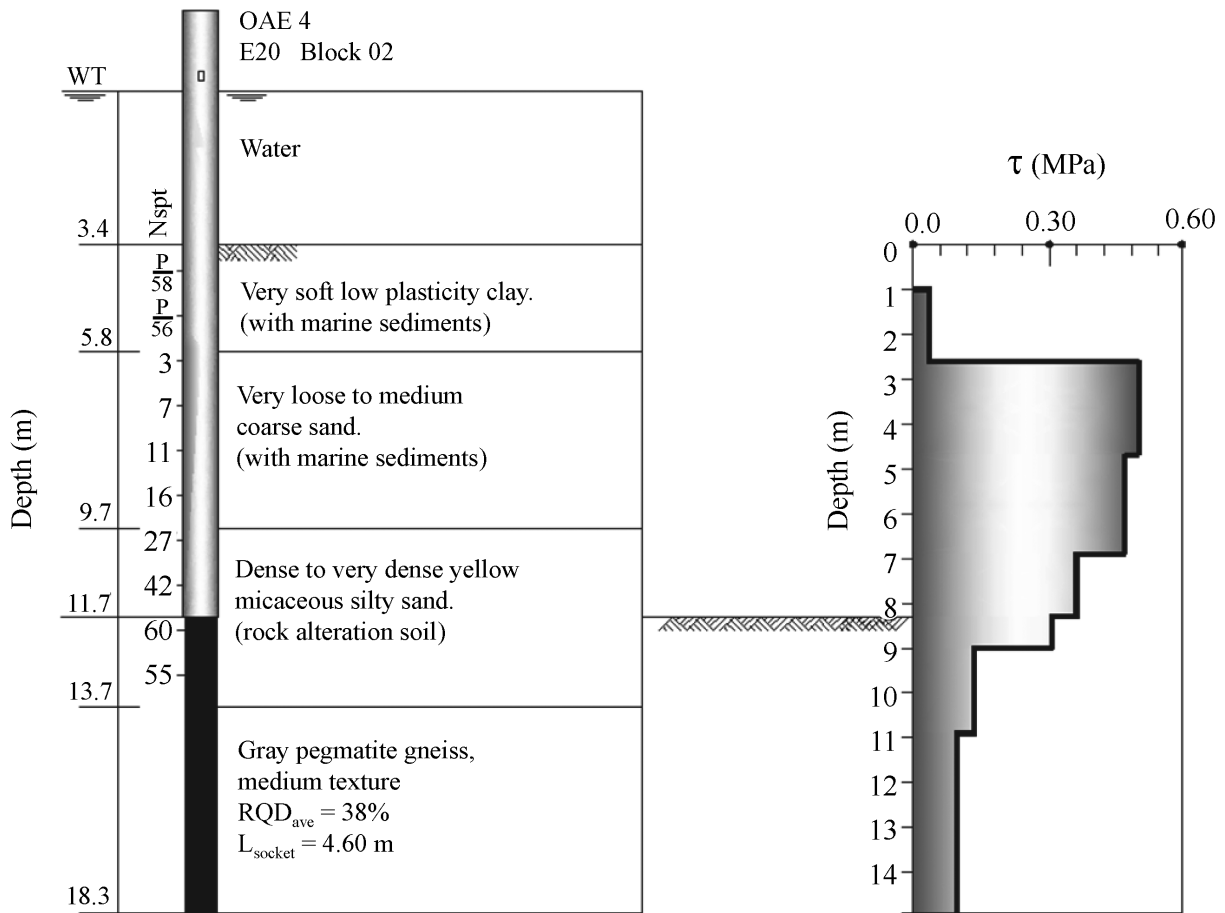


Figure 16 - Ground profile and mobilized shear stresses - OAE 4, Block 02, E20.

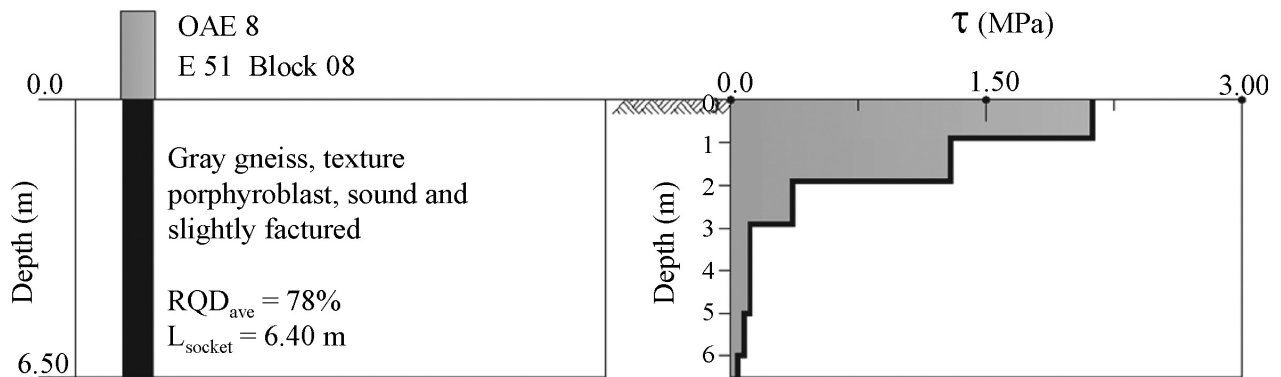


Figure 17 - Ground profile and mobilized shear stresses - OAE 8, Block 08, E51.

dynamic tests (CAPWAP results) with the corresponding q_u at the same level. In this case, q_u were obtained from RQD (at the same level) through Eq. 6. The results are presented in Fig. 20.

An interpretation of Fig. 20 leads to the following proposal for a prediction of the *available side shear* of pile sockets in gneiss of the Rio de Janeiro region:

$$\tau_{avail} = \alpha(5 + 0.6RQD)^\beta \quad (\tau_{avail} \text{ in MPa, } RQD \text{ in } \%) \quad (7)$$

with $\alpha = 0.2$ and $\beta = 0.5$ (very close to those suggested by Horvath, 1978).

Since the set of data points exhibits scattering, Eq. 7 can be understood as leading to reasonable values for design purposes.

7. Conclusions

The paper initially presents the results of laboratory tests performed on gneiss specimens with different RQDs.

Table 4 - Pile socket dimensions, average RQD along the pile socket and average mobilized side shear from dynamic tests.

Bridge/block	Pile no.	RMX (kN)	DMX (mm)	Pile Wave Speed (m/s)		Jc	Boring method	Pile dimensions			Average RQD (%)	Average $\tau_{\text{max, shaft}}$ (MPa)
				in soil	in rock			Diam. (mm)	Length in residual soil (m)	Length in rock (m)		
OAE 2 - Block 9	E19	13050	4.5	4167	3850	0.10	DTH	700	-	4.10	25	0.50
OAE 2 - Block 8	E15	13692	3.5	4167	4000	0.00	DTH	700	-	3.40	80	0.16
OAE 3 - Block 3	E01	18800	5.4	4167	4000	0.00	DTH	700	-	4.00	40	0.95
OAE 3 - Block 1	E02	13138	4.4	4167	4000	0.00	DTH	700	2.00	3.00	50	0.40
OAE 3 - Block 10	E05	14825	3.9	4167	4000	0.00	DTH	700	2.15	4.00	60	0.60
OAE 3 - Block 7	E08	14229	3.6	4167	4000	0.00	DTH	700	0.50	6.00	70	0.75
OAE 4 - Abutment 1	E04	8160	5.0	4167	3850	0.61	Wirth	700	-	3.40	78	1.02
OAE 4 - Block 2	E20	9253	5.8	4167	3850	0.00	Wirth	700	2.00	4.60	38	0.12
OAE 4 - Block 3	E27	8258	7.6	4167	3850	0.48	Wirth	700	-	6.60	20	0.23
OAE 6 - Support 7	E02	5933	3.9	4167	3850	0.53	Wirth	700	6.00	7.82	10	0.12
OAE 6 - Support 8	E01	6405	4.7	4167	3850	0.60	Wirth	700	2.00	5.10	40	0.27
OAE 6 - Support 10	E01	7071	3.3	4167	3850	0.45	Wirth	700	-	7.90	20	0.28
OAE 6 - Module 2	E13	6576	5.0	4167	3850	0.57	Wirth	700	7.00	4.30	30	0.23
OAE 6 - Support 2	E04	9488	5.1	4167	3850	0.22	Wirth	700	-	4.25	0	0.31
OAE 7 - Block 12	E07	9462	7.1	4167	3850	0.58	Wirth	600	3.00	5.00	15	0.17
OAE 7 - Block 13	E05	11718	6.3	4167	3850	0.65	Wirth	700	6.00	3.60	18	0.39
OAE 7 - Block 11	E12	12150	5.8	4167	3850	0.45	Wirth	700	3.00	5.20	13	0.60
OAE 7 - Block 10	E08	12500	7.0	4167	3850	0.03	Wirth	700	1.70	3.90	45	0.37
OAE 1 - Block 4	E02	5218	6.3	4000	4000	0.00	DTH	386	-	6.00	40	0.12
OAE 1 - Block 3	E08	5680	5.6	4000	4000	0.00	DTH	386	-	6.00	40	0.18
OAE 8 - Block 7	E42	4774	2.0	4000	4000	0.00	DTH	386	-	6.30	90	0.34
OAE 8 - Block 8	E51	4852	2.4	4000	4000	0.00	DTH	386	-	5.90	78	0.67
OAE 8 - Block 9	E60	5900	3.8	4000	4000	0.00	DTH	386	-	5.00	95	0.47
OAE 8 - Block 16	E111	5370	4.7	4000	4000	0.00	DTH	386	-	6.00	79	0.26
OAE 8 - Block 17	E117	3950	6.2	4000	4000	0.57	DTH	386	-	5.00	90	0.36
OAE 8 - Block 13	E93	4970	4.1	4000	4000	0.00	DTH	386	-	5.80	87	0.69
OAE 8 - Block 14	E99	4930	4.0	4000	4000	0.00	DTH	386	-	8.00	65	0.42
OAE 8 - Block 14	E100	4922	4.0	4000	4000	0.00	DTH	386	-	8.00	65	0.30
OAE 8 - Block 15	E105	5673	4.3	4000	4000	0.00	DTH	386	-	8.00	55	0.35
OAE 8 - Block 01	E05	5700	3.9	4000	4000	0.00	DTH	386	-	6.40	87	0.59

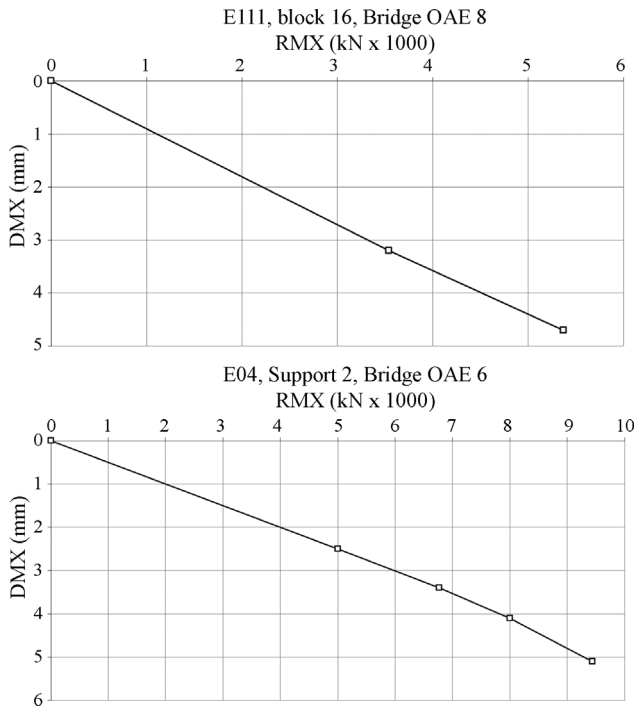


Figure 18 - Maximum displacement (DMX) vs. mobilized pile (total) resistance, in a series of blows with increasing energy, for piles E111, Block 16, Bridge OAE 8 and E04, Support 2, Bridge OAE 6.

If RQD is accepted as an indication not only of rock fracturing but also of rock weathering, a correlation between the uniaxial compressive strength (q_u) and RQD can be sought. Such correlation was obtained through laboratory tests for the gneissic rocks of the Rio de Janeiro region. RQD - q_u correlations have a practical importance due to the fact that, in most projects, a comprehensive laboratory test program is not available and design has to be based on boring data.

A series of dynamic tests, performed on piles of a BRT project in Rio de Janeiro were analyzed. Results show that the contribution to pile capacity of the residual soil overlying the rock is significant, although usually disregarded in design (there are some studies correlating SPT results with side shear in residual soils, a subject outside the scope of this paper). Although pile sockets were bored by two different methods - water assisted rotary drilling and compressed-air assisted down-the-hole hammering - the boring method did not seem to have a significant effect on shear stress mobilization. Test data also provide a relation between *maximum* mobilized side shear ($\tau_{max, mob}$) and q_u , the latter obtained from RQD (correlation mentioned above). An expression for the prediction of pile shaft capacity of piles bored in gneiss, based on the inferred maximum mobilized side shear, is put forward (Eq. 7).

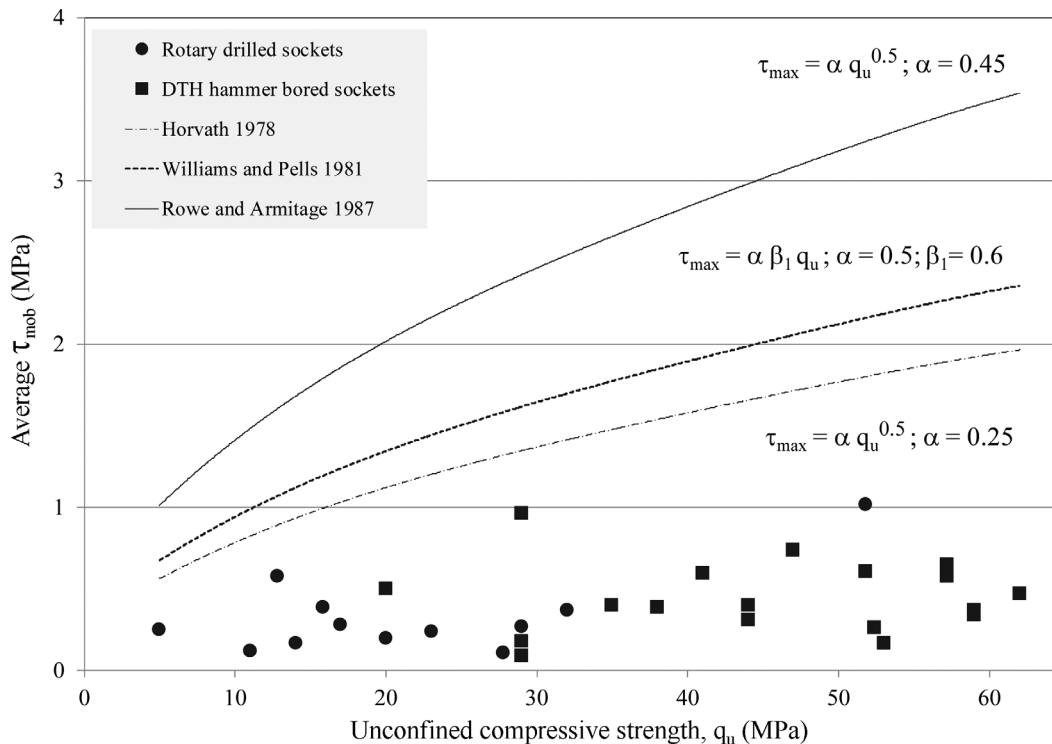


Figure 19 - Average mobilized shear stress from dynamic tests vs. q_u (estimated from average RQD along the pile socket).

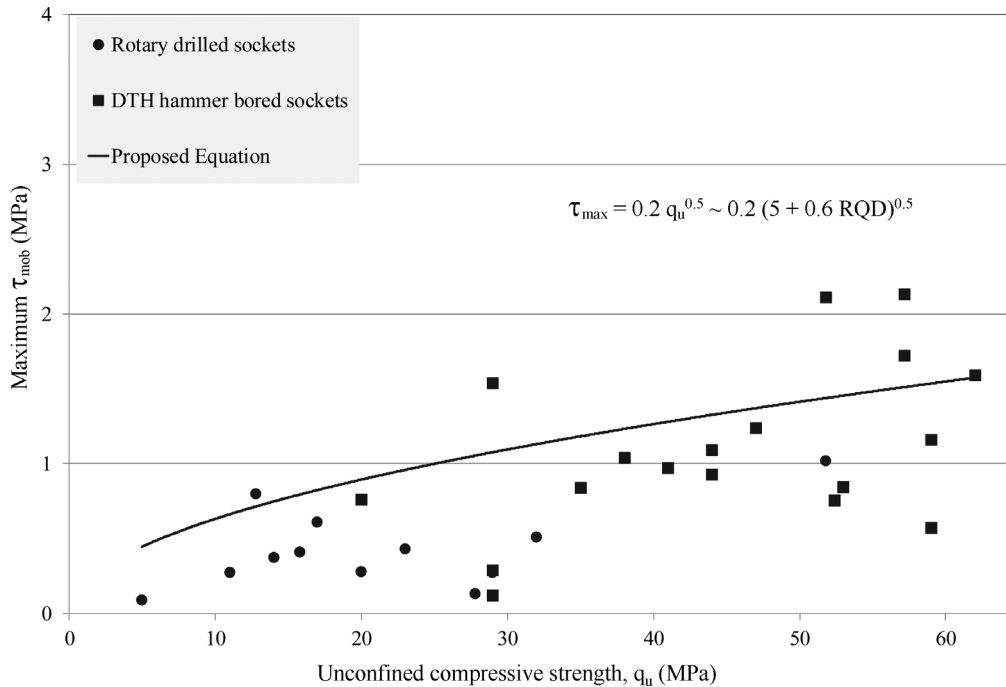


Figure 20 - Maximum mobilized shear stress in dynamic tests vs. q_u (estimated from average RQD along the pile socket).

Acknowledgments

The authors would like to thank the support from the design firm, PROJCONSULT, in the person of engineer Filemon B. Barros, and from the Contractor, TRANS-CARIOCA. Laboratory tests were performed at the Structures Laboratory of COPPE (Graduate School of Engineering), Federal University of Rio de Janeiro, and thanks are due to Prof. Romildo D. Toledo Filho and his staff. Many thanks are also due to geologist José Paulo Coutinho Filho, responsible for the field supervision of pile boring, for sharing his experience with the authors.

References

ABNT (2007). NBR 13208 - Brazilian Technical Standards Association. Dynamic Testing of Piles - Test Method. Rio de Janeiro, Rio de Janeiro, Brazil, 12 p. (in Portuguese).

ASTM (2001). Standard Practices for Preparing Rock Core Specimens and Determining Dimensional and Shape Tolerances - D 4543. ASTM International, West Conshohocken, Pennsylvania, USA, 5 p.

ASTM (2012). Standard Test Method for High - Strain Dynamic Testing of Deep Foundations - D 4945. ASTM International, West Conshohocken, Pennsylvania, USA, 9 p.

Danziger, B.R.; Lopes, F.R.; Costa, A.M. & Pacheco, M.P. (1996). A discussion on the uniqueness of CAPWAP-type analyses. Proc. 5th. Int. Conf. on the Application of Stress-wave Theory to Piles, Miami, v. 1, pp. 394-408.

Deere, D.U. (1969). Geological considerations. In: Stagg, K.G., Zienkiewicz, O.C. eds. Handbook of Rock Mechanics in Engineering Practice. John Wiley & Sons, London, pp. 1-20.

Goodman, R.E. (1989). Introduction to Rock Mechanics. 2nd. ed. John Wiley & Sons, New York, p. 562.

Horvath, R.G. (1978). Field load test data on concrete to rock bond strength for drilled pier foundations. University of Toronto Publication No.78-07. Toronto, Ontario.

Horvath, R.G. & Kenney, T.C. (1979). Shaft resistance of rock-socketed drilled piers. In: F.M. Fuller, ed., ASCE Symposium on Deep Foundations, Atlanta. New York, p. 182-214.

Juvencio, E.L. (2015). Evaluation of the Behavior of Piles Partly Embedded in Gneissic Rock. DSc Thesis, COPPE, Federal University of Rio de Janeiro, 225 p. (in Portuguese).

Mcvay, M.C.; Townsend, F.C. & Williams, R.C. (1992). Design of socketed drilled shafts in limestone. Journal of Geotechnical Engineering, 118(10):1226-1237.

Meigh, A.C. & Wolski, W. (1979). Design parameters for weak rock. In: Proceedings, 7th European Conference on Soil Mechanics and Foundation Engineering, Brighton, UK. London: British Geotechnical Society; v. 5, pp. 59-79.

Pells, P.J.N.; Rowe, R.K. & Turner, R.M. (1980). An experimental investigation into side shear for socketed piles in sandstone. In: Proc. of the Int. Conf. on Structural Foundations on Rock. Sydney, v. 1, pp. 291-302.

Rausche, F.; Morgano, M.; Hannigan, P.; Bixler, M. & Beim, J. (2006). Experiences with heavy drop hammer

- testing of rock-socketed shafts, 31st. Annual Conference on Deep Foundations, DFI, Washington, 9 p.
- Rosenberg, P. & Journeaux, N. (1976). Friction and end bearing tests on bedrock for high capacity socket design. *Canadian Geotechnical Journal*, 13(3):324-333.
- Rowe, R.K. & Armitage, H.H. (1987). A design method for drilled piers in soft rock. *Canadian Geotechnical Journal*, 24(1):126-142.
- Williams, A.F. & Pells, P.J.N. (1981). Side resistance rock sockets in sandstone, mudstone, and shale. *Canadian Geotechnical Journal*, 18(4):502-503.
- Wyllie, D.C. (1999). *Foundations on Rock*. 2nd. ed. E & FN Spon, London, 435 p.
- Zhang, L. (1997). *Analysis and Design of Axially Loaded Drilled Shafts Socketed into Rock*. MSc Thesis in Civil and Environmental Engineering. Massachusetts Institute of Technology, Cambridge, MA, 167 p.
- Zhang, L. & Einstein, H.H (1998). End bearing capacity of drilled shafts in rock. *Journal of Geotechnical and Geoenvironmental Engineering*, 124(7):574-584.

SOILS and ROCKS

An International Journal of Geotechnical and Geoenvironmental Engineering

Publication of

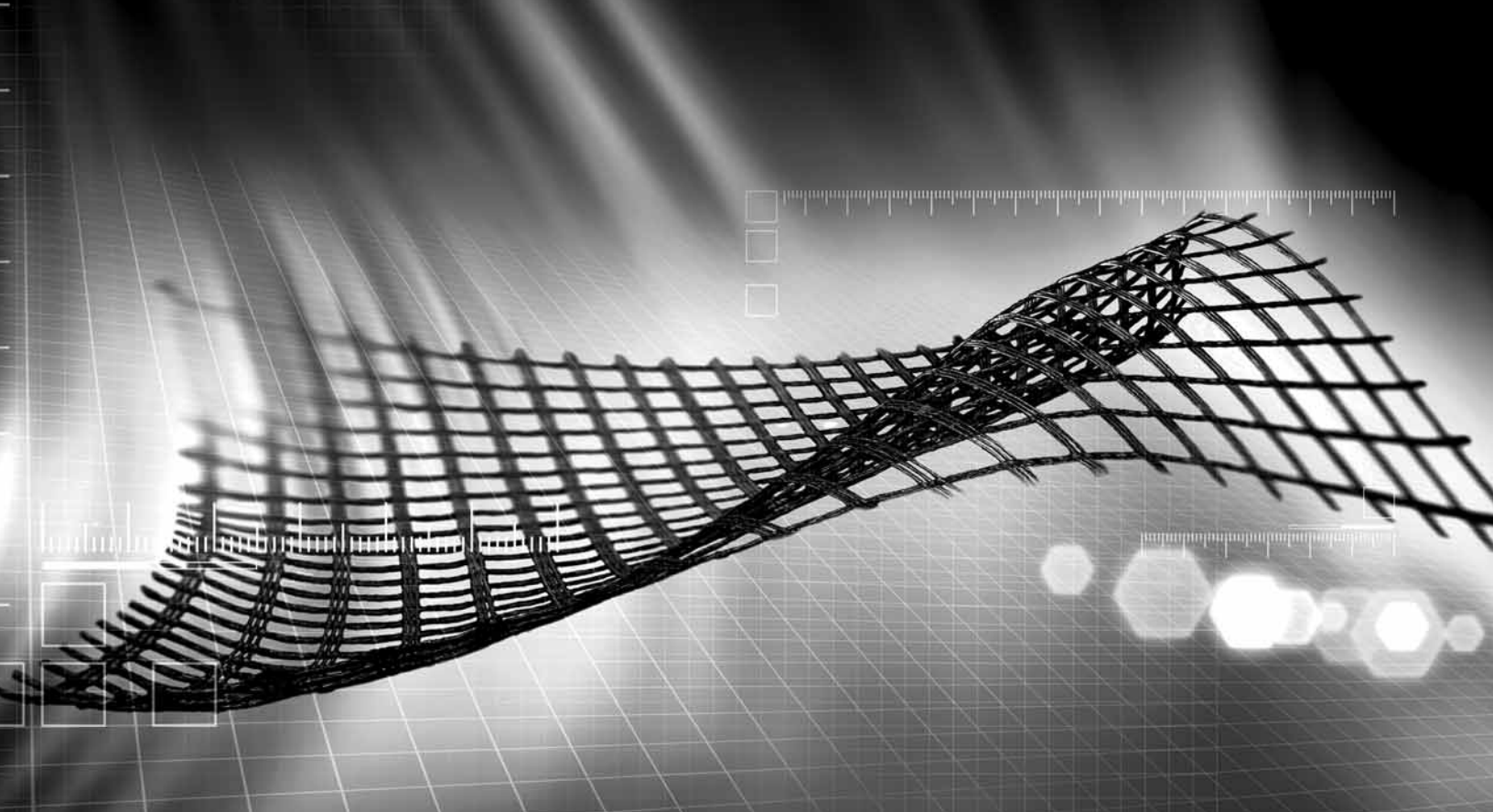
ABMS - Brazilian Association for Soil Mechanics and Geotechnical Engineering

SPG - Portuguese Geotechnical Society

Volume 40, N. 1, January-April 2017

Author index

Araújo Neto, C.L.	51	Melo, M.C.	51
Benetti, L.B.	17	Miranda Neto, M.I.	31
Cordão Neto, M.P.	3	Monteiro, V.E.D.	51
Juvencio, E.L.	61	Nóbrega, B.M.A.	51
Kormann, A.C.M.	17	Nunes, A.L.L.S.	61
Lopes, B.C.F.L.	3	Paiva, W.	51
Lopes, F.R.	61	Passini, L.B.	17
Mahler, C.F.	31	Romero, E.	3
Mascarenha, M.M.A.	3	Silva, P.C.R.	39
Massad, F.	39	Sousa, R.B.A.	51



A strong, lasting connection.

With a history of over 150 years of pioneering in geosynthetics, we strive to create solutions for the most diverse engineering challenges.

Our business areas:



**Earthworks and
Foundations**



**Environmental
Engineering**



Roads and Pavements



Hydraulic Engineering

Talk to HUESKER Brasil:
www.HUESKER.com.br
HUESKER@HUESKER.com.br
+55 (12) 3903 9300

Follow HUESKER Brasil in social media:



HUESKER
Ideen. Ingenieure. Innovationen.



Geotechnic and Rehabilitation

TEIXEIRA DUARTE
ENGENHARIA E CONSTRUÇÕES, S.A.

• **Head Office**
Lagoas Park - Edifício 2
2740-265 Porto Salvo - Portugal
Tel.: [+351] 217 912 300
Fax: [+351] 217 941 120/21/26

• **Angola**
Alameda Manuel Van Dunen 316/320 - A
Caixa Postal 2857 - Luanda
Tel.: [+34] 915 550 903
Fax: [+34] 915 972 834

• **Algeria**
Parc Miremont - Rua A, Nº136 - Bouzareah
16000 Alger
Tel.: [+213] 219 362 83
Fax: [+213] 219 365 66

• **Brazil**
Rua Iguatemi, nº488 - 14° - Conj. 1401
CEP 01451 - 010 - Itaim Bibi - São Paulo
Tel.: [+55] 112 144 5700
Fax: [+55] 112 144 5704

• **Spain**
Avenida Alberto Alcocer, nº24 - 7º C
28036 Madrid
Tel.: [+34] 915 550 903
Fax: [+34] 915 972 834

• **Mozambique**
Avenida Julyus Nyerere, 130 - R/C
Maputo
Tel.: [+258] 214 914 01
Fax: [+258] 214 914 00

BUILDING A BETTER WORLD



TPF

PLANEGE CENOR



Engineering and Architectural Consultancy

Geology, Geotechnics, Supervision of Geotechnical Works
Embankment Dams, Underground Works, Retaining Structures
Special Foundations, Soil Improvement, Geomaterials



www.tpfplanegecenor.pt



- > **Prospecção Geotécnica**
Site Investigation
- > **Consultoria Geotécnica**
Geotechnical Consultancy
- > **Obras Geotécnicas**
Ground Treatment-Construction Services
- > **Controlo e Observação**
Field Instrumentation Services and Monitoring Services
- > **Laboratório de Mecânica de Solos**
Soil and Rock Mechanics Laboratory

Certificada ISO 9001 por

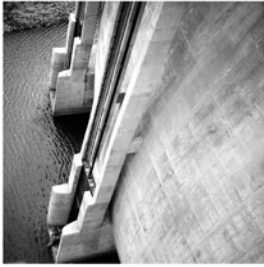


Geocontrole



Parque Oriente, Bloco 4, EN10
2699-501 Bobadela LRS
Tel. 21 995 80 00
Fax. 21 995 80 01
e.mail: mail@geocontrole.pt
www.geocontrole.pt


Geocontrole
Geotecnia e Estruturas de Fundação SA



COBA

GEOLOGY AND GEOTECHNICS

Hydrogeology • Engineering Geology • Rock Mechanics • Soil Mechanics • Foundations and Retaining Structures • Underground Works • Embankments and Slope Stability
Environmental Geotechnics • Geotechnical Mapping



- Water Resources Planning and Management
- Hydraulic Undertakings
- Electrical Power Generation and Transmission
- Water Supply Systems and Pluvial and Wastewater Systems
- Agriculture and Rural Development
- Road, Railway and Airway Infrastructures
- Environment
- Geotechnical Structures
- Cartography and Cadastre
- Safety Control and Work Rehabilitation
- Project Management and Construction Supervision



PORTUGAL

CENTER AND SOUTH REGION
Av. 5 de Outubro, 323
1649-011 LISBOA
Tel.: (351) 210125000, (351) 217925000
Fax: (351) 217970348
E-mail: coba@coba.pt
www.coba.pt

Av. Marquês de Tomar, 9, 6.º.
1050-152 LISBOA
Tel.: (351) 217925000
Fax: (351) 213537492

NORTH REGION

Rua Mouzinho de Albuquerque, 744, 1.º.
4450-203 MATOSINHOS
Tel.: (351) 229380421
Fax: (351) 229373648
E-mail: engico@engico.pt

ANGOLA

Praceta Farinha Leitão, edifício nº 27, 27-A - 2.º Dto
Bairro do Maculusso, LUANDA
Tel./Fax: (244) 222338 513
Cell: (244) 923317541
E-mail: coba-angola@netcabo.co.ao

MOZAMBIQUE

Pestana Rovuma Hotel. Centro de Escritórios.
Rua da Sé nº114. Piso 3, MAPUTO
Tel./Fax: (258) 21 328 813
Cell: (258) 82 409 9605
E-mail: coba.mz@tdm.co.mz

ALGERIA

09, Rue des Frères Hocine
El Biar - 16606, ARGEL
Tel.: (213) 21 922802
Fax: (213) 21 922802
E-mail: coba.alger@gmail.com

BRAZIL

Rio de Janeiro
COBA Ltd. - Rua Bela 1128
São Cristóvão
20930-380 Rio de Janeiro RJ
Tel.: (55 21) 351 50 101
Fax: (55 21) 258 01 026

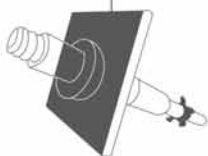
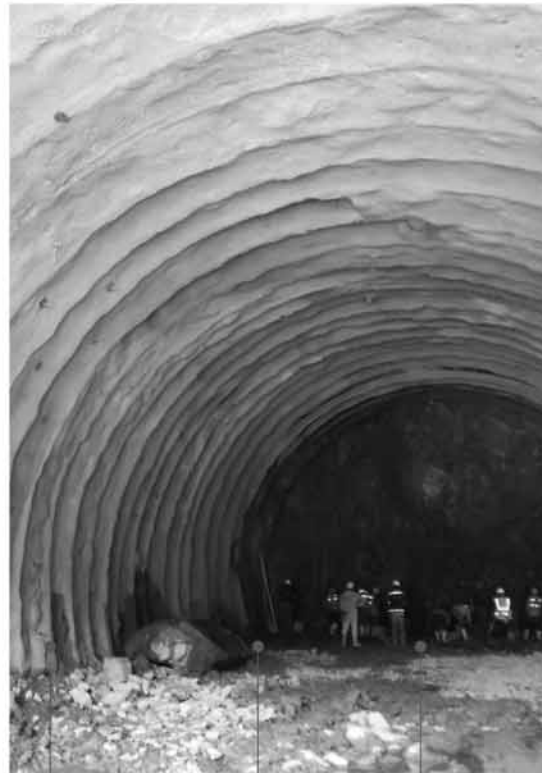
Fortaleza

Av. Senador Virgílio Távora 1701, Sala 403
Aldeota - Fortaleza CEP 60170 - 251
Tel.: (55 85) 3261 17 38
Fax: (55 85) 3261 50 83
E-mail: coba@esc-te.com.br

UNITED ARAB EMIRATES

Corniche Road - Corniche Tower - 5th Floor - 5B
P. O. Box 38360 ABU DHABI
Tel.: (971) 2 627 0088
Fax: (971) 2 627 0087

Much more support to your business.



Incotep - Anchoring Systems

Incotep anchoring Systems is a division of Açotubo Group, which engaged in the development of Anchoring Systems, used in geotechnical and structural applications where high quality prestressing systems are designed to meet diverse needs.

Know our solutions for your processes

- Self Drilling Injection Hollow Bar
- Cold Rolled Thread Bars and Micropiles
- Hot Rolled Thread Bars
- Incotep Tie Rods (Port and Dike Construction)

- Umbrella Tubes Drilling System
- Pipes for Root Piles, among others

www.incotep.com.br
+55 11 2413-2000

INCOTEP
Sistemas de Ancoragem

A company Açotubo Group





Conheça mais:
www.geobrugg.com/pt/taludes



Safety is our nature

TECCO® SYSTEM³ com fio de aço de alta resistência

**SISTEMA ECOLOGICAMENTE
CORRETO PARA ESTABILIZAÇÃO
DE TALUDES**

SPECIALISTS IN GEOTECHNICAL IN-SITU TESTS AND INSTRUMENTATION

GEOTECHNICAL SERVICES (onshore and offshore)

IN-SITU TESTS

- Seismic CPT
- Cone Penetration Testing Undrained-CPTu (cordless system)
- Vane Shear Testing (electrical apparatus)
- Pressuremeter Testing (Menard)
- Flat Dilatometer Test-DMT (Machetti)
- Standard Penetration Test-SPT-T

INSTRUMENTATION

- Instrumentation, installation and direct import
- Routine Monitoring
- Operation and Maintenance
- Engineering analyses
- Consultancy, design & geotechnical engineering services

SAMPLING

- Soil sampling and monitoring
- Groundwater sampling and monitoring
- Field and laboratory testing

ENVIRONMENTAL

- Environmental Services
- Soil and groundwater sampling and monitoring
- Field and laboratory testing



0800 979 3436

São Paulo: +55 11 8133 6030

Minas Gerais: +55 31 8563 2520 / 8619 6469

www.deltageo.com.br deltageo@deltageo.com.br

Whatever your geotechnical challenge

Reinforced soil slopes with Green Terramesh®

Dynamic Rockfall barriers

Rock slope protection with SteelGrid®

we can engineer a better solution

Reinforced Soil Walls with Terramesh® System

Follow us:



/maccaferri /maccaferribrazil @Maccaferri_BR #MaccaferriWorld /maccaferriworld

For technical data, software and more, visit:
www.maccaferri.com/br

MACCAFERRI

Instructions for Submission of Manuscripts

Category of the Papers

Soils and Rocks is the international scientific journal edited by the Brazilian Association for Soil Mechanics and Geotechnical Engineering (ABMS) and the Portuguese Geotechnical Society (SPG). The aim of the journal is to publish (in English) original research and technical works on all geotechnical branches.

According to its content the accepted paper is classified in one of the following categories: Article paper, Technical Note, Case Study or Discussion. An article paper is an extensive and conclusive dissertation about a geotechnical topic. A paper is considered as a technical note if it gives a short description of ongoing studies, comprising partial results and/or particular aspects of the investigation. A case study is a report of unusual problems found during the design, construction or the performance of geotechnical projects. A case study is also considered as the report of an unusual solution given to an ordinary problem. The discussions about published papers, case studies and technical notes are made in the Discussions Section.

When submitting a manuscript for review, the authors should indicate the category of the manuscript, and is also understood that they:

- assume full responsibility for the contents and accuracy of the information in the paper;
- assure that the paper has not been previously published, and is not being submitted to any other periodical for publication.

Manuscript Instructions

Manuscripts must be written in English. The text is to be typed in a word processor (preferably MS Word), **single column**, using ISO A4 page size, left, right, top, and bottom margins of 25 mm, Times New Roman 12 font, and line spacing of 1.5. All lines and pages should be numbered. The text should be written in the third person.

The first page of the manuscript must include the title of the paper followed by the names of the authors with the abbreviation of the most relevant academic title. The affiliation, address and e-mail must appear below each author's name. An abstract of 200 words follows after the author's names. A list with up to six keywords at the end of the abstract is required.

Although variations on the sequence and title of each section are possible, it is suggested that the text contains the following sections: Introduction, Material and Methods, Results, Discussions, Conclusions, Acknowledgements, References and List of Symbols. A brief description of each section is given next.

Introduction: This section should indicate the state of the art of the problem under evaluation, a description of the problem and the methods undertaken. The objective of the work should be clearly presented at the end of the section.

Materials and Methods: This section should include all information needed to the reproduction of the presented work by other researchers.

Results: In this section the data of the investigation should be presented in a clear and concise way. Figures and tables should not repeat the same information.

Discussion: The analyses of the results should be described in this section.

Conclusions: The content of this section should be based on the data and on the discussions presented.

Acknowledgements: If necessary, concise acknowledgements should be presented in this section.

References: References to other published sources must be made in the text by the last name(s) of the author(s), followed by the year of publication, similarly to one of the two possibilities below:

...while Silva & Pereira (1987) observed that resistance depended on soil density... or It was observed that resistance depended on soil density (Silva & Pereira, 1987).

In the case of three or more authors, the reduced format must be used, e.g.: Silva *et al.* (1982) or (Silva *et al.*, 1982). Two or more citations belonging to the same author(s) and published in the same year are to be distinguished with small letters, e.g.: (Silva, 1975a, b, c.). Standards must be cited in the text by the initials of the entity and the year of publication, e.g.: ABNT (1996), ASTM (2003).

Full references shall be listed alphabetically at the end of the text by the first author's last name. Several references belonging to the same author shall be cited chronologically. Some examples are listed next:

Papers: Bishop, A.W. & Blight, G.E. (1963). Some aspects of effective stress in saturated and unsaturated soils. *Geotechnique*, 13(2):177-197.

Books: Lambe, T.W & Whitman, R.V. (1979). *Soil Mechanics*, SI Version. John Wiley & Sons, New York, 553 p.

Book with editors: Sharma, H.D.; Dukes, M.T. & Olsen, D.M. (1990). Field measurements of dynamic moduli and Poisson's ratios of refuse and underlying soils at a landfill site. Landva, A. & Knowles, G.D. (eds), *Geotechnics of Waste Fills - Theory and Practice*, American Society for Testing and Materials - STP 1070, Philadelphia, pp. 57-70.

Proceedings (printed matter or CD-ROM): Jamiolkowski, M.; Ladd, C.C.; Germaine, J.T. & Lancellotta, R. (1985). New developments in field and laboratory testing of soils. Proc. 11th Int. Conf. on Soil Mech. and Found. Engn., ISSMFE, San Francisco, v. 1, pp. 57-153. (specify if CD ROM).

Thesis and dissertations: Lee, K.L. (1965). *Triaxial Compressive Strength of Saturated Sands Under Seismic Loading Conditions*. PhD Dissertation, Department of Civil Engineering, University of California, Berkeley, 521 p.

Standards: ASTM (2003). *Standard Test Method for Particle Size Analysis of Soils - D 422-63*. ASTM International, West Conshohocken, Pennsylvania, USA, 8 p.

Internet references: Soils and Rocks available at <http://www.abms.com.br> and downloaded on August 6th 2003.

On line first publications must also bring the digital object identifier (DOI) at the end.

Figures shall be either computer generated or drawn with India ink on tracing paper. Computer generated figures must be accompanied by the corresponding digital file (.tif, .jpg, .pcx, etc.). All figures (graphs, line drawings, photographs, etc.) shall be numbered consecutively and have a caption consisting of the figure number and a brief title or description of the figure. This number should be used when referring to the figure in text. Photographs should be black and white, sharp, high contrasted and printed on glossy paper.

Tables shall be numbered consecutively in Arabic and have a caption consisting of the table number and a brief title. This number should be used when referring to the table in the text. Units should be indicated in the first line of the table, below the title of each column. Acronyms should be avoided. When applicable, the units should come right below the corresponding column heading. Additional comments can be placed as footnotes.

Equations shall appear isolated in a single line of the text. Numbers identifying equations must be flushed with the right margin. International System (SI) units must be used. The definitions of the symbols used in the

equations must appear in the List of Symbols. It is recommended that the symbols used are in accordance with Lexicon in 8 Languages, ISSMFE (1981) and the ISRM List of Symbols.

The text of the submitted manuscript (including figures, tables and references) intended to be published as an article paper or a case history should not contain more than 30 pages, formatted according to the instructions mentioned above. Technical notes and discussions should have no more than 15 and 8 pages, respectively. Longer manuscripts may be exceptionally accepted if the authors provide proper explanation for the need of the required extra space in a cover letter.

Discussion

Discussions must be written in English. The first page of a discussion should contain:

The title of the paper under discussion;

Name of the author(s) of the discussion, followed by their position, affiliation, address and e-mail. The author(s) of the discussion should refer to himself (herself/themselves) as the reader(s) and to the author(s) of the paper as the author(s).

Figures, tables and equations should be numbered following the same sequence of the original paper. All instructions previously mentioned for the preparation of article papers, case studies and technical notes also apply to the preparation of discussions.

Editorial Review

Each paper will be evaluated by reviewers selected by the editors according to the subject of the paper. The authors will be informed about the results of the review process. If the paper is accepted, the authors will be required to submit a version of the revised manuscript with the suggested modifications. If the manuscript is rejected for publication, the authors will be informed about the reasons for rejection. In any situation comprising modification of the original text, classification of the manuscript in a category different from that proposed by the authors, or rejection, the authors can reply presenting their reasons for disagreeing with the reviewer comments.

Submission

The author(s) must upload a digital file of the manuscript to the Soils and Rocks website.

Follow Up

The online management system will provide a password to the corresponding author, which will enable him/her to follow the reviewing process of the submitted manuscript at the Soils and Rocks website.

Volume 40, N. 1, January-April 2017**Table of Contents***ARTICLES*

<i>A Microstructural Cam Clay Model for Hydro-Mechanical Behavior of Unsaturated Soils</i> M.P. Cordão Neto, B.C.F.L. Lopes, M.M.A. Mascarenha, E. Romero	3
<i>Pile Setup over a Period of Seven Years Based on Dynamic Load Tests in Overconsolidated Clay</i> L.B. Passini, L.B. Benetti, A.C.M. Kormann	17
<i>Study of the Shear Strength of a Tropical Soil with Grass Roots</i> M.I. Miranda Neto, C.F. Mahler	31
<i>Cavity Expansion Analysis to Predict Side Shear Set-Up in Clayey Soils</i> P.C.R. Silva, F. Massad	39
<i>Statistical Modeling of Municipal Solid Waste Settlement from a Lysimeter</i> C.L. Araújo Neto, B.M.A. Nóbrega, R.B.A. Sousa, M.C. Melo, W. Paiva, V.E.D. Monteiro	51
<i>An Evaluation of the Shaft Resistance of Piles Embedded in Gneissic Rock</i> E.L. Juvencio, F.R. Lopes, A.L.L.S. Nunes	61